

# Renaissance of Analogue Optical Computing

Nikita Stroeve<sup>1</sup> and Natalia G. Berloff<sup>2\*</sup>

<sup>1</sup>*Department of Physics of Complex Systems,*

*Weizmann Institute of Science, Rehovot 76100, Israel and*

<sup>2</sup>*Department of Applied Mathematics and Theoretical Physics,*

*University of Cambridge, Cambridge CB3 0WA, United Kingdom*

## Abstract

This review paper examines the physics and mathematics of optical computing, which utilizes photons and optics-related technologies for effective and efficient computational purposes. We discuss the history and development of optical computing, as well as modern analogue computing platforms and architectures, focusing on neural network implementations. Furthermore, we cover special-purpose optimisers and mathematical descriptions of optical optimisers, as well as their various applications and interconnections. We also explore the main directions of technological development in optical computing and estimates of its efficiency. Finally, we discuss future perspectives and the domain of optical quantum computing. This review provides a comprehensive overview of the current state-of-the-art in optical computing and its potential applications.

---

\* correspondence address: N.G.Berloff@damtp.cam.ac.uk

## I. INTRODUCTION

In 1965 Intel co-founder Gordon Moore formulated an empirical observation that the number of transistors in a microprocessor will double nearly every two years, the statement which is known as Moore's law [1, 2]. This prediction was followed by the forecast of reaching a saturation point by 2015. The progress of conventional computer architectures was very close to Moore's vision. However, reaching the saturation point was just a matter of time. The miniaturization of silicon transistors recently managed to break the 7-nanometre barrier, which was believed to be the limit. Also, Moore's law usually comes with several essential indicators, such as the processor's thread performance and clock frequency, which reached the point of saturation much faster than the density of the transistors. All of these factors limit the scaling performance of modern computers. However, there are other reasons for the saturation of conventional computing power growth, which are the consequences of Moore's law. For example, increasing the number of transistors allows one to obtain more powerful systems. Still, the processing speed will inevitably decrease with the concomitant increase in heat production, while increased energy consumption is connected with the growth of the performance. Another critical issue is the so-called von Neumann bottleneck [3], arising from the architecture design. It refers to the computer system throughput limitation due to the characteristic of bandwidth for incoming and outgoing data [4, 5]. All these issues pose severe problems to the future of conventional computer development. As a result, the alternatives to von Neumann systems started to emerge [6, 7].

One turns to alternative hardware architectures and purpose-built devices to keep up with the scaling performance. As such, universal quantum computing promises to decrease the algorithmic complexity of solving challenging tasks by exploiting the entangled states. However, in contrast to this high-risk and high-reward strategy (also discussed in the current review in the optical setting), there is an option to replace electrons with photons but remain in the scope of classical or classical with a transient quantum coherence regime of optical computing. The motivation for such transition is clear since photons move at the speed of light, have low heat production, have high density and can be efficiently coupled to matter to exploit nonlinear behaviours. Moreover, optical technologies have matured and entered our everyday lives, such as fibre optic channels that carry the global traffic of information or optical readers of compact disks. However, the conversion of photons into electrons is

required for compatibility with CMOS architectures. Such conversion takes a significant portion of energy, slows down the overall process of information processing, and presents a severe technological bottleneck in this type of hybrid technology.

Despite these difficulties, optical hardware is exploited in computing devices. For example, different application-specific photonic hardware can operate on a reasonable scale in data centres for heavy machine learning (ML) applications and large-scale optimization. Moreover, neural network (NN) architectures are nearly ideally suited for optical hardware with the potential to achieve high efficiency, fast computing times, and low energy consumption due to the desired physical properties of the photonic systems. Nevertheless, at this point, optical computing can not be associated with mainstream technology. It is unlikely that optics will ever replace electronics as the universal platform in the foreseeable future. The additional reason is the technological inertia accumulated through the years by significant investments in CMOS technologies. Partially, the rapid development of what we call conventional computers in the early years led to an ever-increasing gap with computing using photonics, which will occupy its own place in the domain of application-specific hardware.

There are many excellent reviews on the topic of optical computing. The challenges of modern computing and new opportunities for optics are discussed in [8]. This work presents the latest research progress of analogue optical computing, focusing on three main directions: vector/matrix manipulation, reservoir computing (RC) and photonic Ising machine. Moreover, it covers the topic of computing efficiencies, such as the ratio of performance and power dissipation and the error/precision interplay of such hardware. Another excellent review considers analogue optical computing in the context of artificial intelligence (AI) applications [9]. This work provides an overview of the latest accomplishments of optical computing, considering the realization of different AI models and NN paradigms. One can find additional information in other reviews [10–14], which appeared due to the recent interest in deep learning methods and their success in many domains.

What differentiates our review from those listed above is that we treat analogue optical computing using the concept of universality of the underlying dynamical systems description. The advantage of optical computing comes from ultrafast emulation of the dynamics [15]. We focus on physical optimisers that exploit bifurcation dynamics and threshold operation and aim at solving nonlinear problems, therefore, going beyond the speed-up of performing the linear operations that optics is so efficient at.

We organised our review as follows. Section II provides a short history of optical computing together with the modern analogue computing platforms focusing on NN implementation and other neuromorphic systems. Section III discusses the special-purpose optimisers and several examples of such devices. This section connects the operational regimes of such machines with the complexity classes and addresses the scalability of this approach. Section IV focuses on the physics of optical computing devices based on laser networks, optical parametric oscillators (OPOs) in fibre, photon or polariton networks, as well as their mathematical models. The second part of this review investigates the mathematical structures of different assignments and their emulation by the physical systems. The following Section V lists a wide range of possible applications across different applied domains. The final part consists of our subjective perspective on the future technological development of optical computing field in Section VI and passing remarks about quantum optical devices in Section VII. Finally, Section VIII summarises the results.

## **II. ANALOG OPTICAL COMPUTING**

Modern technologies demand vast data flows, creating various challenges for the development of the semiconductor industry and pushing classic electrical circuits to their physical limits. The developments range from more mainstream such as optical components that can be integrated into traditional computers or play the role of specific hardware, dealing with computationally heavy tasks or supplementing such calculations, to ambitious ones, such as all-optical digital computer architecture.

### **II.1. Brief prehistory of the optical computing**

Although optical computing is an emerging technology that has gained more momentum over time (especially considering the popularity and efficiency of the latest data-driven approaches), many significant advances have been made in previous decades. Therefore, before describing the particular systems, their advantages and their applications, we briefly discuss the progress that enabled. More information and additional details can be found in [16].

The generic optical processor architecture comprises three plane parts: the input, the processing and the output planes. Early on, the input plane was a fixed image slide with

its later change to a spatial light modulator (SLM), introduced to perform the input signal conversion. The processing plane can be composed of lenses, nonlinear components, or holograms, while the final output part is composed of photodetectors or a camera.

The first promising applications for optical processors were pattern recognition tasks, which influenced the prototypes of optical correlators. The simple architecture called 4-f was based on the work on spatial filtering, see [17]. The Fourier transform property of a lens is the standard function of many optical computing schemes, taking advantage of the speed and parallelism of light. The second type of correlator architecture was presented in 1966 by Weaver and Goodman [18], which is called the joint transform correlator (JTC), see Fig. 1

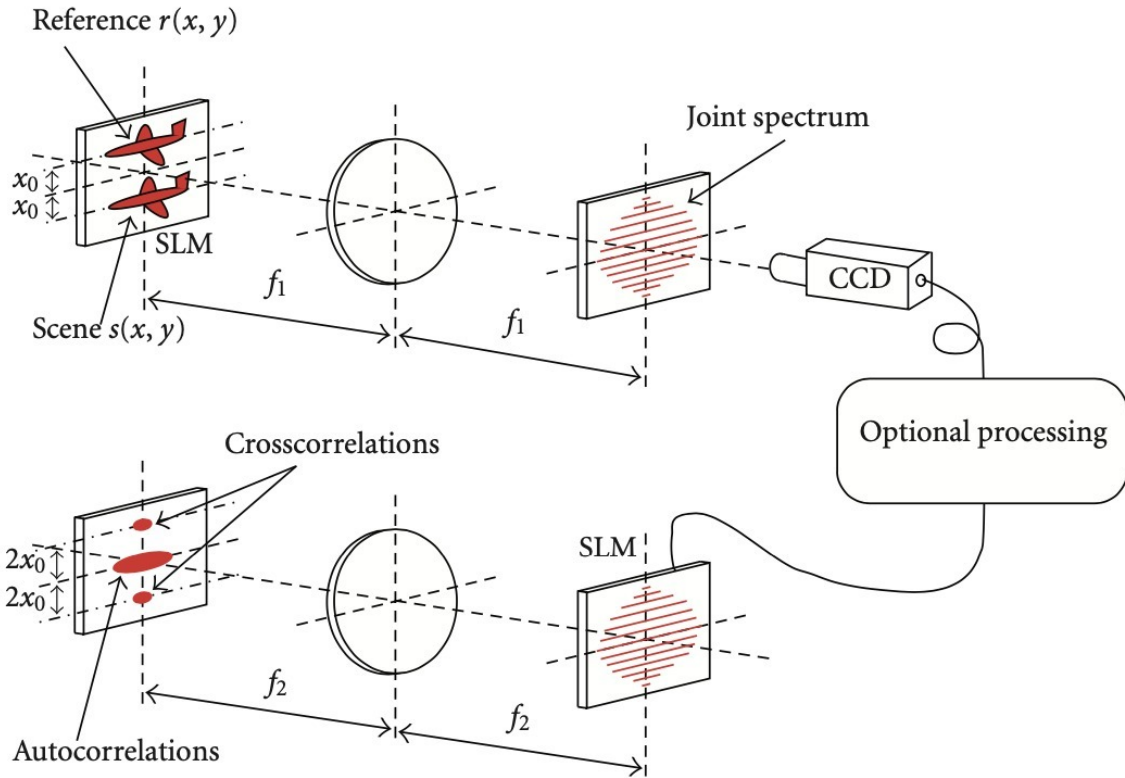


FIG. 1. The optical setup of the joint transform correlator (JTC). The figure is taken from [16].

Before 1950 there were significant steps in development of optical technologies such as the theory of image formation in the microscope [19], developed by Abbe, the development of phase contrast filter by Zernike [20] and the appearance of the information optics after Elias Snitzer in 1952 [21, 22]. Other major inventions of that period were holography

(by Gabor, 1948) [23] and the development of the laser in 1960 [24, 25]. The consequent introduction of the off-axis hologram allowed the separation of the different terms of the reconstruction giving remarkable 3D reconstructions [26, 27] in 1962 by Leith and Upatnieks, which basically led to practical holography and was further enhanced by Lohmann, creating the first computer-generated hologram [28, 29] in 1966. Early SLMs were based on the Pockels effect with few prospective devices [30–32]. Liquid crystal technology is the most commonly used technology for SLMs today. Another significant step was the invention of the first optical transistor [33], the hope for small integrated circuits.

The period from 1980 to 2004 was vibrant and productive. Active progress was going in the field of holography, particularly new encoding methods and the point-oriented methods were developed to achieve high quality and high diffraction efficiency optical reconstructions of the CGHs [34]. More than 50 types of SLM were introduced in the eighties and nineties [35]. Optical transistors presented another active area of research with the appearance of the micro-electromechanical systems (MEMS) technology [36]. In the 1990s, vertical-cavity surface-emitting lasers (VCSELs) and the self-electrooptic effect (SEED) devices became available [37]. In general, many aspects of modern optical interconnections and their components were introduced and studied during this period.

The optical technologies development provided the necessary experience in the capabilities of the optical devices and led to the maturation of the experimental element base. Optical computing received a second chance after the success of so-called deep NNs, which share many similarities with the previous neural-like optical architectures.

## II.2. Modern optical computing

Today, numerous research topics benefit from the progress in optical computing; therefore, the field is no longer so well defined. For example, some of the algorithms initially developed for pattern recognition using optical processors are now used successfully in digital computers. Other fields, such as biophotonics, largely benefit from past optical processing research.

The fundamental building block of modern electronic computers is a transistor. Therefore, one must find an equivalent optical transistor to replace electronic components with optical ones. To assemble such transistors into the higher-level components to create an

all-optical computer’s central processing unit (CPU), one has to design the optical processor and optical storage and organise the optical data transfer. However, such an approach faces many challenges, while the potential of optics in large architecture consisting of higher-level components can be seen as somewhat speculative [38]. Among persisting problems are the scalability of the optical logic devices due to the bad logic-level restoration, cascadability, fan-out and input-output isolation, energy consumption issues and non-miniature device footprint. Moreover, coupling these potential devices with the electrical components will require data format conversion from photons to electrons, which is relatively slow and energy-consuming.

However, the development of integrated photonics continued [39]. It led to attempts to create linear logic elements, such as all-optical logic gates [40, 41], improve the existing optical transistors and develop new ones in the context of the all-optical processing [42, 43]. One can use SLM, micro-lens array and holographic elements in free space to realize optical linear interconnection. Such linear elements are essential components in various optical computing devices.

Nonlinearity is another essential component in optical schemes; however, its realisation meets specific difficulties as light beams pass through each other unperturbed in a pure vacuum. To force these beams to interact, one has to set up a high-energy experiment, which is challenging to realise in practice. There are two other ways to realise the nonlinearity: introduce the digital readout mechanism, implemented by the charged-coupled device (CCD), send it to a computer with further nonlinear processing before feeding it back to SLM, or develop fully optical nonlinear activation materials with high enough intensity of the beams (utilising absorption, refraction or scattering processes). Nonlinearities can be divided into local (as needed in neural architectures) and global systems (such as reservoir computing systems, see below). Combining the linear and nonlinear elements led to the developing of specialised isolated devices. As a result, optical computing research has seen a resurgence in activity, centring around new developments in photonic hardware accelerators and neuromorphic computing.

Neuromorphic computing usually denotes the use of integrated systems to mimic neurobiological architectures. Although it is very close to the domain of AI, with the stress on the word “artificial”, which deals with the intelligent designed machines or agents, we will use neuromorphic computing in the general sense to describe any neural systems, be it

brain or nature-inspired or artificially designed. Modern key focus areas are concerned with emulating the neural structure and operation of the human brain, including probabilistic computing, which creates algorithmic approaches to dealing with uncertainty, ambiguity, and contradiction in the natural world. Optics has required ingredients to emulate NNs [13, 44].

### II.3. Optical neural networks

Optics has long been a promising medium for matrix multiplication and interconnects. Artificial neural networks (ANN) have been widely used for industrial and fundamental applications, and this new technological demand created a renewed case for photonic NNs. Although most ANN hardware systems are electronic-based, their optical implementation is particularly attractive because of their intrinsic parallelism and low energy consumption. Disparate ANNs vary by types of constituent elements, mathematical operations and the architecture used. In photonic approaches to ANN, the mathematical operations are mapped to the dynamics of optical propagation set by programmable linear optics and nonlinearity. A scalar synaptic weight describes pairwise connections between artificial neurons. At the same time, the layout of interconnections can be represented as a matrix-vector operation, where the input to each neuron is the dot product of the output from connected neurons with assigned weights.

Photonic realizations of ANNs fall into three categories. First, free-space systems rely on diffraction, Fourier transforms, etc. [45, 46]. They have high scalability and can simultaneously process large numbers of neurons but suffer limited connectivity. One example is a reconfigurable, scalable two-layer NN for the classifying phases of a statistical Ising model [47]. Second, SLMs program linear operations and Fourier lenses implement the summation by collecting the light power encoded signal. However, in the case of free optics, the nonlinear optical activation functions are realized in a complicated manner, e.g. with the laser-cooled atoms with electromagnetically induced transparency [47]. Finally, on-chip approaches based on wavelength multiplexing [48] or beamsplitter meshes [49] can achieve programmable all-to-all coupling but need to scale better. One on-chip design was proposed in [50], where the optical platform takes advantage of encoding information in both phase and magnitude, thus making it possible to execute complex arithmetic by optical interfer-



ence, which suits performing handwriting recognition tasks. Mach–Zehnder Interferometers (MZIs) can perform many functions, such as dividing and modulating the light signals, separating the reference and the main light beams, and implementing a complex-valued weight matrix.

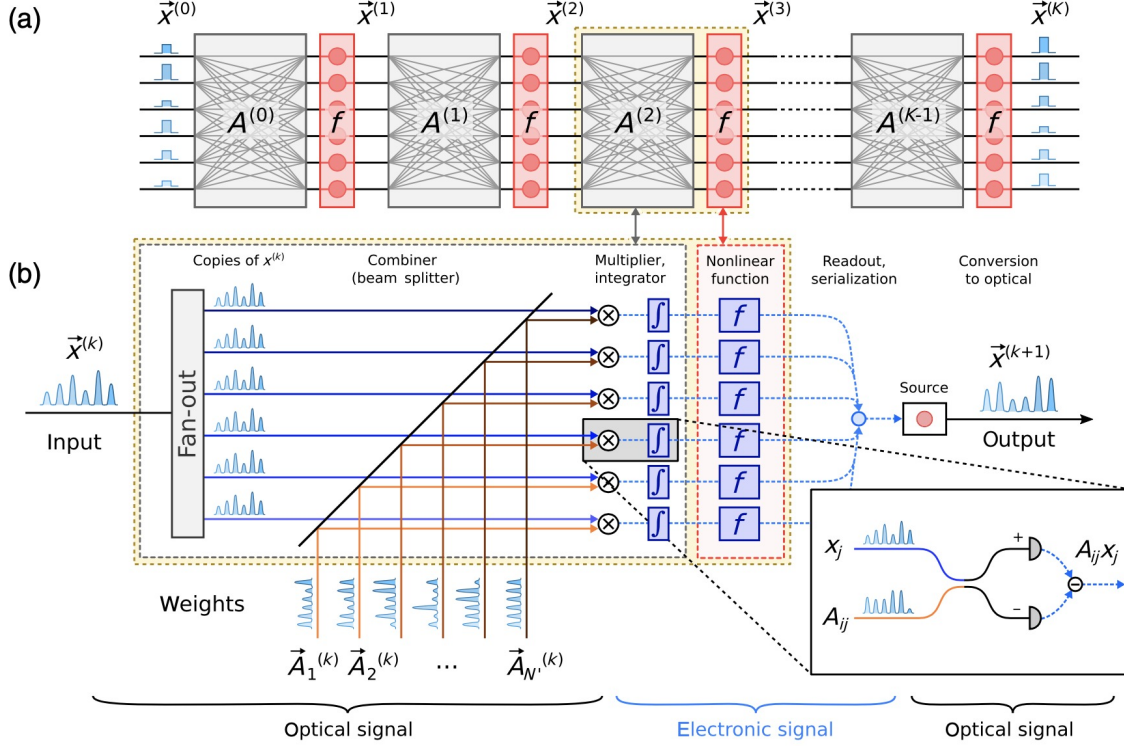


FIG. 2. (a) One layer of an optical NN with  $k$  layers consists of matrix-vector multiplication (grey) and non-linearities (red). (b) One-level implementation. Matrix multiplication is performed by combining the input and weight signals and performing balanced homodyne detection. The final signals are sent through a non-linear function (red), serialized, and sent to the following layer's input. Figure from [51]

Tunable waveguides can multiply optical signals, while wavelength-division multiplexing can add signals. Wavelength-division multiplexing can be achieved by the accumulation of carriers in semiconductors [52, 53], electronic currents [54, 55], or photon-induced changes of the material [56]. To achieve the full potential in on-chip architectures, one must require long-range connections between neurons, assisted with photonic waveguides that outperform metal wires connections of conventional electronics but fall behind free-optics solutions. In particular, silicon photonic platforms demonstrated efficient neuromorphic architectures [48, 49, 54]. An array of beam splitters and phase shifters can implement unitary matrix

transformations using interference between different paths of coherent input light, where inputs are assigned to different waveguides and power modulated [57]. Modulating the effective refractive index of signal-carrying waveguides is another optical mode-based approach to weight configuration. Non-volatile synapse implementations have been referred to as all-optical because they do not need electrical inputs for tuning. These may use optically induced changes in chalcogenide materials to control the light propagation in waveguides [58]. Weight configurations based on non-volatile optical materials could lead to improved heat dissipation.

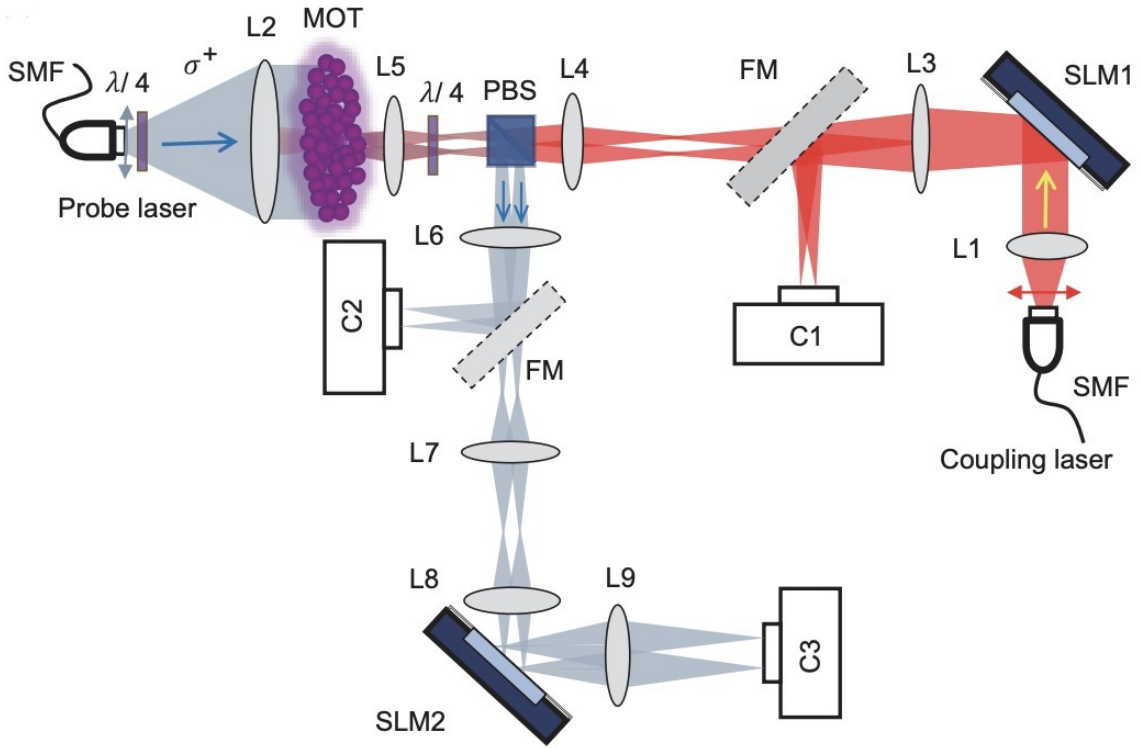


FIG. 3. In fully functional 2-layer all optical NN the first layer comprises a linear operation by the first SLM (SLM1) which encodes a certain pattern and a nonlinear activation function based on the electromagnetic induced transparency at magneto-optical trap (MOT). The second layer contains the second SLM (SLM2), converting four beams into two output beams at camera C3. The collimated coupling laser beam passing lens L1 is incident on the SLM1, which generates four beams at the focal plane of L3, which is monitored by a flip mirror (FM) and camera C1. Four beams are imaged on the MOT through a 4-f system comprising L4 and L5. A probe laser is going opposite the coupling beam, which is imaged on camera C2 through L5 and L6. L7 and L8 achieve further amplification. Four beams are incident on SLM2, generating two beams and then focusing on camera C3. Figure from [47].

A scheme based on homodyne detection has several scaling advantages over on-chip ap-

proaches, including linear (rather than quadratic) chip-area scaling and constant circuit depth [51]. The input vector in this implementation is encoded onto a pulse train, which is fanned out to an array of homodyne detectors where each detector computes a product between the input and a row of a matrix encoded into optical pulse trains. The accumulated charge on the homodyne detector performs matrix-vector multiplication. The output is sent through an electrical nonlinearity and converted back to optical signal using a modulator. The advantage of the homodyne detection scheme is that the matrix elements (weights) are encoded optically and can be dynamically reconfigured. This procedure requires a reduced number of photonic components: the number of modulators, detectors, and beamsplitter grows linearly with the number of neurons. The homodyne detection architecture can be parallelized to implement general matrix-matrix multiplication by routing the light out of plane [51]. This is useful in practical NNs that reuse weights (either natively in convolutional layers or through batching).

Nonlinearity in ANN is required to implement the thresholding effect of the neuron. Some photonic devices exhibit nonlinear neuron-like (gate-like) transfer functions. However, the challenge is to achieve cascability. Photonic neurons must be capable of reacting to multiple optical inputs, applying a nonlinearity and producing an optical output suitable to drive other photonic neurons. Integrated photonic solutions use either optical/electrical/optical (O/E/O) or all-optical design to achieve such cascability. In the O/E/O approach, nonlinearities may be introduced during the E/O conversion stage by employing lasers, saturated modulators or photodetector–modulators [59] or in the electronic domain only (e.g. the nonlinear dynamics of spiking photonic neurons could be implemented with a superconducting electronic signal pathway [60]).

NN architectures can take different forms: feed-forward and back-forward, layered and recurrent, spiking or continuous etc. Each neural model has a different signal representation, training method and network topology. Weight configurations can differ depending on the training type: supervised training, unsupervised or programmatic ‘compilation’. Topology describes the graph structure of neuron connectivity, and often it is advantageous to ANN operation to constrain the topology to guide weight configurations. Therefore, hardware implementation details may differ between different ANN, while the key technologies necessary for practical realization include active on-chip electronics and light sources. Many photonic architectures have already been demonstrated: recurrent ANN, continuous-time and

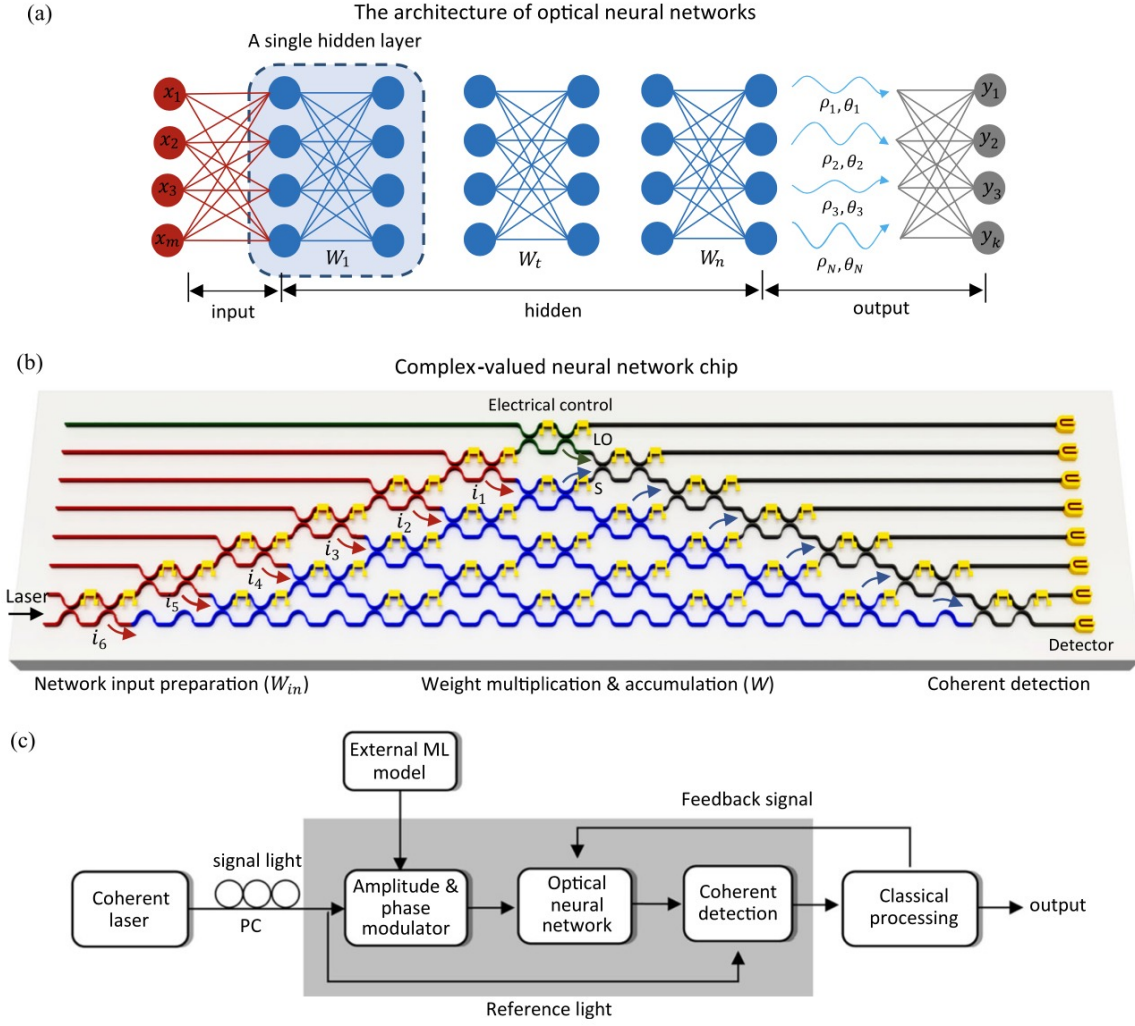


FIG. 4. Complex-valued coherent optical NN. (a) Scheme with an input layer, multiple hidden layers, and an output layer. (b) The schematic of the optical neural chip in implementing complex-valued networks. The single chip performs all stages, such as the input preparation, weight multiplication and coherent detection. The division and modulation of the light signals ( $i_1 - i_6$ ) are realized by the MZIs (red). Green MZI separates the reference light. Blue MZIs are used to implement the  $6 \times 6$  complex-valued weight matrix. Grey MZIs are used for on-chip coherent detection. (c) The workflow of the ONC system. Figure from [50].

programmed by compiler [48]; feed-forward, single-valued and externally trained ANN [49]; spiking, feed-forward ANN with both external and local training [56]; feed-forward multilayer ANN with semiconducting few-photon light-emitting diodes and superconducting-nanowire single-photon detectors [54]; diffractive networks with a nonlinearity [47]. The computational tasks solved by these platforms cover the main functions attributed to ML and AI: image and audio recognition and classification, simulation of dynamical systems, combina-

torial optimization and many other applications, which we will discuss in Section V. Some of the architectures and their different experimental realizations are shown in Fig. 2, 3 and 4.

The key merit of NN hardware is the level of energy consumption, which can be evaluated as petaMAC (multiply-accumulate operations) per second per  $\text{mm}^2$  processing speeds [61] and attojoule per MAC energy efficiencies [62]. In general, current optoelectronic hardware offers great advantages for implementing ANN, but eliminating the electrical contribution will inevitably be beneficial. For practical applications of neuromorphic photonic systems, one needs to reduce heat dissipation during information transfer between electrons and photons. Such reduction can be achieved by improving optical sources, high-efficiency modulators, and photonic analogue-to-digital interfaces. Current photonic platforms lack the functionality of electronic processors such as logic gates, high-level compilers and assemblers, analogue-digital-analogue conversion and memory. Although photonics provides advantages in connectivity and linear operations over electronics, on-chip memory is challenging. ‘In-memory’ computing, where processing is performed in situ with an array of memory devices called memristors, has been established [63, 64]; however, reading and writing at high frequencies is still challenging. The recent trends in the development of the ANN show the increasing demand to lower the power consumption of the devices. At the same time, the requirements for parallelism and scalability remain the same through the years [65]. Thus, the optical domain offers a promising solution to future hardware requirements.

#### **II.4. Reservoir and other neuromorphic computing systems**

Reservoir computing (RC) is a recurrent NN-based framework for computation that maps input signals into a specific computational space of the fixed nonlinear system dynamics. This system is usually called a “reservoir”, and its state is passed to a simple readout mechanism, specifically trained to get the final output [66]. The original concepts of RC can be traced to the liquid-state machines [67] and echo-state networks [68]. Many physical systems can reproduce this computational framework, and the optical/photonics domain is no exception. The extension of RC to deep hierarchical RC allows one to create more efficient models and simultaneously investigate the inherent role of layered composition in recurrent structures. Another promising research direction is to combine RC with quantum

physical systems to access larger computational space.

The idea of RC is to exploit the rich nonlinear dynamics of controllable nonlinear systems and simultaneously overcome the disadvantages of recurrent architectures with their challenging and time-consuming training for both hardware and software systems. The RC training is performed only at the readout stage, as the reservoir dynamics are fixed. This readout framework enjoys the benefits of a particular photonic physical system, such as speed or energy consumption, reducing learning costs. Another RC benefit is learning temporal (dynamic) dependencies compared to the feed-forward architectures used for static (non-temporal) data processing. The simplicity of the training procedure in RC is attractive. However, accessing complex dynamics without rigorous understanding can lead to many problems. Operating within the RC framework usually needs extensive experiments and experimental verification due to the need for a unified theory of RC. Another disadvantage is the performance instability due to the noise present, typical for nearly chaotic dynamical systems.

Nevertheless, many successful cases of RC are being applied to practical problems, such as temporal pattern classification, time series forecasting, pattern generation, adaptive filtering and control, and system approximations. Moreover, RC can be used conventionally for static data processing. The first all-optical implementation of RC was demonstrated within a simple optical delayed feedback loop combined with the nonlinearity of an optical amplifier [70]. Concerning the free-space optics principles, an image processing task was successfully solved using a predesigned configuration with a diffraction grating and Fourier imaging with randomly interconnected microring resonators [71]. The reservoir consisting of a diffractive optical element was described based on an  $8 \times 8$  laser array (of VCSELs) and an SLM. It showed rich dynamics with the potential for scaling up [72]. Further modifications of this setup with a laser illumination field and digital micro-mirror device allowed one to realise the large-scale RC scheme with 2025 diffractively coupled photonic nodes applied to a time series prediction task [73]. The recurrent 24-node silicon photonic NN, in which microring weight banks configure connections, was programmed using a “neural compiler” to solve a differential system emulation task with a 294-fold acceleration against a conventional benchmark [48].

Some hybrid architectures, such as opto-electronic devices, similarly benefit from the RC concept. For example, excellent performance has been obtained for speech recognition



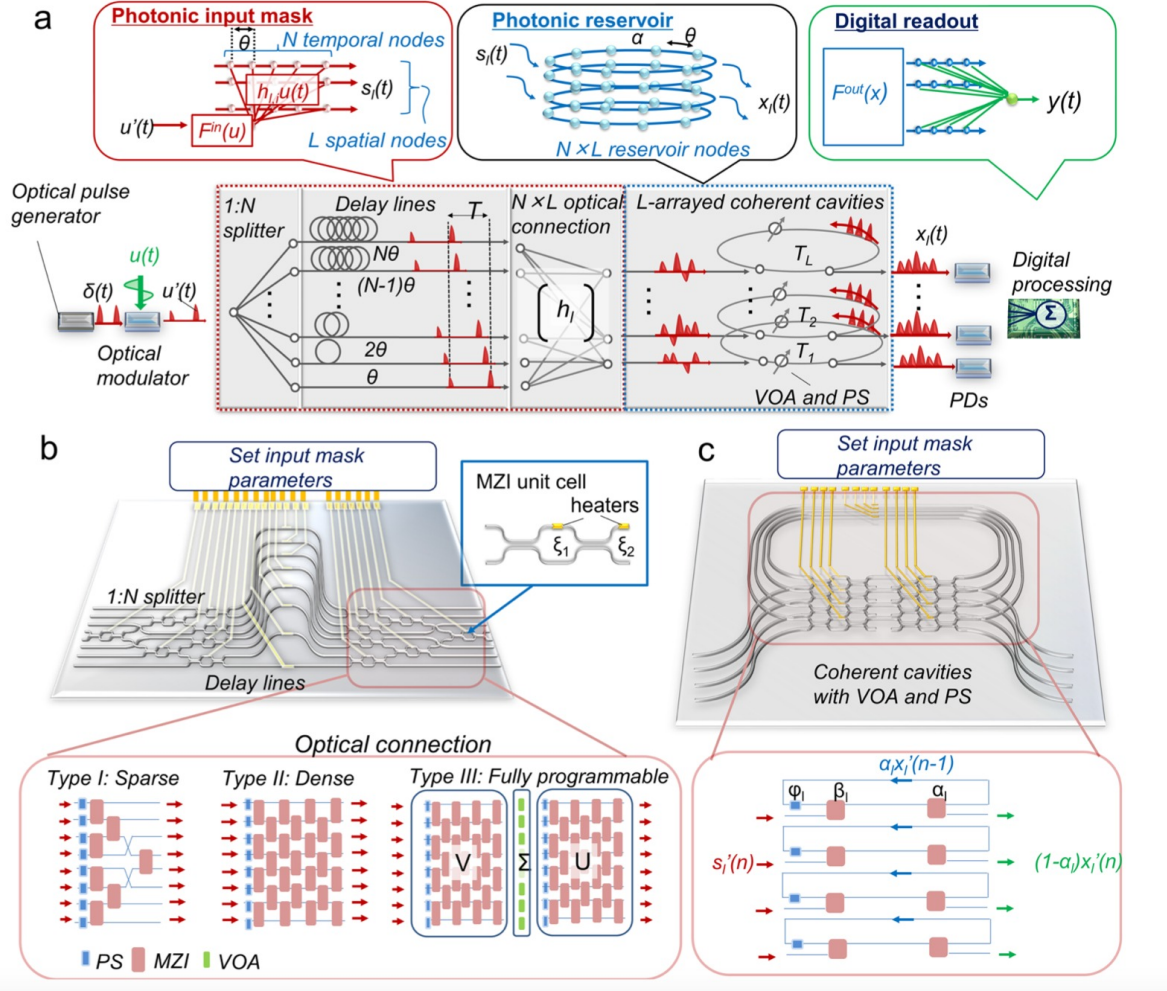


FIG. 5. (a) Schematics of proposed reservoir computing (RC) architecture. The electric input signal  $u(t)$  is coded on optical pulse,  $\delta(t)$  is coded by optical modulator. The sinusoidal nonlinearity is achieved by the electro-optic conversion ( $F^{in}$ ). RC system comprises the  $L$ -array of optical cavities with  $N$  temporal nodes with  $N \times L$  virtual nodes. Photodetectors (PDs) get the output signals from optical circuit and generate nonlinear conversion ( $F^{out}$ ). The digital processing unit detects signals  $|x_l|^2$  and weights and sums them to obtain the final output  $y(t)$ . (b) Schematic of the waveguide layout for input mask circuit with the three types of installations for optical connection, and (c) - input mask reservoir circuit. The input weights  $h_l$  and reservoir parameters can be tuned by the phase shifter, MZI and variable optical attenuator setup. Figure from [69].

[74–76], chaotic time series prediction [75, 77, 78], and radar signal forecasting [79], with the operating speed in the megahertz range and the potential to increase it to gigahertz speed, at the same time preserving the state-of-the-art numerical accuracy. Additional cases of successful RC have been reported in literature [66, 74, 80]. We will consider the NN and RC architectures cases involving quantum effects in Section VII.1. Another example is

illustrated by Fig. 5.

### III. NONLINEAR OPTIMIZATION SPECIFIC OPTICAL MACHINES

A large class of problems that can be solved by optical hardware includes nonlinear programming problems. They seek to minimize a nonlinear objective function  $E(\mathbf{x})$  of real or complex variables in  $\mathbf{x}$  subject to a series of constraints in the form of equalities or inequalities, i.e.  $g(\mathbf{x}) \leq 0$  and  $h(\mathbf{x}) = 0$ . Such a general framework can include many applications across social sciences, finance, telecommunications, aerospace, biological and chemical industries [81].

Many nonlinear optimisation problems present a significant challenge as the number of operations to solve them usually grows exponentially fast with the number of variables. This algorithmic complexity is the reason for using specialised techniques such as genetic algorithms, particle swarm optimisation, simulation and population annealing. Quadratic programming (QP) for minimising quadratic functions of variables subject to linear constraints is a usual simplification of such problems because nonlinear optimisation problems are quadratic to second order around the vicinity of the optimal solution. Such approximation can be successfully performed even outside the feasible solutions space. QPs can be met in the least squares regression or as a part of a bigger problem, such as support vector machine (SVM) training. The apparent correspondence between the QP objective function and 2-local spin Hamiltonians of various physical systems allows one to map the problem into the physical setup. Here, the degrees of freedom  $\mathbf{x}$  are associated with “spins” and the cost function  $E(\mathbf{x})$  is associated with a “Hamiltonian” that specifies the interactions patterns and strengths between spins.

There are several possible ways such a system can find the optimal solution or the ground state of the corresponding spin Hamiltonian. Depending on the nature of the system, it can use either quasi-equilibrium or non-equilibrium regimes. The system in thermodynamic equilibrium may find the optimal solution by quantum annealing, which is executed with the time-dependent Hamiltonian

$$H(t) = \left(1 - \frac{t}{\tau}\right)H_0 + \frac{t}{\tau}H_{\text{objective}}, \quad (1)$$



where  $H_0$  is the initial trivial Hamiltonian with known ground state, and  $H_{\text{objective}}$  is the final Hamiltonian at  $t = \tau$  which encodes an original objective function  $E$ . One can keep the system at the ground state during adiabatic evolution from  $H_0$  to  $H_{\text{objective}}$ . For the adiabatic transformation, the time scaling  $\tau$  for the system to remain in the ground state must be much larger than that defined by the inverse of the spectral gap [82]. However, the process becomes inefficient for larger systems and sophisticated (glassy)  $H_{\text{objective}}$  because the spectral gap typically shrinks exponentially fast with the system size. The excited states lead to large errors while simultaneously slowing down the annealing procedure.

Many open non-equilibrium gain-dissipative systems, such as lasers and photonic or polaritonic condensates are non-Hermitian systems and, therefore, do not have a ground state. Instead, they tend to minimise losses on the route to coherence. One can use geometric analogies to describe their operational principle as the approach of the surface of the optimisation cost function (loss landscape) from below. There are two main processes that lead to loss minimisation: bosonic stimulation below the threshold and the coherence of operations at the threshold responsible for the quality of the solution. After increasing the gain to the point where it overcomes the linear losses and is stabilised by the nonlinearity of the gain saturation, the emergent coherent state minimises the losses (equivalent to maximisation of the total number of particles). It hence achieves the loss minimisation mapped into the objective spin Hamiltonian. The system elements' resulting evolution closely resembles the Hopfield Networks' dynamics, proposed to be used to solve quadratic optimisation problems forty years ago [83]. Despite the successes and a lot of excitement generated back then, the optimisers based on Hopfield networks were almost forgotten primarily due to the high connectivity required between neurons and the concomitant evolution time of the networks used by classical architecture. The recent interest in Hopfield networks reemerged as it became possible to emulate them with physical systems such as electronic circuits or photonic NNs. Photonic systems have an advantage over their electronic counterparts due to the picosecond to the femtosecond time scale of their operation. At the same time, many signals can flow through a single optical waveguide. As a result, a photonic implementation of Hopfield networks as optimisers can have large dimensionality, dense connectivity, and a fast convergence time to the optimum solution.

### III.1. Spin Hamiltonians

The most real-life decision or optimisation problems present a severe challenge to conventional classical computers, with classic examples of a so-called “hard optimisation task” being the travelling salesman problem, the dynamic analysis of financial markets, the prediction of new chemical materials, and ML. Mathematically, many of these optimisation problems admit a reformulation into the problem of finding the ground state of a particular spin Hamiltonian, which can be emulated with a given simulator (e.g. solid-state or optical system). The overhead in the number of additional variables needed during this mapping is, at most, polynomial [84]. However, better still, such a system needs to easily map the variables of the desired objective function into spin Hamiltonian elements (spins, currents etc.). Additionally, one wants to independently tune short and long-range interactions between the elements and perform measurements to obtain the answer with the required precision. Such spin model Hamiltonians are experimentally challenging to implement and control. Still, the possible advantages in dealing with large problem sizes lead to an intensive search for a superior simulator. Such simulators have been realised to various extents in different physical systems and are covered in this review. Through all these systems, two classes of spin Hamiltonians are generally considered: Ising and XY. The Ising model attracts the most attention since an extensive range of challenging discrete combinatorial optimisation problems, e.g. travelling salesman, graph colouring, graph partitioning, etc., can be mapped into it [84]. This model is formulated for  $N$  classical “spins”  $s_j$  that take discrete values  $\{-1, 1\}$  to minimise the quadratic unconstrained binary optimisation problem (QUBO):

$$\min_{s_i} - \sum_{i=1}^N \sum_{j=1, j < i}^N J_{ij} s_i s_j + \sum_{i=1}^N h_i s_i, \quad \text{subject to } s_i \in \{-1, 1\}, \quad (2)$$

where  $h_i$  represents an external (magnetic) field, this term can be incorporated in the  $\mathbf{J}$  matrix by considering  $N + 1$  spins and thus will be omitted for the rest of the chapter. Experimental realization of the **nonlinear** terms beyond quadratic in the Ising Hamiltonian would lead to a  $k$ -local spin Hamiltonian with  $k > 2$  and would allow for a direct mapping of higher-order binary optimization problems (HOBQ) including Max-SAT [85] or number

factorization [86]

$$\min_{s_i} - \sum_{i_1, i_2, \dots, i_k}^N Q_{i_1, i_2, \dots, i_k} s_{i_1} s_{i_2} \dots s_{i_l} \dots s_{i_k} \quad \text{subject to} \quad s_{i_l} \in \{-1, 1\}. \quad (3)$$

In the XY model “spins” are continuous vectors  $\mathbf{s}_j = (\cos \theta_j, \sin \theta_j)$  and the corresponding quadratic continuous optimization problem (QCO) can be formulated as

$$\min_{\mathbf{s}_i} - \sum_{i, j < i} J_{ij} \mathbf{s}_i \cdot \mathbf{s}_j = \min_{\theta_i} - \sum_{i, j < i} J_{ij} \cos(\theta_i - \theta_j) \quad \text{subject to} \quad \theta_i \in [0, 2\pi), \quad (4)$$

and directly applicable for phase retrieval problems [87–90]. When phases  $\theta_j$  are limited to discrete values  $2\pi/n$  with an integer  $n > 2$  the model (4) recovers the  $n$ –state Potts model with applications in protein folding [91].

The appearance of continuous spins is a common feature in many optical systems because short photonic impulses can be characterized through amplitude and phase variables. Some of the optical hardware for ML take advantage of this feature. For example, complex-valued NNs [50], or more unusual concept of analogue transformations using a nonlinear set of functions were proposed [92].

### III.2. P, NP, NP-complete problems

The computational complexity of a problem is determined through the dependence of the problem’s size on time or the number of operations required to solve it. A problem belongs to a  $\mathbb{P}$  class when a polynomial algorithm exists for solving it (e.g. searching for the maximum element in an array with no prior information). Suppose there exists a polynomial algorithm for verifying a solution. In that case, the problem belongs to a non-deterministic polynomial-time ( $\mathbb{P} \ni \mathbb{NP}$ ), which does not always have an efficient (polynomial time) method of finding a solution. Whether  $\mathbb{P} = \mathbb{NP}$  true or not is a major unsolved problem in computer science, although it is widely believed to be untrue. Most difficult problems in  $\mathbb{NP}$  are called  $\mathbb{NP}$ -complete. They are equivalent to each other in that either all of them or none admit a polynomial-time algorithm (e.g. the travelling salesman problem, spin glass models and integer linear programming are in general  $\mathbb{NP}$ -complete problems). A problem is called  $\mathbb{NP}$ -hard (informally, the hardest problems in  $\mathbb{NP}$ ) if the existence of an efficient algorithm for

its solution implies the existence of such an algorithm for all the  $\text{NP}$ -complete problems.

In general, if a decision problem with a yes or no answer (e.g. does a particular Ising Hamiltonian have a ground state energy less than some value?), is  $\text{NP}$ -complete, then its corresponding optimization problem (e.g. what is the ground state energy of this Ising Hamiltonian?), is said to be  $\text{NP}$ -hard. It means that  $\text{NP}$ -hard problems are not any easier to solve than the corresponding  $\text{NP}$ -complete decision problems. The computational complexity of the Ising model has been studied before [93] where the Ising model with a magnetic field (2) and equal antiferromagnetic couplings was shown to be  $\text{NP}$ -hard for planar graphs.  $\text{NP}$ -hardness was demonstrated for the three-dimensional Ising model with nearest neighbour interactions and coupling strengths randomly drawn from  $\{-1, 0, 1\}$ . The  $\text{NP}$ -hardness implies the hardness of the hardest instances for the considered problems, while the average problem can be polynomially easy.

The existence of universal spin Hamiltonians has been established [94]. Universality means that all classical spin models can be reproduced within such a model, and certain simple Hamiltonians, such as the 2D Ising model on a square lattice with transverse fields and nearest neighbour interactions of infinite precision are universal [94]. Thus, due to  $\text{NP}$ -hardness of the Ising model, there should exist a polynomial time mapping of many practically relevant  $\text{NP}$ -complete problems to the Ising Hamiltonian, whose decision version solves the  $\text{NP}$ -the complete problem of interest. The mapping of various  $\text{NP}$  problems, including Karp's 21  $\text{NP}$ -complete problems, to Ising models with a polynomial overhead were explicitly formulated [84].

A problem belongs to  $\mathbb{P}$  class only if all its instances can be solved in polynomial time, while for a problem to be  $\text{NP}$ -complete is enough to have some instances that are hard to solve. Such instances are said to represent worst-case scenario behaviour. How to distinguish hard instances from simple ones is a cornerstone question of analogue physical optimisers. Such understanding is necessary to evaluate their scalability and efficiency [95].

It is believed that the procedure for creating “hard” instances for spin Hamiltonians may be found at the intersection of computational complexity and statistical physics, e.g. the hardness of problems can be connected to the existence of a first-order phase transition in a system (see [96–99] and references therein). Indeed, even a medium size hard instance is difficult to solve on a classical computer due to the exponential growth of operations with size. Thus, the time required to find the ground state energy depends on the coupling matrix

structure  $\mathbf{J}$ . For instance, finding the global minimum of the XY model for positive definite matrices remains NP-hard due to the non-convex constraints. Still, it can be effectively approximated using a semidefinite programming relaxation with some performance guarantee [100, 101]. Sparsity also plays an important role, and for sufficiently sparse coupling matrices, fast methods exist [102]. Having a unified set of optimization problems with tunable hardness and known solutions is an ongoing research direction. It will allow for an objective benchmark of classical and/or quantum simulators and algorithms. Otherwise, it would be hard to evaluate the performance of state-of-the-art platforms and methods.

Current research made a good starting point in developing a standardised procedure for performance evaluation. For example, the “optimisation simplicity criterion” was recently proposed to identify computationally simple instances [95]. Optical machines with their mode selection operation often follow the dominant eigenvalue of the coupling matrix and find minimisers that correspond to the signs of the principal eigenvector components. If the minimisers of a given problem have this property, the solution will be found easily in polynomial (at most quadratic) time. One such popular example is the Ising model on the Möbius ladder graph [95]. By rewiring the Möbius ladder graph to random 3-regular graphs, one can probe an intermediate computational complexity between  $\mathbb{P}$  and NP-hard classes with several numerical methods. Another way to construct instances for testing involves planted ensemble technique [99, 103].

#### IV. DESCRIPTION OF PHYSICAL OPTICAL PLATFORMS FOR OPTIMIZATION

Rather than trying to model nature, one can consider a reverse idea of exploiting physical phenomena for solving NP-complete problems. The concept of using simulators or analogue processing devices is quite old; see, for example, [104]. However, in the last years, one can observe a competition of different physical platforms in solving classical optimization problems faster than it can be achieved on conventional hardware. This competition resulted in the rapid emergence of a new field of Hamiltonian simulators at the intersection of laser and condensed matter physics, engineering and complexity theories. Here we discuss various physical systems that appeared as promising platforms for solving computational problems.

#### IV.1. Complex laser networks

A new generation of complex lasers such as degenerate cavity lasers, multimode fibre amplifiers, large-aperture VCSEL, and random lasers have many advantages compared with the relatively simple traditional laser resonators of their computing properties [105]. They have many spatial degrees of freedom, their nonlinear interactions within the gain material can be controlled by adjusting the spatial structures of lasing modes, the spatial coherence of emission can be tuned over a wide range, and the output beams may have arbitrary profiles. These properties allow the complex lasers to be used for RC [106] or mapped to hard computational problems.

In laser networks, the coupling can be engineered by mutual light injection from one laser to another. This introduces losses that depend on the relative phases between the lasers. Such dissipative coupling drives the system to a phase-locking that minimises losses. If the amplitudes of lasers are about the same, a steady-state minimum of the XY Hamiltonian is found [107]. Degenerate cavity lasers are beneficial as solvers as all their transverse modes have nearly identical  $Q$ . This implies that a large number of transverse modes lase simultaneously since they all have similar lasing thresholds [105].

The evolution of the  $N$  single transverse and longitudinal modes class-B lasers can be described by the rate equations [108, 109] on the amplitude  $A_i$ , phase  $\theta_i$ , and gain  $G_i$  of the  $i$ -th laser

$$\frac{dA_i}{dt} = (G_i - \alpha_i) \frac{A_i}{\tau_p} + \sum_j J_{ij} \frac{A_j}{\tau_p} \cos(\theta_i - \theta_j), \quad (5)$$

$$\frac{d\theta_i}{dt} = \Omega_i - \sum_j J_{ij} \frac{A_j}{\tau_p A_i} \sin(\theta_i - \theta_j), \quad (6)$$

$$\frac{dG_i}{dt} = \frac{1}{\tau_c} [P_i - G_i(1 + |A_i|^2)], \quad (7)$$

where  $P_i, \alpha_i, \Omega_i$  represent the pump strength, loss, frequency detuning of laser  $i$ , respectively, whereas  $\tau_p$  and  $\tau_c$  denote the cavity round trip time and the carrier lifetime, respectively. The coupling strengths between  $i$ -th and  $j$ -th lasers are represented by  $J_{ij}$ . If the amplitudes of all lasers are equal, Eq. (6) reduces to the Kuramoto equation of coupled phase oscillators

$$\frac{d\theta_i}{dt} = \Omega_i - \frac{1}{\tau_p} \sum_j J_{ij} \sin(\theta_i - \theta_j). \quad (8)$$

Equation (8) is a celebrated Kuramoto model of identical oscillators, which is widely used to describe the emergence of coherent behaviour in complex systems [110, 111]. By LaSalle invariance principle [112], every trajectory of the Kuramoto model converges to a minimum of the XY Hamiltonian.

It was shown that the probability of finding the global minimum of the XY Hamiltonian agrees between the experimental realization of the laser array and with the numerical simulation of Eqs. (5-7). However, simulating the Kuramoto model Eq. (8) on the same matrix of coupling strength gives a much lower probability of finding the global minimum. This result implies that the amplitude dynamics described by Eq. (5) provide a mechanism to reach lower energy states by pumping from below [109]. Consequently, the cavity lasers can be used as an efficient physical simulator for finding the global minimum of the XY Hamiltonian and, therefore, for solving phase retrieval problems. A particularly successful in these tasks was a digital degenerate cavity laser [90]. It is an all-optical system that uses a nonlinear lasing process to find a solution that best satisfies the constraint on the Fourier magnitudes of the light scattered from an object. To ensure that the solution to the phase retrieval problem is found, the compact support aperture is introduced inside the cavity, ensuring that different configurations of laser phases compete to find the one with minimal losses. The system combines the advantages of short round-trip times of the order of 20ns and high parallelism in selecting the winning mode.

#### **IV.2. Coherent Ising machine**

A network of coupled optical parametric oscillators (OPOs) is an alternative physical system for solving the Ising problem ([113–119] and references therein). Each OPO is a nonlinear oscillator with two possible phase states above the threshold that can be interpreted as the Ising spins. These artificial Ising spins are encoded by the optical phase of short laser pulses generated by a nonlinear optical process, i.e. optical parametric amplification. The OPO-based simulator, coherent Ising machine (CIM), is a gain-dissipative system in which the ground state of the Ising Hamiltonian corresponds to the lowest loss configuration. The optimal solution is found by driving the system close to the near-threshold regime, where other local energy minima are still unstable.

Currently, most successful implementations of CIMs use a fibre-based degenerate OPOs

(DOPOs) and a measurement-based feedback coupling, in which a matrix-vector multiplication is performed on the FPGA embedded in the feedback loop, see the scheme depicted in Fig. 6. The computational performance of such a scalable optical processor, bounded by the electronic feedback, was demonstrated for various large-scale Ising problems [113–115]. The comparison of a possible CIM’s speedup over classical algorithms is an ongoing study [116, 120]. Furthermore, the ability to implement arbitrary coupling connections [113] between any two spins implies better scalability than the solid-state based annealer, i.e. D-Wave machine [114].

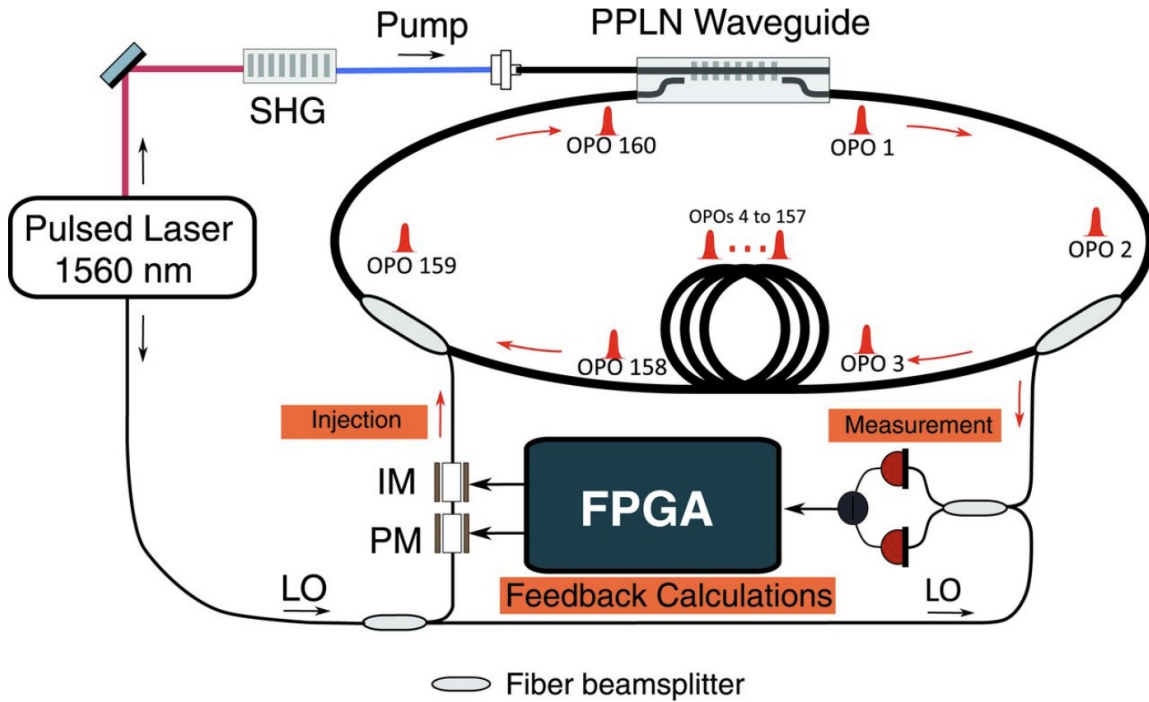


FIG. 6. Schematics of the coherent Ising machine (CIM) with the feedback mechanism. The time-multiplexed pulse degenerate parametric oscillator is formed by a non-linear crystal (periodically polarized lithium niobate (PPLN)) in a fibre optic ring cavity containing 160 pulses. The feedback signal couples the independent pulses in the cavity and is computed from the measurements from different pulse fractions. IM - intensity modulator; PM - phase modulator; LO - local oscillator; SHG - second-harmonic generation; FPGA - field-programmable gate array. The figure is taken from [113].

In CIM, each Ising spin corresponds to a DOPO that is described by a stochastic equation for the complex amplitude of the signal field  $a_i$ :

$$\frac{da_i}{dt} = pa_i^* - a_i - |a_i|^2 a_i + \sum_j J_{ij} a_j, \quad (9)$$



where the dynamics is defined by a linear pump term  $p$ , normalised linear and nonlinear losses, and mutual couplings  $J_{ij}$ . To experimentally realise these couplings, a portion of the light is extracted from the cavity after each round trip. That light is then homodyned against a reference pulse to produce  $a_i$  that is supplied to the FPGA, where a feedback signal is computed for each pulse. Lastly, an optical modulator is applied to convert the signal back to light for the next round trip. The equations (9) are often reformulated in terms of the in-phase and quadrature components  $a_i = c_i + is_i$  giving the equations in real terms:

$$\frac{dc_i}{dt} = \left( p - 1 - (c_i^2 + s_i^2) \right) c_i + \sum_j J_{ij} c_j \quad (10)$$

$$\frac{ds_i}{dt} = \left( -p - 1 - (c_i^2 + s_i^2) \right) s_i + \sum_j J_{ij} s_j. \quad (11)$$

The computational effectiveness of these equations has been demonstrated by tackling small size Ising type problems of order up to 20 [118]. In part devoted to polariton condensates, we will show that for achieving the global minimum, the realisation of an individual pump variation  $p_i$  for equalising all signal amplitudes  $|a_i|$  is crucial.

Phase stability for the cavity's whole length is required, making the DOPOs system highly susceptible to external perturbations that can affect performance [114]. Furthermore, the nonlinear DOPO generation process demands powerful laser systems and temperature-controlled nonlinear materials, which results in large and complex optical setups. These issues have led to recent proposals of other physical platforms for implementing a CIM-like machine. A CIM based on optoelectronic oscillators with self-feedback was suggested to be more stable and cheaper based on solving Ising optimisation problems on regular and frustrated graphs with up to 100 spins, and similar or better performance compared to the original DOPO-based CIM [117]. An analogue all-optical implementation of a CIM based on a network of injection-locked multicore fibre lasers demonstrated the possibility of solving Ising Hamiltonians for up to thirteen nodes [121]. The dynamics of a network of injection-locked lasers were based on nonlinear coupled photon rate equations, and the couplings were implemented using SLMs. The couplings were reported to be dependent on the photon numbers that have yet to be discovered beforehand, which can be a significant obstacle in solving a given Ising Hamiltonian with the proposed photonic CIM. To resolve this issue

approaches similar to gain feedback [122, 123] may be considered in future. Another large-scale optical Ising machine based on the use of an SLM was experimentally demonstrated by using the binary phases in separated spatial points of the optical wavefront of an amplitude-modulated laser beam and realising configurations with thousands of spins with tunable all-to-all pairwise interactions [124].

CIM's essential elements are DOPOs with an unconventional operating mechanism called mode selection or gain-dissipative principle. Here we briefly describe this operational regime: Each neuron is prepared in a linear superposition state of different excitations to implement a quantum parallel search. The cost function is mapped to the effective loss, photon decay rate, of the given network by setting the coupling coefficient proportional to the  $J_{ij}$ , which encodes the information about the given task. The ground state of the Ising Hamiltonian corresponds to an oscillation mode with the minimum network loss. The system reaches the ground state with a minimum loss at the threshold pump rate. It starts oscillating as a single stable mode, which triggers photons' stimulated emission and affects the saturation for all the other modes. Detecting this single oscillation mode will give us the solution to the desired problem.

### IV.3. Photon and polariton networks

Photons have both attractive and not properties concerning computational assignments. However, despite the commonly known optical platforms, such as free optical setups or systems of lasers, it is possible to bind the photons with the matter wave excitations. This gives rise to unique designs, combining the photons with matter, such as exciton-polaritons. Microcavity exciton-polaritons, or simply polaritons, are quasi-particles that result from the hybridisation of light confined inside semiconductor microcavities and bound electron-hole pairs (excitons). The steady states in these nonequilibrium systems are set by the balance between the pumping intensity, coming from the interconversion rate of the exciton's reservoir into polaritons, and losses, happening due to the leakage of photons. Polaritons are bosons and obey Bose-Einstein statistics. Therefore, they can form a condensed (coherent) state above a critical density [125]. Thus, polaritons offer a unique playground to explore nonequilibrium condensation and related effects in solids. The advantage for such explorations comes from the polariton's small effective mass of 4-5 orders of magnitude

smaller than the electron's mass. The design and choice of material allow one to control the polariton mass and realise such solid-state nonequilibrium condensates not only at cryogenic temperatures but also at room temperature in organic structures. The weak coupling at high temperatures and high pumping intensities transitions continuously to strong coupling at lower temperatures and lower pumping intensities. In the limit of a small gain, i.e. small losses, solid-state condensates resemble equilibrium Bose-Einstein condensates (BECs). They approach the lasers in the regime of high gain, i.e. high losses. This transition from the equilibrium BECs to normal lasers was described with a unified approach via polariton condensates [126].

In another system, closely resembling the physics of polariton condensates, macroscopic occupation of the lowest mode for gas of photons confined in a dye-filled optical microcavity was recently shown [127–130]. The rapid thermalization of rovibrational modes of the dye molecules by their collisions with the solvent and phonon dressing of the absorption and emission by the dye molecules leads to the thermal equilibrium distribution of photons and concomitant accumulation of low-energy photons. Such systems resemble microlasers [131], but unlike microlasers, they exhibit a sharp threshold that occurs far below the inversion.

Many techniques have been proposed and realised in experiments to construct the lattices of polariton or photon condensates. Polariton lattices can be optically engineered by injecting polaritons in specific areas of the sample using the SLM [132–136]. Various potential landscapes to confine polariton or photons have also been engineered [137–139]. The rate equations describing the evolution of gain-dissipative condensates in a lattice were derived using the tight-binding approximation of the space and time-resolved mean-field equations [123, 140] and take the form of the Stuart-Landau equations

$$\dot{\Psi}_i = -iU|\Psi_i|^2\Psi_i + (\gamma_i - |\Psi_i|^2)\Psi_i + \sum_{j \neq i} \mathcal{C}_{ij}\Psi_j, \quad (12)$$

where  $\Psi_i = \sqrt{\rho_i} \exp[i\theta_i]$  is the complex amplitude of the  $i$ -th condensate,  $U$  is the strength of self-interactions between the quasi-particles,  $\gamma_i$  is the effective injection rate (the difference between the pumping of the quasi-particles into the system and linear losses). The coupling strength  $\mathcal{C}_{ij} = J_{ij} + iG_{ij}$  is generally a complex number and consists of the Heisenberg coupling  $J_{ij}$  mediated by the injection reservoir and the Josephson part  $G_{ij}$  that comes from exchange interactions between the condensates. The system described by Eq. (12) reaches

the fixed point when  $J_{ij} \gg G_{ij}$  and the pumping feedback is introduced in the system [123]. The feedback on the pumping intensity ensures that all the occupations are the same at the fixed point by adjusting the pumping if the occupation exceeds the set threshold value  $|\Psi_i|^2 = \rho_{\text{th}}$ . The total injection of the particles in the system of  $N$  condensates at the fixed point is given by

$$\sum_{i=1}^N \gamma_i = N\rho_{\text{th}} - \sum_{i=1}^N \sum_{j<i}^N J_{ij} \cos(\theta_i - \theta_j). \quad (13)$$

Choosing the lowest possible total particle injection  $\sum \gamma_i$  that leads to the occupation  $\rho_{\text{th}}$  for each condensate guarantees that the minimum of the  $XY$  Hamiltonian is reached. To find the actual global minimum, the system has to slowly be brought to the condensation threshold while spending enough time in its neighbourhood to span various phase configurations driven by the system noise (classical and quantum fluctuations). When the system reaches a phase configuration in the vicinity of the minimum of the  $XY$  Hamiltonian, it quickly converges to it by the gradient descent given by the imaginary part of Eq. (12):

$$\dot{\theta}_i = -U\rho_{\text{th}} - \sum_{j \neq i}^N J_{ij} \sin(\theta_i - \theta_j). \quad (14)$$

This idea has been theoretically justified [123] and experimentally realised for simple polariton graphs [136]. It was also proposed how to extend the scheme to discrete optimisation problems such as QUBO (minimising the Ising Hamiltonian) or  $n$ -states Potts Hamiltonians [141]. When the resonant excitation is combined with a non-resonant one, the spins are forced to take the discrete values aligning with the directions set by the resonant excitation. If  $n : 1$  resonant drive is added to the system, the dynamics of the coherent centres obey

$$\dot{\Psi}_i = -iU|\Psi_i|^2\Psi_i + (\gamma_i - |\Psi_i|^2)\Psi_i + \sum_{j \neq i} J_{ij}\Psi_j + h(t)\Psi_i^{*(n-1)}, \quad (15)$$

where  $h(t)$  is an increasing function that reaches a constant value  $H > \max_i \sum_j |J_{ij}|$  at the threshold. At the fixed point, Eq. (13) is replaced with

$$\sum_{i=1}^N \gamma_i = N\rho_{\text{th}} - \sum_{i=1}^N \sum_{j<i}^N J_{ij} \cos(\theta_i - \theta_j) - H\rho_{\text{th}}^{n/2-1} \cos(n\theta_i). \quad (16)$$

At  $n = 2$ , the last term on the right-hand side provides the penalty to phases deviating from 0 or  $\pi$ , reducing the optimization problem to QUBO. For  $n > 2$ , the  $n$ -state Potts Hamiltonian is minimized. The minimization of HOBO may be achieved when the system operates much above the threshold, and higher-order terms must be addressed [142].

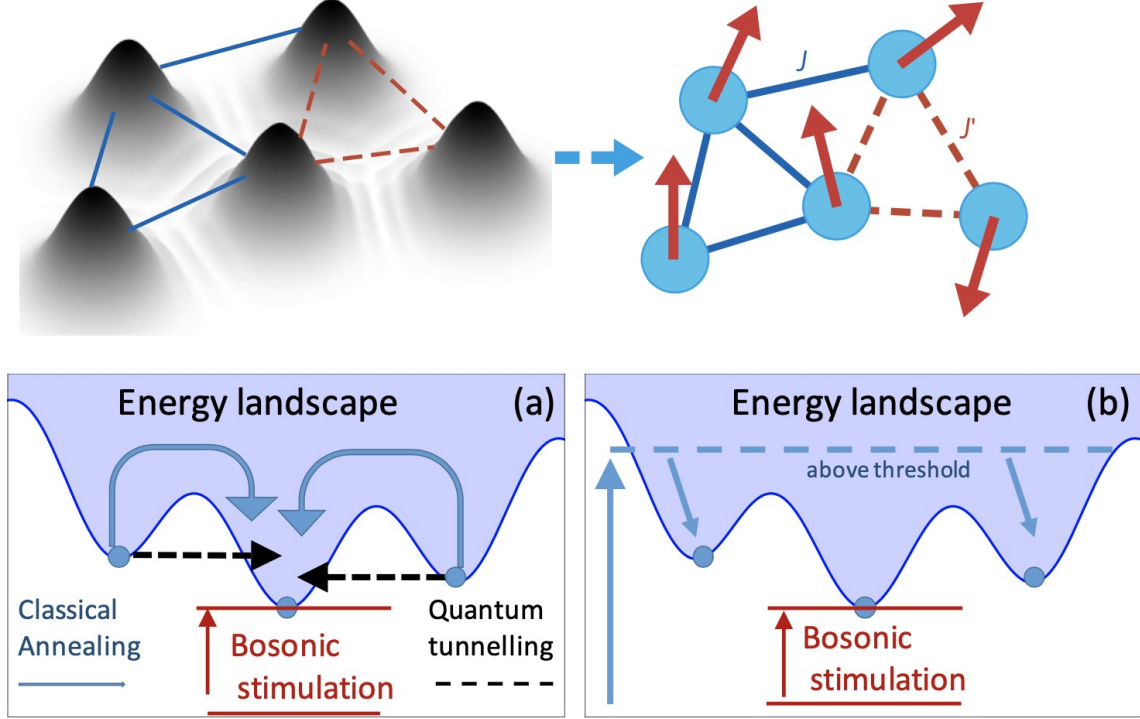


FIG. 7. Top: Schematic of the condensate density map for a five-vertex polariton graph. The sign of the coupling depends on the separation distance between the sites and is either ferromagnetic (solid-blue lines) or anti-ferromagnetic (dashed-red lines). Each vertex of the graph polaritons represents a local phase mapped to a classical vector spin. Bottom: schematics of different types of annealing for finding the global minimum of the energy landscape of the simulated XY Hamiltonian [136].

If the time evolution of the reservoir of noncondensed particles is slow, the system of  $N$  interacting coherent centres is better described by the following equations [140]:

$$\dot{\Psi}_i = -iU|\Psi_i|^2\Psi_i + (R_i - \gamma_c)\Psi_i + \sum_{j \neq i} J_{ij}\Psi_j, \quad (17)$$

$$\dot{R}_i = \Gamma_i - \gamma_R R_i - R_i|\Psi_i|^2, \quad (18)$$

where  $R_i$  is the occupation of the  $i$ -th reservoir,  $\Gamma_i$ ,  $\gamma_R$  and  $\gamma_c$  characterize the rate of particle injection into the reservoir and the linear losses of the reservoir and condensate,

respectively. If one replaces  $\Psi_i$  by the electric field and  $R_i$  by the population inversion of the  $i$ -th laser, the result is a form of the Lang-Kobayashi equations normally derived to describe the dynamical behaviour of coupled lasers from Lamb's semiclassical laser theory [143, 144]. The total injection of the particles in the system of  $N$  condensates at the fixed point is given by

$$\sum_{i=1}^N \Gamma_i = (\gamma_R + \rho_{\text{th}})[N\gamma_c - \sum_{i=1}^N \sum_{j<i}^N J_{ij} \cos(\theta_i - \theta_j)]. \quad (19)$$

Similar to Eq. (13), if the total injection into the system is minimal, the phases of coherent centres minimize the XY Hamiltonian.

#### IV.4. Mathematical description of optical optimisers

Many existing optical machines can be described as the evolution of a set of  $N$  classical degrees of freedom. The variety of optical platforms, such as atoms, polaritons, excitons, photons, etc., shares many similar features in their mathematical description. We present here the structured list of the main equations used in the context of nature-inspired physical systems and algorithms in Fig. 8. There are a few main reasons to highlight the unified picture of these equations. The first one is to show that all of the presented equations represent the same phenomena of the minimization principle and bifurcation dynamics, unifying many equations from math, physics, theory of neural networks, etc., see [145]. The second important feature is represented through the structure of the list. One can easily find the correct transformation between two chosen equations. This is the reason we non-rigorously placed them in the order so that the canonical Andronov-Hopf oscillators (AHO) model resides at the top of the list and the most straightforward gradient resides at the bottom. One can land at the required equations starting from the canonical model by using the proper transformation in the neighbourhood of the bifurcation leading to the solution or omitting some of the terms or derivatives. Moreover, the difference between the presented equations appears to lie only in the chosen parametrization of the system. The optimization process can be done differently, even in the scope of classical dynamical systems depending on the chosen parameters. Such a unified framework allows one to merge many empirical results or to work in the same framework of a universal model for a better comparison of

results.

The Principle of Least Action, the Principle of Minimum Power Dissipation (or Minimum Entropy Generation) or the Variational Principle are good demonstrations that “optimization is built into physics” [146]. In Hamilton’s formulation, the fundamental Principle of Least Action states that a true dynamical trajectory of a system between an initial and final configuration in a specified time is found by choosing the one among the set of possible imaginary trajectories that makes the action locally stationary (in other words have least action). Such a variational task is an excellent example of physics spawning complex problems. For even more complicated tasks, one can consider the formulations of the Principle of Least Action for classical and quantum field theories. We do not include the explicit Hamiltonian equations ( $\dot{q}_i = \frac{\partial H}{\partial p_i}$ ,  $\dot{p}_i = -\frac{\partial H}{\partial q_i}$ ) in the second block in the Fig. 8. However, they also connected with the presented equations and served as a perfect entry point for considering the whole list from the physicist’s point of view. Within the scope of this review, we restrict ourselves to classical systems with a discrete number of degrees of freedom and focus on PDEs that can be mapped into Newtonian-like equations of motion. Additionally, we do not pay much attention to the changes in the original equations of motion, such as Lagrange multipliers, holonomic constraints or relativistic factors.

Another good entry point of Fig. 8 is the well-known classical gradient-descent dynamics with the target cost function defined by the gradients  $-\sum_{j \neq i} Q_{ij}(x_j)$ , which is the most straightforward equation among the presented dynamical systems. One can connect it with gradient descent with momentum (see the centre of Fig. 8) or the classical momentum (CM) method [147], or it’s improved version – Nesterov accelerated gradient-descent [148]).

Kuramoto model - is a well-known mathematical model used to describe synchronization phenomena occurring in a system of coupled oscillators [149–151]. One can obtain this model from the AHO equations using the transformation that involved the eigenvalues and eigenvectors of the coupling matrix at the neighbourhood of the Hopf bifurcation, directly derive it from a nontrivial dissipative Hamiltonian or look at this model as the gradient descent over the cost function corresponding to the classical XY Hamiltonian.

The bottom part of Fig. 8 consists of Hopfield NN and coherent Ising machine description. Hopfield NN is a recurrent artificial NN and can be viewed as the gradient descent variant with the effective projection term with characteristic time  $\tau$  and the gradient terms  $-\sum_{j \neq i} Q_{ij}(x_j)$ , which are usually represented through  $-\sum_{j \neq i} J_{ij}\varphi(x_j)$ , where  $\varphi(x_j)$  is the

projection function and  $J_{ij}$  are the coupling strengths [83]. CIM equations are very close to the Hopfield description. CIM is a network of OPOs, in which the “strongest” collective mode of oscillations corresponds to an optimum solution while going above the threshold of a particular Ising problem [113, 114]. The main difference between the classical description of CIM (which is debated to be essentially non-classical [152, 153]) and Hopfield NN is the additional pumping term  $p$  and saturation mechanism  $-x_i^2$ .

The middle part of the Fig. 8 contains simulated bifurcation machine (SBM) equations, which are inspired by the adiabatic evolution of classical nonlinear Hamiltonian systems exhibiting bifurcation phenomena [154–156]. The higher derivative makes the connection with the physics more visible and improves the simulation algorithm’s performance for specific parameters.

An alternative perspective on the connections between the physical Lagrangian/Hamiltonian systems and neural network evolution is given by the Modern Hopfield networks, or dense associative memories [157, 158]. Modern Hopfield networks operate with feature  $x_i$  and memory (hidden)  $h_\mu$  neurons that evolve as continuous variables in continuous time. The characteristic times for each group are  $\tau_f$  and  $\tau_h$ . The symmetric coupling functions are chosen according to  $Q_{i\mu}(h_\mu) = \xi_{i\mu}f_\mu$  and  $G_{\mu i}(x_i) = \xi_{\mu i}g_i$  and connect only neurons from different groups, i.e. a feature neuron  $i$  to the memory neuron  $\mu$  and reverse. The outputs of the memory neurons and the feature neurons are denoted by non-linear functions  $f(\{h_\mu\})$  and  $g_i = g(\{x_i\})$  correspondingly. These functions can be represented as derivatives of the Lagrangian functions for the two groups of neurons  $f_\mu = \frac{\partial L_h}{\partial h_\mu}$  and  $g_i = \frac{\partial L_x}{\partial x_i}$ . Choosing the specific Lagrangian will define the network’s dynamics (or updates rule), which minimises the energy function. One can recover an effective theory of evolution by integrating out hidden neurons.

The upper part of Fig. 8 contains the Andronov-Hopf oscillators model [159, 160], the canonical model describing the appearance of the bifurcations, which are among the essential phenomena observed in neuron dynamics, responsible for the periodic activity. The functions  $Q_{ij}$  are accountable for the interaction between the  $i$  and  $j$  oscillators, while  $\gamma_i$ ,  $\omega_i$ ,  $\sigma_i$ ,  $U_i$  represent the effective gain, self-frequency, nonlinear dissipation and self-interactions respectively. Many lasers [161], photonic, polaritonic [140], and biological systems [162] exhibit the so-called Andronov-Hopf bifurcation at the threshold that can spawn the limit cycle behaviour. AHO can be an attractive choice for the unifying framework for many



models presented here, which demonstrate a variety of collective phenomena [145]. Another important property of the AHO model is its canonicity, which means that in the vicinity of bifurcation, one can get every equation in Fig. (8) below AHO by a certain transformation, which is not true in the reverse case. One can also investigate the bifurcation phenomena and the time-dependent behaviour of the coefficients near the bifurcation point since it is the crucial mechanism for the system to find a solution to the optimization task. AHO shares its canonicity with another model - weakly interacting neural networks. The network consists of  $N$  neural oscillators comprised of excitatory ( $x_i(t)$ ) and inhibitory ( $y_i(t)$ ), that evolve according to the presented dynamical equations [162]. In the local context, functions  $f, g$  are responsible for the internal behaviour of the  $i$ th part of the system. At the same time,  $p, q$  represents the external interactions, the strength of which is parametrized by the  $\epsilon$  parameter. The explicit transformations between the equations can be found in [163–165].

We will omit the explicit description of the transformations that lead from the top equations to the bottom, while the detailed discussion and corresponding references can be found in [145]. Although the coupled microelectromechanical systems (MEMs) do not contain the optical elements, they are governed by similar optical second-order differential equations [165]. The transition from the AHO to the CIM, Hopfield or SBM equations can also be found in [145]. It is important to remember that introducing sophisticated time dynamics of the parameters can improve the minimisation properties of each of the presented types of equations. For example, it is possible to introduce specific time schedules (e.g. the chaotic amplitude method that anneals the coupling terms depending on the discrepancy between the oscillator amplitude and its saturation point [166]) or to introduce the high-order terms (e.g.  $\dot{\psi}_{i_k} \sim \sum_{i_1, i_2, \dots, i_{k-1}}^N Q_{i_1, i_2, \dots, i_{k-1}, i_k} \psi_{i_1} \psi_{i_2} \dots \psi_{i_{k-1}} \psi_{i_k}^*$  [142]).

An additional note should highlight the Principle of Minimum Power Dissipation and its role in analogue optimization machines. It was shown that many physical systems act through this principle and perform Lagrange function optimization [146]. The Lagrange multipliers are given by the gain or loss coefficients or their time-varying parametrization; see, for example, the equations of the CIM. Depending on the characteristics of the machine, it can be helpful in many other applied domains.

The operation of optical machines consisting of  $N$  elements can be described in a unified fashion as an evolution of a set of  $N$  classical or quantum oscillators. The difference between classical and quantum comes from the system's initial state. It affects the speed and proba-

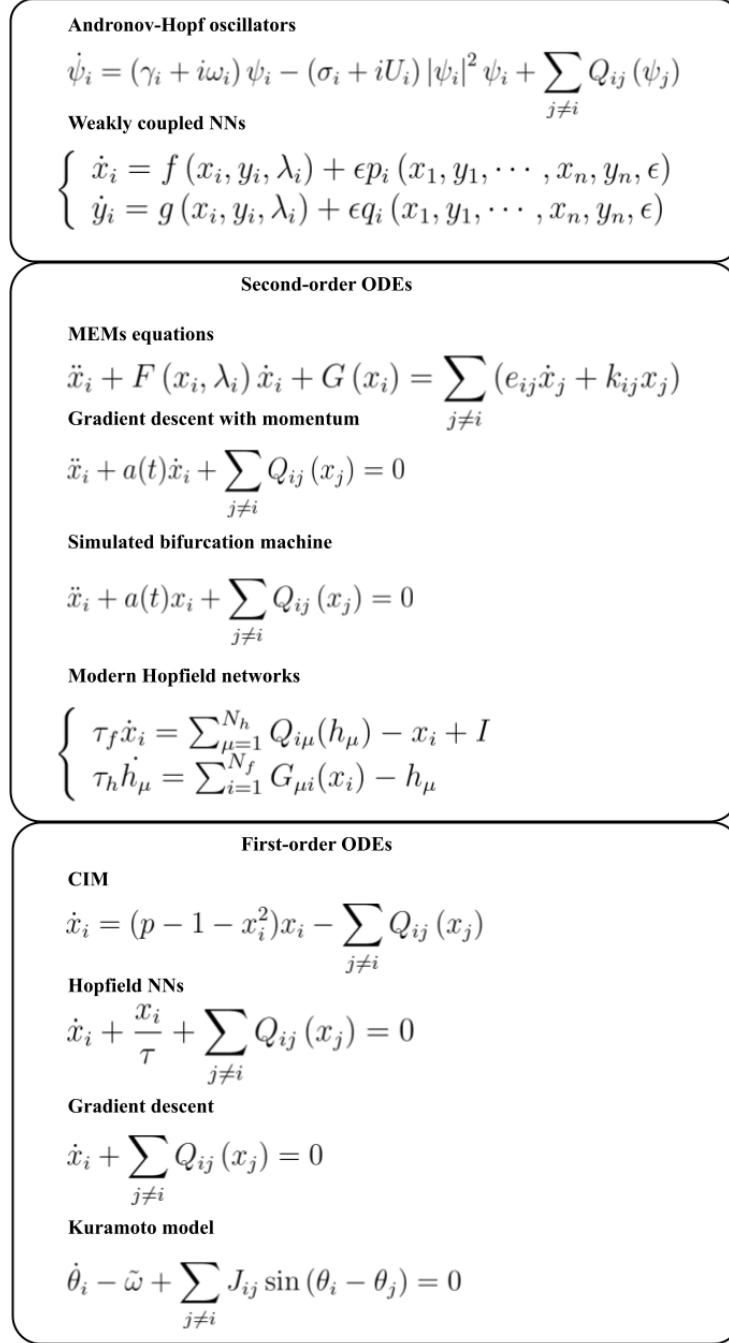


FIG. 8. The ordered list of the main models from different branches of science used in the context of the optimization. The most general equations are closer to the top, starting with the canonical AHO model, which encompasses all equations below through certain transformations. In contrast, the simpler ones, like gradient descent, are located at the bottom. We non-rigorously group the models according to their use of the second-order derivative terms. The functions  $\sum_{j \neq i} Q_{ij}(x_j)$  can have different forms such as  $\eta \frac{\partial E}{\partial x_i}$  in gradient descent case,  $Q_{ij}(x_j) = J_{ij} x_j$  or  $Q_{ij}(x_j) = J_{ij} \varphi(x_j)$  in case of the Hopfield NNs.

bility of finding the final state (usually a solution to a problem). If the occupation numbers of oscillators are large and somewhat uncertain and interactions are weak, then the system evolves as an ensemble of classical fields with corresponding classical-field action [167]. This analogy is valid for any bosonic oscillators, including optical: atoms, polaritons, excitons, photons, etc. For instance, the density matrix of a completely disordered, weakly interacting Bose gas with large and somewhat uncertain occupation numbers is almost diagonal in the coherent-state representation. The initial state can be viewed as a statistical ensemble of coherent states. To the leading order, each coherent state evolves along its classical trajectory. The evolution leads to an explosive increase of occupation numbers in the low-energy region of wave number space where the ordering process takes place [167]. Even if the occupation numbers are of order unity in the initial state, so that the classical matter field description is not yet applicable, the evolution, which can be described at this stage by the standard Boltzmann quantum kinetic equation, inevitably results in the appearance of large occupation numbers in the low-energy region of the particle distribution. Therefore, one can switch from the kinetic equation to the matter field description for the long-wavelength component of the field at a particular moment of the evolution when the occupation numbers become appropriately large. The optical system can be described using a classical matter field when this happens. However, the quantum dynamics before this moment plays a crucial role. This fully quantum dynamics with entanglement and superposition of states allows for complete scanning of the high dimensional space of the system until the coherent state is found. After that, the system behaves classically. While this coherent state settles to a fixed point that is a solution to a problem. During the passage to the coherent state, the quantum effects should enhance the search for the optimal state and potentially lead to the quantum speed-up.

#### IV.5. Associative memory model

In this section, we present the associative memory model as one of the NN models, which exploits the links with spin Hamiltonians. This correspondence implies that many physical systems with nontrivial (nonzero) interaction potentials can be used as computational devices.

The standard model of associative memory [83] uses a system of  $N$  binary neurons, with values  $\pm 1$ . A configuration of all the neurons is denoted by a vector  $\sigma_i, i = 1, \dots, N$ . The

model stores  $K$  memories, denoted by  $\xi_i^\mu, \mu = 1, \dots, K$ , which are also binary. The model is defined by an energy function (or, further Lyapunov function), which is given by

$$E = -\frac{1}{2} \sum_{i,j=1}^N \sigma_i J_{ij} \sigma_j, \quad J_{ij} = \sum_{\mu=1}^K \xi_i^\mu \xi_j^\mu, \quad (20)$$

and a dynamical update rule that decreases the energy at every update. The fundamental problem is that when presented with a new pattern, the network should respond with a stored memory that most closely resembles the input. Many physical systems we considered in Section IV can follow the gradient of this Lyapunov function, which automatically converts them into the ANN.

The theory of Hebbian learning addressed the associative memory [168, 169] and describes how to prescribe the coupling coefficients between the neurons  $J_{ij}$  (usually normalised by the number of patterns  $K$ ). Usually,  $J_{ij}$  is taken as the sum of the outer products of the stored patterns. One can find more ways to define coupling coefficients in the associative memory, e.g. pseudoinverse rule, Storkey learning rule or others. There has been a lot of work investigating this model's capacity, defined as the maximal number of memories that the network can store and reliably retrieve. It has been demonstrated that in the case of random memories, this maximal value is of the order of  $K^{\max} \approx 0.14N$  [83, 170, 171]. If one attempts to store more patterns, several neighbouring memories in the configuration space will merge, which produces a global minimum of the energy (20), thus preventing recovery of the stored memories. It is possible to improve the capacity close to  $K^{\max} = N$  by modifying the Hamiltonian (20) in a way that removes second-order correlations between the stored memories [172].

The simple associative memory model (20) has many benefits. Firstly, it is quadratic in variables, which means that the energy gradient is linear to these variables. Therefore, one can easily calculate the corresponding updates of the neurons that lower the energy function (20). The following consequence of this mathematical structure is that one can reproduce the energy function (20) together with required dynamical behaviour using various physical hardware systems. To build an associative memory machine, one needs to connect the elements representing the analogue variables via nontrivial interaction potential proportional to the strength  $J_{ij}$  and project the final stable state into the discrete domain to obtain the binary states of neurons. Furthermore, the model's simplicity allows one to easily modify

and incorporate other extensions. Finally, the model's universality means it is possible to solve different tasks via associative memory by mapping between tasks; for example, the classification task can be reduced to pattern recognition/restoration.

Another well-known name for the associative memory model is the Hopfield NN, a form of recurrent ANN with binary threshold nodes. Moreover, Hopfield NN shares many other similarities with the physical spin-glass model and several combinatorial optimization tasks. For example, the Hopfield model is isomorphic to the Ising model of magnetism (for zero temperature) [173], which has been extensively analyzed in physical contexts. In combinatorial optimization, finding the ground state of the Ising model is NP-hard and can be related to the QUBO (2). Moreover, computing the statistical sum of the spin-glass has the same NP-hard complexity class, which was a significant obstacle in calculating its various thermodynamic quantities. Other examples of tasks are the Boolean satisfiability problem or SAT [174] and weighted MAX-2-SAT.

To fully define the associative memory model, one has to specify the dynamical update rule of the neurons. For instance, the update rule can describe the discrete state of neurons in discrete time steps:

$$\sigma_i(t+1) = \begin{cases} 1, & \text{if } \sum_j J_{ij}\sigma_j(t) > 0, \\ -1, & \text{otherwise,} \end{cases} \quad (21)$$

with the same notation used in 20. The continuous version has the form:

$$\frac{dx_i}{dt} = -\frac{x_i}{\tau} + \sum_j J_{ij}g(x_j) + h_i, \quad (22)$$

where  $x_i$  denotes the mean state of the  $i$ -th neuron that can get continuous values in the initially defined range,  $h_i$  is a direct input or bias coefficient in case the Lyapunov function (20) has non-zero field,  $g$  is a monotone function that bounds the continuous states and converts them into the discrete in the final state of convergence, i.e. makes the correspondence between the variables  $\sigma_i = g(x_j)$ , and  $\tau$  is the characteristic time (22) of the convergence to an optimal or suboptimal solution.

The analogue computation with the NN can be described as an evolution of the vector-state variables in the high-dimensional continuous space. One can precisely trace it using Eq. (22). The vital aspect of such a differential equation structure is an existence of a Lyapunov function. This Lyapunov function  $H$  behind the Hopfield NN can lead to the un-

derstanding of possible final states, which appear to be attractors of the system’s dynamical behaviour. For both models, one can realise the dynamical state update using a particular hardware system described previously. However, one should differentiate between different regimes that can be realised on the hardware level: the task of finding the ground state (the global minimum) of the model and pattern restoration (descending on the surface of the Lyapunov function towards its nearest minimum).

The explicit formula for the Lyapunov function in the discrete variant of the model with the non-zero field is:

$$H = -\frac{1}{2} \sum_{i,j=1}^N \sigma_i J_{ij} \sigma_j - \sum_{i=1}^N h_i \sigma_i. \quad (23)$$

In the case of continuous variables Eq. (22), the same function has a slightly different forms:

$$H = -\frac{1}{2} \sum_{i,j=1}^N \sigma_i J_{ij} \sigma_j - \sum_{i=1}^N h_i \sigma_i + \frac{1}{\tau} \sum_{i=1}^N \int^{\sigma_i} g^{-1}(Z) dZ, \quad (24)$$

where the last term appears due to the correspondence between the discrete and continuous state  $\sigma_i = g(x_i)$ . For  $g(x)$ , one usually picks the  $g(x) = \tanh(x/\beta)$  function, where the  $\beta$  parameter tends to zero value during the evolution of the Hopfield NN forcing the last term of the Eq. (24) to disappear, see [175] with the additional emphasis on the optimization problems. The essential property of the dynamical update rules is that the energy decreases through the system evolution, which leads to the final stable patterns in the phase space.

The classical Hopfield NN has many modifications for the Lyapunov function, variables update rules and other features. One version is known as modern Hopfield NNs [157]. Modern Hopfield networks with continuous states can be integrated into deep learning architectures because they are continuous and differentiable with respect to their parameters. Moreover, they retrieve patterns with just one update, conforming to deep learning layers. For these reasons, modern Hopfield networks can serve as specialised layers in deep networks to equip them with memories. Possible applications of Hopfield layers in deep network architectures find their way in multiple instance learning, defence against adversarial attacks [176], processing of and learning with point sets, sequence analysis and time series prediction, storing and retrieving reference data, e.g. the training data, outliers, high error data points, prototypes and many other purposes [157]. Even more importantly, the functionality of the modern Hopfield networks can be compared with various methods from the ML domain,

such as SVMs, random forest, boosting, decision trees, Bayesian methods and many others [177, 178].

As we mentioned above, many optical systems can perform optimization tasks. Since there are intrinsic similarities between this task and the associative memory model, one can exploit this relation to realize Hopfield NN on the optical setup. Such realizations include previously discussed laser networks, Ising machines, photon [179] and polariton systems [136], and confocal cavity QED NN [180], see Fig. 9. The connection between the optical networks and the Hopfield model is important since it allows one to incorporate such layers into more complex optical architectures without complicated adjustments.

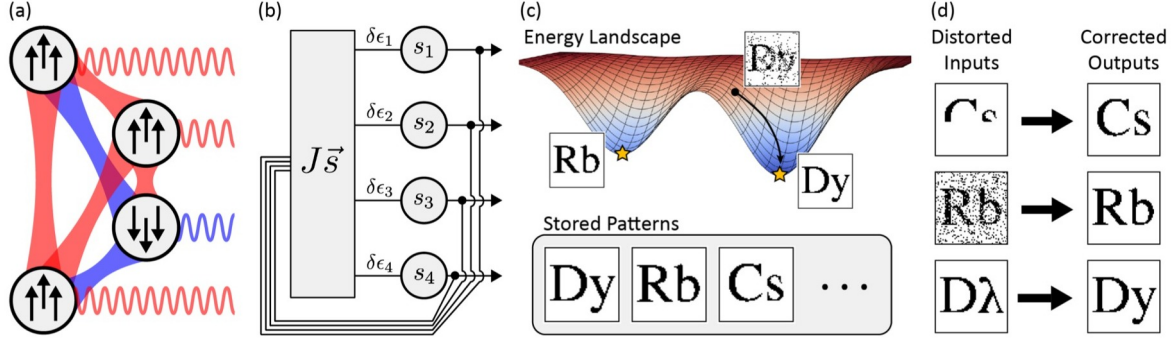


FIG. 9. (a) Four nodes with the all-to-all coupling and sign-changing connectivity between spin ensembles. Blue and red show ferromagnetic versus antiferromagnetic  $J_{ij}$  links. One can find the physical details in [181]. (b) The realization of the Hopfield NN by the spin ensemble. Binary neurons  $s_i$  of a single-layer network are recurrently fed back and subjected to a linear transform  $J$  with the consequent element-wise threshold operation. (c) The Hopfield model exhibits an energy landscape with many metastable states. Energy-minimizing dynamics drive similar spin configurations to the stored local minimum, characterized by the basin of attraction. Too many memories make the basins of attraction vanish. (d) Schematic of the associative memory problem - recalling multiple stored patterns by completing distorted input images. Figure from [181].

#### IV.6. Higher-order systems

One significant extension of the Hopfield model is incorporating the tensor terms, which depend on the  $\sigma_i$  variables polynomially in  $n$  [182]. The such extension allows one to increase the number of stored patterns to  $K^{max} = \alpha_n N^{n-1}$ , where  $\alpha_n$  is a numerical constant. Moreover, it is possible to observe the so-called "feature to prototype transition" when increasing  $n$  in the NN training. The prototype theory provides an alternative approach to

learning in which objects are recognized as a whole. Although tensor terms are assumed not to be biologically plausible [158], they can be reproduced on some artificial physical setups [142]. From this perspective, artificial tensor platforms can significantly benefit from such technological opportunities. The higher order Hopfield NNs [183] can be written as

$$\frac{dx_l}{dt} = -\frac{x_l}{\tau} + \sum_{\bar{\Omega}} \mathbf{A}_{l,i_1,\dots,i_k}^k s_{i_1} \cdots s_{i_k}; \quad s_l = g\left(\frac{x_l(t)}{\beta}\right), \quad (25)$$

where  $x_l$  are real continuous variables,  $g(x)$  is the threshold function and  $\beta$  is the scaling parameter that can depend on time. Such systems can solve HOBQ, see Eq. (3), because of the  $k$ -local coupling.

It was shown [142] that polariton systems above the threshold are described by

$$\frac{d\Psi_l}{dt} = \Psi_l(\gamma_l(t) - |\Psi_l|^2) + \sum_{\bar{\Omega}} \mathbf{A}_{i_1,\dots,i_k}^k \Psi_{i_1} \cdots \Psi_{i_k}^*, \quad (26)$$

$$\frac{d\gamma_l}{dt} = \epsilon(\rho_{\text{th}} - |\Psi_l|^2), \quad (27)$$

where  $\bar{\Omega}$  is the set of indices that excluded index  $l$ . Eq. (27) describes the feedback mechanism that drives all  $\rho_i$  to a priori set values  $\rho_{\text{th}}$ ,  $\epsilon$  characterizes how fast  $\gamma_i$  adjusts to changes in  $\rho_i$ . Next, we proceed with the different ways of connecting the practical computational tasks with the actual physical behaviour of the presented systems.

## V. MATHEMATICAL FORMULATION OF APPLICATIONS

This section considers a range of generic applications that follow from the network's ability to solve optimization problems or/and act as Hopfield networks. We start with the simple problems from classical computer science with the corresponding mapping to the QUBO problem. We then move to modern tasks that differ in information capacity and are considered to suffer from the so-called "curse of dimensionality", where it is more suitable to work with the probability distributions instead of the individual variables. However, in both cases, we do not pay attention to whether the presented mapping is efficient (like in the following subsection) or not (when one needs multiple sequential operations with a considerable amount of pre and post-processing in between). Some of the inefficient embeddings can still possess mathematical challenges and can be improved either in the



general formulation or with task-specific information. At the end of this chapter, we discuss the NN architectures and their capabilities.

### V.1. Direct encoding/decoding

This subsection describes the connections/correspondences between different computational tasks established during the last 50 years [174, 184, 185].

The propositional satisfiability problem (SAT) lies at the heart of such correspondence. It is a fundamental problem determining whether a set of sentences in propositional logic is satisfactory. A clause is built as the disjunction, the logical OR (denoted by  $\vee$ ) of some Boolean variables or their negations. A set of several clauses, which must be satisfied simultaneously, is the conjunction, logical AND (denoted by  $\wedge$ ) of the clauses. One can write a satisfiability problem in the general form:

$$(x_1 \vee x_2 \vee \dots) \wedge (y_1 \vee y_2 \vee \dots) \wedge \dots(\dots), \quad (28)$$

where the  $x_i, y_i$  are "literals", any of the original variables or their negations. The form (28) is called a conjunctive normal form (CNF), and one can easily see that any logical statement between Boolean variables can be written as a CNF.

SAT is the first problem that was proven to be NP-complete [174, 184]. Currently, no known algorithm efficiently solves each SAT instance. The question of its existence is equivalent to the famous P vs NP problem. Nevertheless, many heuristics SAT algorithms can solve problem instances involving a significant number of variables, sufficient for many applications. Additionally, many versions of the SAT problems exist, like 3-SAT and the generalization k-SAT, HORN-SAT, and XOR-SAT, which can better suit particular unconventional tasks.

One specific SAT version - weighted MAX-2-SAT allows one to easily reformulate the task as QUBO, often appearing in this review. A simple 2-SAT has  $m$  clauses of 2 literals each. A MAX-2-SAT is the problem of assigning values that maximize the number of satisfied clauses. Weighted MAX-SAT gives each clause a positive weight so that the measure of violating the cost appears in the problem. To reformulate a weighted MAX-2-SAT problem as a QUBO, one has to use the fact that maximizing the weight of satisfied clauses is equivalent

to minimizing the weight of unsatisfied clauses, and using the logic  $\overline{x_i \vee x_j} = \overline{x_i} \wedge \overline{x_j}$ . The final form looks then:

$$\max_{x_i} \sum_{i,j < i} w_{ij} x_i x_j, \quad (29)$$

which is the QUBO that has the same form as Eq.(2). Thus, the connection between the SAT (that can be easily converted into weighted MAX-2-SAT by use of the Boolean logic) and QUBO is revealed.

The vital work [84] provided Ising formulations for many NP-complete and NP-hard problems and covered all of Karp's 21 NP-complete problems. For example, one can find number partitioning, graph partitioning, clique existence, binary integer linear programming, exact cover, set packing (or maximal independent set), vertex cover, satisfiability (with the emphasis on 3SAT to MIS reduction), set cover, knapsack with integer weights, graph colouring, Hamiltonian cycles and paths, travelling salesman problem, Steiner trees, feedback vertex set, feedback edge set, graph isomorphisms among the covered problems, as well as some useful tricks for the near-term quantum adiabatic optimization devices. We mention some of them in a slightly different form below.

## V.2. Logistics

Logistic and planning problems are usually related to the well-known travelling salesman problem. For example, a salesman travels in  $N$  cities that are connected with weighted edges  $w_{uv} \geq 0$  from the set  $E$  (these can represent distances and other costs associated with travelling between the cities), and can be formulated as the following Ising problem of size  $N^2$ :

$$\begin{aligned} H_{\text{TSP}} = & A \sum_{i=1}^N \left( 1 - \sum_{v=1}^N x_{v,i} \right)^2 + A \sum_{v=1}^N \left( 1 - \sum_{i=1}^N x_{v,i} \right)^2 + A \sum_{(uv) \notin E} \sum_{i=1}^N x_{u,i} x_{v,i+1} \\ & + B \sum_{(uv) \in E} w_{u,v} \sum_{i=1}^N x_{u,i} x_{v,i+1}. \end{aligned} \quad (30)$$

Each spin  $x_{v,i} \in \{0, 1\}$  in Eq. (30) represents the vertex  $v$  and its order  $i$  in a path. The first three terms regulate all valid routes in this representation. Each city should be in the route (first term) and appear only once (second term). Any adjacent cities in the route should be

connected (third term), while the search for the optimal route is realised by minimising the sum of weights of all cities in a route (fourth term). The reasonable choice of constants  $A$  and  $B$  (e.g.  $A$  should be big enough for  $B > 0$ ) guarantees that only the space of valid routes is explored. Reshaping this two-dimensional spin matrix with elements  $x_{v,i}$  to a spin vector of size  $N^2$  allows one to recover the coupling matrix  $\mathbf{J}$  and magnetic field  $\mathbf{h}$  to formulate the corresponding Ising Hamiltonian. One can reduce the size of the Ising problem to  $(N - 1)^2$  by fixing a particular city to be the first in the route. Note that the Hamiltonian  $H_{\text{TSP}}$  can represent both directed and undirected graphs, and the generalisation for the cycles optimisation problem is straightforward. It has also been used for finding transportation routes that minimise costs.

### V.3. Portfolio optimization

Optimizing the portfolio selection means finding the most optimal combination of investments for an institution or individual. One of the modern portfolio optimization problem formulations has the following form [186]:

$$\min_{0 \leq x_i \leq 1} \lambda \left[ \sum_{i=1}^N \sum_{j=1}^N J_{ij} x_i x_j \right] - (1 - \lambda) \left[ \sum_{i=1}^N \mu_i x_i \right], \quad \sum_{i=1}^N x_i = 1, \quad (31)$$

where  $N$  is the number of different assets, and  $x_i$  is the decision variable representing the proportion of capital invested in asset  $i$ . Here coupling coefficient  $J_{ij}$  represents the covariance between returns of assets  $i$  and  $j$ ,  $\mu_i$  is the mean return of asset  $i$ , and  $\lambda \in [0, 1]$  is the risk aversion parameter. When  $\lambda = 0$ , the model maximizes the portfolio's mean return, and the optimal solution will be formed only by the assets with the greatest mean return. When  $\lambda = 1$ , only the total risk associated with the portfolio is minimized.

There are different modifications to the portfolio optimization problem. For instance, one can introduce bounding and cardinality constraints that specify that there should be  $K$  different assets in the portfolio or/and the portion of some assets should be within certain bounds. This is achieved by

$$\sum_{i=1}^N z_i = K, \quad \epsilon_i z_i \leq x_i \leq \delta_i z_i, \quad z_i \in \{0, 1\}. \quad (32)$$

The cardinality-constrained mean-variance model is a mixed quadratic and integer programming problem in the  $\text{NP}$ -hard class of problems. Although the problem is not a combinatorial optimisation, we take advantage of the fact that the objective function has the same form as the energy function in Hopfield networks. Consequently, it will be minimised if we follow the Hopfield dynamics. Hopfield NNs have efficiently solved this problem [187, 188]. The discrete dynamics becomes

$$x_i(t+1) = G_i[-2\lambda \sum_j J_{ij}x_j(t) + (1-\lambda)\mu_i], \quad (33)$$

where  $G_i$  is a sigmoid with values in  $[\epsilon_i, \delta_i]$ . When solving any optimization problem, constraints usually appear in the energy function. However, in many cases of Hopfield networks, this is not necessary. Constraints on  $x_i$  are satisfied using a sigmoid's activation function since its outputs already lie inside the desired interval. To fulfil the cardinality constraints, we begin with  $3K/2$  neurons. After getting a minimum for the objective function, we remove the asset with the smallest output and repeat this process until the network has precisely  $K$  assets. These remaining assets solve the original portfolio selection problem. To satisfy the constraint  $\sum x_i = 1$ , one can use various adjustments, for instance, to evaluate the feasibility of every portfolio and change the proportions of capital  $x_i$  to be invested in each selected asset [187].

#### V.4. Phase retrieval

The minimisation of the XY model (solving QCO) is directly related to the notoriously hard-to-solve phase retrieval problem. The problem's objective is to recover a general signal (or image) from the magnitude of its Fourier transform [87–89]. This problem arises because the signal detectors can usually record only the modulus of the diffraction pattern, therefore, losing the information about the phase of the optical wave. Mathematically, one needs to recover a signal  $\mathbf{x} \in \mathbb{C}^m$  from the amplitude  $\mathbf{b} = |\mathbf{Ax}|$ , where  $\mathbf{A} \in \mathbb{C}^{n \times m}$ ,  $\mathbf{b} \in \mathbb{R}^n$ . Then the phase recovery problem [189] can be formulated as:

$$\min_{x_j, u_i} \sum_i \left( \sum_j A_{ij}x_j - b_i u_i \right)^2 \quad (34)$$

where  $\mathbf{u} \in \mathbb{C}^n$  is a phase vector that satisfies  $\mathbf{Ax} = \text{diag}(\mathbf{b})\mathbf{u}$ ,  $|u_i| = 1$  for  $i = \overline{1, n}$ . This optimization problem can be further rewritten as

$$\min \sum_{ij} M_{ij} u_i u_j \quad \text{subject to} \quad |u_i| = 1, i = \overline{1, n}, \quad (35)$$

where  $\mathbf{M} = \text{diag}(\mathbf{b})(\mathbf{I} - \mathbf{AA}^\dagger)\text{diag}(\mathbf{b})$  is the Hermitian matrix,  $\mathbf{I}$  is the identity matrix, and  $\mathbf{A}^\dagger$  is the Moore-Penrose inverse of a matrix  $\mathbf{A}$  (see [189] for details).

### V.5. Machine learning

The data growth now surpasses our capabilities to process it concerning human and computational resources. The development of data-driven methods also marks the transition from the classical computer science paradigm to the modern ML setting. The related questions concerning the abilities of the precisely crafted algorithms and worst-case scenarios are changed by the most probable cases and the design of the NN architectures.

One of the main ML field's goals is to predict specific outcomes from the given data. The richness of the data dramatically influences the methods' performance, making it easier to find patterns and expect accurate results. Considering complicated methods and deep NN architectures, there are three crucial components in ML: data, features, and algorithms.

Practically speaking, one can meet the data in many ways: e-mails, stock prices time-series, users databases and collection of the experimental measurements. Moreover, one can collect in different ways, either manually, usually quite long and costly, with few errors or automatically feeding everything to some sorting algorithms. Depending on the context, the collected data (or datasets) can be of great value, determining the demand for suitable rare datasets.

Features represent the properties of the considered objects. Therefore, a small amount of essential and sorted features in most cases can guarantee the success of the ML approach to the problem. However, it is very time-consuming to determine the feature in the so-called 'raw' big datasets and select the right ones. Moreover, sometimes one has to avoid human-based decisions to prevent introducing subjectivity and opinion-based bias to optimize the model performance. Therefore, the latest deep learning success is partially tied to automatic feature engineering compared to the previous partially empiric ML models.

The last part of the considered scheme is the algorithm. Choosing the method of solving a particular task depends on the context and influences such parameters as the final model's accuracy, speed, and computational complexity. In general, one can solve a problem in many different ways.

The components were presented according to their significance in the ML pipeline. Simply saying, one can only extract useful information from a noisy and meaningful dataset. The following subsection starts the discussion with the simple classical algorithms, which are the basis of many existing applications. Then, we outline the central ideas behind the main ML methods that will be the centre of attention for transferring into the special-purpose hardware. At the end of this chapter, we cover the wide range of capabilities of the NNs.

#### V.5.1. Regression

Regression analysis is one of the earliest methods in statistical modelling that allows estimating the relationships between a dependent variable and independent variables. The most common form of regression analysis is linear regression. This model assumes that the dependent variables denoted by  $y_i$  have a linear relationship depending on the  $m$ -vector of points  $\{x_{i1}, \dots, x_{im}\}_{i=1}^n$  with an addition of the disturbance terms  $\epsilon_i$  in each case. This relationship can be written in the following form:

$$y_i = \beta_0 + \beta_1 x_{i1} + \dots + \beta_m x_{im} + \epsilon_i = \sum_{j=0}^m \beta_j x_{ij} + \epsilon_i. \quad (36)$$

To shorten notation we use the matrix form  $\mathbf{y} = \mathbf{X}\boldsymbol{\beta} + \boldsymbol{\epsilon}$  where:  $\mathbf{y} = \{y_i\}$ ,  $\mathbf{X} = \{x_{ij}\}$ ,  $\boldsymbol{\beta} = \{\beta_j\}$ ,  $\boldsymbol{\epsilon} = \{\epsilon_i\}$ ,  $(i = 1, \dots, n)$ ,  $(j = 0, \dots, m)$ , with  $x_{i0} = 1$ . The linear regression task is the estimation of the values of the regression coefficients  $\beta_j$  given the data points  $x_{ij}$  and observables  $y_i$ , so that the error term  $\boldsymbol{\epsilon} = \mathbf{y} - \mathbf{X}\boldsymbol{\beta}$  is minimized. One can use different metrics for that purpose, such as the sum of squared errors of  $\epsilon_i$  or others.

The most common parameter estimation technique is called the least-squares estimation. Here, the optimum parameter is defined through the minimization of the sum of the mean squared loss

$$\min_{\beta_j} \sum_{i=1}^n \left( \sum_{j=0}^m \beta_j x_{ij} - y_i \right)^2, \quad (37)$$

which can be connected with the conventional QP. The optimal solution can be obtained by differentiating Eq. (37) and equating it to zero with respect to parameters  $\beta_j$ . In matrix notation, the solution can be written as

$$\boldsymbol{\beta} = (\mathbf{X}^T \mathbf{X})^{-1} \mathbf{X}^T \mathbf{y}. \quad (38)$$

There exist different modifications of the proposed procedure: generalized least squares, where one introduces a certain degree of correlation between the residuals  $\epsilon_i$  (37), or the weighted least squares, where the knowledge of the variance of observations is incorporated as the coefficients  $w_k$  before each of the residual. Moreover, intrinsically different techniques can be based on maximum likelihood estimation, Bayesian methods, or regularization.

A natural extension of linear regression is in replacing linear dependence with a polynomial. In the case of one argument, it is possible to rewrite Eq. (36) as

$$y_i = \beta_0 + \beta_1 x_i + \beta_2 x_i^2 + \cdots + \beta_m x_i^m + \epsilon_i = \sum_{j=0}^m \beta_j x_i^j + \epsilon_i. \quad (39)$$

Given the data points  $x_i^j$ , the task is the same as Eq. (37) except for the change in variables  $x_{ij} \rightarrow x_i^j$ . Similarly, it is possible to replace the polynomial basis with a set of some nonlinear functions  $f(x_i)_j$ , so that  $x_i^2 \rightarrow f(x_i)_j$ .

Multiple linear regression is a generalization of linear regression with more than one independent variable. The basic model for multiple linear regression can be written in a similar form:

$$\mathbf{y}_i = \beta_0 + \beta_1 \mathbf{X}_{i1} + \beta_2 \mathbf{X}_{i2} + \cdots + \beta_m \mathbf{X}_{im} + \mathbf{e}_i = \sum_{j=0}^m \beta_j \mathbf{X}_{ij} + \mathbf{e}_i, \quad (40)$$

where instead of variables  $x_{ij}$  one has a set of matrix elements  $\mathbf{X}_{ij}$  of size  $k \times k$ . Depending on the chosen norm for the matrix, it is possible to formulate the task of finding the regression coefficients. Taking the square Frobenius norm of the matrix, the search for optimal coefficients  $\beta_i$  is equivalent to solving Eq.(37), except for the additional sum over the  $k^2$  matrix elements:

$$\min_{\beta_j} \sum_{l=1}^{k^2} \sum_{i=1}^n \left( \sum_{j=0}^m \beta_j x_{ij}^l - y_i^l \right)^2. \quad (41)$$

This can be extended further for multivariate linear regression or combined with the nonlinear basis with minor consequences concerning the parameters search and hardware operations, except for the much more complicated procedure for preprocessing the coefficients for any modification. Regression can be considered the simplest form of supervised learning.

### V.5.2. Classification

Classification is one of the popular tasks for ML. The purpose of classification is to sort the objects among the initially defined classes. The earliest algorithms include naive Bayes and decision trees. Here, we only consider Markov random field (MRF) encoding, which is the general case for such models.

The  $k$ -nearest neighbours algorithm is a non-parametric classification method used in statistics [190, 191]. It aims to classify the objects by considering their  $k$  nearest neighbours with the defined class. The consequent attaching objects to a particular group is repeated until the convergence. We omit the explicit corresponding formulas because of their similarity with the  $k$ -means, the unsupervised clusterization algorithm, presented below. Both methods are usually based on Euclidean distances and can easily be transferred to special-purpose optimization hardware.

Another classification method is called a support vector machine (SVM). SVM is a supervised learning model that analyses data for classification purposes. It aims to construct a hyperplane between the classes of training data points in a high-dimensional space, emphasising a good separation achieved by maximising its margin. SVM was introduced in [192] and standardised in [193].

Linear SVM deals with the  $n$  points  $\mathbf{x}$  in the  $m$ -dimensional space, where each point has been assigned a binary class  $y_i = \pm 1$ . The task is to construct a hyperplane that divides these two groups with the maximum distance between them. The so-called "hard margin" scenario assumes that the initial data is linearly separable. One can start by constructing two parallel hyperplanes, separating groups of different classes with the largest distance between these two surfaces. The target surface between these hyperplanes is called the maximum margin hyperplane. To mathematically describe these surfaces, one can write:

$$\mathbf{w}^T \mathbf{x}^i - b = \sum_j w_j x_j^i - b = \pm 1, \quad (42)$$



where  $w_j$  are the components of the normal vector for both of the hyperplanes,  $x_j^i$  are  $m$ -dimensional coordinates of the vector with the serial number  $i$ ,  $b$  defines the surface shift concerning the zero coordinates and  $\pm 1$  defines the class. Everything above  $y = 1$  belongs to one class, and everything below  $y = -1$  belongs to another. The offset of the hyperplane is determined by  $b / \|\mathbf{w}\|$ , while the marginal distance equals  $2 / \|\mathbf{w}\|$ . To maximize the marginal distance, one has to minimize the norm of  $\|\mathbf{w}\|$  and hence its square  $\|\mathbf{w}\|^2$ . This task can be reformulated as the optimization problem, adding the constraints that prevent data points from being positioned into the margin

$$\begin{aligned} & \min \|\mathbf{w}\| \\ & \text{s.t. } y_i (\mathbf{w}^T \mathbf{x}^i - b) \geq 1, \text{ for } i = 1, \dots, n \end{aligned} \quad (43)$$

The natural extension of SVM is in considering a so-called "soft margin" case. It is assumed that the given data points are not linearly separable. In this case, one has to introduce a new kind of variable  $\xi_i = \max(0, 1 - y_i (\mathbf{w}^T \mathbf{x}^i - b))$  for each point  $i$ , which is usually referred to as the hinge loss function, playing a regularizer role. Thus, it is possible to rewrite Eq. (43) as

$$\begin{aligned} & \min \frac{1}{n} \sum_{i=1}^n \xi_i + C \|\mathbf{w}\|^2 \\ & \text{s.t. } y_i (\mathbf{w}^T \mathbf{x}^i - b) \geq 1 - \xi_i \text{ and } \xi_i \geq 0, \text{ for all } i, \end{aligned} \quad (44)$$

where the constant  $C$  regulates the interplay between the pure hard margin classifier and the soft margin one. We can reformulate the problem using the Lagrangian duality:

$$\begin{aligned} & \max_{a_i} \sum_{i=1}^n a_i - \frac{1}{2} \sum_{i=1}^n \sum_{j=1}^n y_i a_i (\mathbf{x}_i^T \mathbf{x}_j) y_j a_j \\ & \text{s.t. } \sum_{i=1}^n a_i y_i = 0, \text{ and } 0 \leq a_i \leq \frac{1}{2nC} \text{ for all } i, \end{aligned} \quad (45)$$

where the norm vector  $\mathbf{w}$  is expressed through the new variables  $a_i$ , so that  $\mathbf{w} = \sum_{i=1}^n a_i y_i \mathbf{x}^i$ , and the initial task of determining the offset of the surface is expressed via  $b = \mathbf{w}^T \mathbf{x}^i - y_i$ . Thus, it is possible to obtain the problem, which has an exact QP formulation. This problem can be solved with the standard quadratic algorithms, thus, can be solved using special-

purpose hardware.

It is helpful to mention the nonlinear extension of the SVM, which solves nonlinear classification task and can exploit the different functional forms of kernels. One can modify the scalar dot product in the quadratic form Eq. (45) by a different kernel function  $k(\mathbf{x}_i, \mathbf{x}_j)$  depending on the properties of the analogue hardware.

### *V.5.3. Finding the principal eigenvector*

Finding the principal (dominant) eigenvector of a given matrix  $\mathbf{J}$  belongs to the  $\mathbb{P}$ -class of problems. However, finding such a dominant eigenvector on an ever-growing large matrix becomes a computationally intensive task incompatible with Moore’s law. At the same time, a range of real-life problems would benefit from fast calculation of the principal eigenvector. For instance, the PageRank algorithm [194, 195] evaluates the relative importance of pages by exploiting the web link structure. The web network is represented as a directed graph, where each page is a node of the graph, and each hyperlink is an edge connecting one page to another. For the entire database of web pages, the PageRank algorithm computes a single score vector, the PageRank. The algorithm’s key underlying assumption is that pages transfer the importance to other pages via links; hence, PageRank components determine the importance of pages. Mathematically, finding the PageRank vector is equivalent to calculating the principal eigenvector of the link-structure matrix, Google matrix. Besides, calculating the principle eigenvector is required in social network analysis, recommendation systems, bibliometrics, bioinformatics, DNA sequencing, and distributed computing systems [196–198].

There are numerous applications of PageRank to chemistry and engineering sciences networks to investigate and analyse complex systems. As engineered systems grow in size, they become increasingly complex, with networks and submodules interacting in unpredictable, nonlinear ways. Network analysis methods like PageRank help to organise and study these complexities [197]. For instance, MonitorRank diagnoses root causes of issues in a modern distributed system: error logs and tracing debugging information [199]. PageRank has been used for road and urban space networks, which help predict traffic flow and human movement. It was shown that PageRank is the best network measure in predicting traffic on individual roads [200].

The advantage of using optical systems for calculating the principal eigenvector has been recently shown [198]. For a certain choice of control parameters of these optical systems, the steady state of optical networks can solve an eigenvalue maximization problem [201], which results in finding the energy state dictated by signs of the eigenvector corresponding to the largest eigenvalue of the interaction matrix, i.e. principal eigenvector. In particular, the estimates presented [198] show that special-purpose optical machines for PageRank calculations may provide dramatic improvements in power consumption over classical computing architectures.

#### V.5.4. Dimensionality reduction

Dimensionality reduction involves the transformation of data from the space with many dimensions into a low-dimensional space, usually preserving meaningful and valuable properties from the original data. It isn't easy to handle high-dimensional data in practice due to the growth of the space volume. Dimensionality reduction is standard in data-intensive fields. It can be used in signal processing, neuroinformatics, and bioinformatics [202, 203]. One can find its applications in recommender systems [204], semantic search [205] or as a primary tool in many domains involving numerical analysis.

One of the well-known methods for dimensionality reduction is the principal component analysis (PCA) [206]. The idea behind PCA is to approximate particular data with linear manifolds of lower dimensions. PCA can be alternatively interpreted as finding subspaces of lower dimension in the orthogonal projection on which the data variation is maximum.

The initial task behind the PCA is to find the best approximation of the data points using lines and surfaces. Given the set of vectors  $\mathbf{x}_1, \mathbf{x}_2, \dots, \mathbf{x}_m \in \mathbb{R}^n$ , the aim is at finding the sequence of  $k$   $k$ -dimensional affine spaces  $L_k \subset \mathbb{R}^n$  that find

$$\min_{L_k} \sum_{i=1}^m d^2(\mathbf{x}_i, L_k) = \min_{a_{jl}} \sum_{i=1}^m \sum_{l=1}^n \left( x_{il} - a_{0l} - \sum_{j=1}^k a_{jl} \sum_{q=1}^n a_{jq} (x_{iq} - a_{0q}) \right)^2, \quad (46)$$

for each  $k$ , where  $d(\mathbf{x}_i, L_k)$  is the Euclidean distance from the point  $\mathbf{x}_i$  to the  $L_k$ . Affine spaces  $L_k$  are defined as the sets of linear combinations  $L_k = \{\mathbf{a}_0 + \alpha_1 \mathbf{a}_1 + \dots + \alpha_k \mathbf{a}_k\}$  with coefficients  $\alpha_i \in \mathbb{R}$ , while the vectors  $\{\mathbf{a}_1, \mathbf{a}_2, \dots, \mathbf{a}_k\} \subset \mathbb{R}^n$  form orthonormal basis in  $\mathbb{R}^n$ .

Eq. (46) is an optimization problem. The initial vector  $\mathbf{a}_0$  is simply defined as the solution

to

$$\min_{\mathbf{a}_0} \sum_{i=1}^m d^2(\mathbf{x}_i, L_0) = \frac{1}{m} \sum_{i=1}^m \mathbf{x}_i. \quad (47)$$

The next component is found iteratively by subtracting the projection  $\mathbf{x}_i = \mathbf{x}_i - \mathbf{a}_0 (\mathbf{a}_0^T \mathbf{x}_i)$  (with the scalar product  $\mathbf{a}_0^T \mathbf{x}_i$ ) for the vectors corresponding to  $L_j$ :

$$\mathbf{a}_j = \operatorname{argmin}_{\|\mathbf{a}_j\|=1} \left( \sum_{i=1}^m (\mathbf{x}_i - \mathbf{a}_j (\mathbf{a}_j^T \mathbf{x}_i))^2 \right). \quad (48)$$

The iterations continue until the number of the affine space  $k$  reaches the  $n - 1$  of the initial problem space dimension. Using the identity  $\|\mathbf{x}_i - \mathbf{a}_j (\mathbf{a}_j^T \mathbf{x}_i)\|^2 = \|\mathbf{x}_i\|^2 - (\mathbf{a}_j^T \mathbf{x}_i)^2$ , one can easily map this task into the QP in  $\mathbf{a}_i$  variables with the normalization constraints and the coupling matrix  $J_{ij} = -x_i x_j$ . To shorten the presented notation, the iterative procedure can be written similarly to maximization tasks

$$\hat{\mathbf{X}}_k = \mathbf{X} - \sum_{s=1}^{k-1} \mathbf{X} \mathbf{w}_{(s)} \mathbf{w}_{(s)}^T, \quad (49)$$

$$\mathbf{w}_{(k)} = \arg \max_{\|\mathbf{w}\|=1} \left\{ \left\| \hat{\mathbf{X}}_k \mathbf{w} \right\|^2 \right\}, \quad (50)$$

where  $k$  is the number of principal component,  $\mathbf{X}$  is the data matrix of size  $n \times m$ ,  $\mathbf{w}_s = (w_1, \dots, w_m)_{(s)}$  are the weight coefficients. If the sequential operation is limited on the specific hardware system, one can still use the first iteration of the PCA method to obtain the largest eigenvalues of a matrix. One can find many alternative formulations of the PCA task, such as cancelling correlations between coordinates, i.e. covariance matrix diagonalization or singular value decomposition.

Singular value decomposition (SVD) is a special form of a rectangular matrix decomposition in the form

$$\mathbf{X} = \mathbf{U} \mathbf{\Sigma} \mathbf{V}^T, \quad (51)$$

where  $\mathbf{U}$  is the unitary matrix (representing the rotation as the linear transformation of the space in the geometrical interpretation),  $\mathbf{\Sigma}$  is the rectangular diagonal matrix with non-negative real numbers on the diagonal (which are called the singular values, the action of the matrix has the interpretation of the corresponding scaling by diagonal elements) and

$\mathbf{V}^\top$  is another unitary matrix (with the same additional rotation interpretation).

SVD is essentially vital in the standard techniques of the latent semantic analysis (LSA) [207, 208], which purpose is to process documents and detect the relationship between libraries and terms.

There is a direct correspondence between PCA and SVD decomposition. To perform the PCA, one has to find the eigenvectors of the covariance matrix  $\mathbf{X}\mathbf{X}^\top$  (without the appropriate scaling factor  $\frac{1}{n-1}$ ). The covariance matrix is diagonalizable, and with the normalized eigenvectors, one can write

$$\mathbf{X}\mathbf{X}^\top = \mathbf{W}\mathbf{D}\mathbf{W}^\top. \quad (52)$$

Applying SVD to the same data matrix  $\mathbf{X}$  gives

$$\mathbf{X}\mathbf{X}^\top = (\mathbf{U}\mathbf{\Sigma}\mathbf{V}^\top) (\mathbf{U}\mathbf{\Sigma}\mathbf{V}^\top)^\top = (\mathbf{U}\mathbf{\Sigma}\mathbf{V}^\top) (\mathbf{V}\mathbf{\Sigma}\mathbf{U}^\top), \quad (53)$$

which gives

$$\mathbf{W}\mathbf{D}\mathbf{W}^\top = \mathbf{U}\mathbf{\Sigma}^2\mathbf{U}^\top, \quad (54)$$

Using this correspondence, one can perform the SVD decomposition as PCA on the special-purpose hardware.

#### *V.5.5. Clusterization*

The most detailed description of clusterization is the separation of the objects on a specific basis. The goal can be defined as a classification without any prior information about the classes. The machine can set the number of clusters in advance or define them automatically. The algorithm determines objects' similarity by their marked features and puts the objects with many similar features in the same class. There are successful applications of clusterization in market analysis (consumer analytics), image compressing, data analytics, and anomaly detection.

$K$ -means clustering is a clustering method that aims to partition  $n$  observations into  $k$  clusters. Each of these observations is located in the cluster with the nearest mean, also called a centroid [209–211]. There are heuristic algorithms that deal with such an assignment;

however, the problem is NP-hard.

Given a set of observations  $\{\mathbf{x}_1, \dots, \mathbf{x}_n\}$  in a  $d$ -dimensional space k-means algorithm aims to partition these observations into  $k$  sets  $\{S_1, S_2, \dots, S_k\}$  to minimise the within-cluster sum of squares (or variance):

$$\arg \min_{S_i} \sum_{i=1}^k \sum_{\mathbf{x} \in S_i} \|\mathbf{x} - \boldsymbol{\mu}_{S_i}\|^2, \quad (55)$$

where  $\boldsymbol{\mu}_{S_i}$  is the mean of points in the set  $S_i$ . One usually uses an iterative technique consisting of two steps to perform such an optimisation task. Given an initial set of  $k$  means  $\mathbf{m}_1^1, \dots, \mathbf{m}_k^1$ , the first step is to assign each observation to the cluster with the nearest mean, according to the Euclidean distance. The next step is to recalculate the centroids:  $\mathbf{m}_i^{t+1} = \sum_{\mathbf{x}_j \in S_{i,(t)}} \mathbf{x}_j$ . Finally, the loop is run until the convergence. The algorithm uses the assigning of objects to the nearest cluster by Euclidean distance, and it is a suitable method for transferring its sequential operations to the specific hardware.

Mean shift is a high-dimensional-space analysis method for locating the maximum density function given a discrete number of data sampled from this arbitrary density function. It is helpful in complex hierarchical algorithms and is used in different computer vision or image processing domains.

Given data points  $\mathbf{x}_i$  in  $n$ -dimensional space, one can use the kernel function  $k(r)$ , acting on the norm value  $r$ , to determine the mean shift's value. The kernel function has to be non-negative, non-increasing and continuous. One can use the flat kernel so that  $k(r) = 1$  if  $r < r_0$  and 0 outside. Each iteration consists of calculating the function

$$F(x) = \sum_i k\left(\frac{(\mathbf{x} - \mathbf{x}_i)^2}{\alpha^2}\right), \quad (56)$$

where there are  $\alpha$  states. The maximum of  $F(x)$  is computed using the square norm.

## V.6. Neural networks

ANNs are often associated with ML. We considered the associative memory model, a simple recurrent shallow NN in the subsection IV.5. This model can be extended to higher-order systems, simultaneously gaining many useful properties. However, optical systems are not tied only to this type of architecture [10].

Any NN can be defined as a set of neurons and connections between them. An artificial neuron's task is to take input numbers, process them in a certain way (executing a special function), and output the results. The standard mathematical transformation of one NN layer can be written as  $\varphi(\sum_{i=0}^N w_i x_i + b)$ , where  $w_i$  denote the weights for the input data points  $x_i$  (or independent variables), and the constant  $b$  is the shift called bias. Here, the  $\varphi$  is a nonlinear activation function. A single-layer NN that performs a similar transformation and produces a single output number is called a perceptron. The perceptrons, assembled into multilayered structures, are called multilayer perceptrons. The introduction to the NNs is presented in [212–214] with more modern work [215] and the latest results after the deep learning breakthrough [216].

The activation function  $\varphi$  plays an essential role in the NN design because the output signal would be simply a linear function in its absence. There are many functional activation functions, such as binary step function, sigmoid (or logistic function), hyperbolic tangent, etc. They allow a NN to map an input to the output appropriately. Thus, NN is considered a universal function approximator [217]. To choose the NN weights, one usually uses the backpropagation procedure [218, 219], although there are many alternatives. Backpropagation consists of tuning the NN weights according to the difference between the actual output value of the network and the predicted one, with the final goal of minimizing this discrepancy or the cost function. The tuning procedure involves computing the total discrepancy gradients on each layer, starting from the final one and updating the corresponding weight values. Through the extensive number of such iterations, there is a chance that the weights will be tuned in the desired way.

Many deep NN (NN with many layers) can be mapped into a shallow one with a significant overhead on the number of neurons in the standard layer. That means that any deep NN functionality can, in principle, be performed on a physical device suitable to a shallow architecture. With an appropriate mapping, both networks will have the same approximation qualities [220–223].

A well-trained NN can approximate many complicated algorithms, some of which are presented in this review. However, one has to provide enough input conditions and good output answers, especially when the problem is of high computational complexity. In addition, however, the resulting correlations need to be better understood. The valuable properties of the NNs go far beyond the optimization domain. We will consider some of them below.

### *V.6.1. Neural networks and dynamical systems*

Using ML models in the domain of physical sciences, i.e. incorporating physical laws and domain knowledge into neural architectures, is called physics-informed machine learning (PIML). It provides a powerful approach to modelling different physical phenomena. This rapidly growing field can pursue many other goals. Among them are constructing better predictive models with high accuracy and reliable generalization abilities, increasing data processing rate, accelerating the dynamical processes through optimized architecture, and solving inverse problems with interpretable models. One should expect that emulating complex nonlinear dynamics should benefit from the PIML. This can be seen in the applications in weather forecasting [224], modelling of turbulence [225, 226], nonlinear dynamics [227, 228], applications of the ML to the Koopman operator theory [229]. Optical hardware can be potentially used to speed up these applications.

The correspondence between NN architectures and dynamical systems is straightforward. Some of the NN can be viewed as discretizations of dynamical systems, which is true in reverse order - one can design NNs to have specific properties, such as invertibility [230]. This correspondence can broaden the applicability of the potential optical hardware. Their connection with dynamical systems and deep learning can be found in [231]. The generalization of the optimization algorithms inspired by different optical systems has canonical universality property [232].

## **V.7. Probabilistic graphical models**

Graphical models provide a natural tool for dealing with uncertainty and complexity throughout applied mathematics and engineering. The graph theoretic side of graphical models offers an appealing interface where one can model a data structure that lends itself naturally to the design of efficient general-purpose algorithms. Many models in statistics, systems engineering, information theory, and pattern recognition are special cases of the general graphical model formalism. It is vital for representing joint probability distribution and inference based on the given observations [233–235].

Probabilistic graphical models (PGMs) are graphs with the nodes represented by random variables, while edges connecting them represent conditional independence assumptions.



PGM can be thought of as a compact representation of joint probability distributions. There are two main kinds of graphical models: undirected, which are known as Markov random fields (MRFs), widely used in the physics and vision communities, and directed, also known as Bayesian networks (BNs), belief networks or causal models that are more popular with the AI and ML communities [233].

The spin Hamiltonians are particularly useful for PGMs. We recall the Ising spin model of Eq. (2) with zero-field coefficients ( $h_i = 0$ ). Each spin variable  $s_i$  can be treated as a random binary variable so that their coupling strengths serve as the connections between random variables. Certain configurations of spin variables  $X = (x_1, \dots, x_N) \in \{-1, +1\}^N$  is called an assignment. The probability of an assignment in the PGM is given by

$$P(s_i = x_i) = \frac{1}{Z} \exp \left( - \sum_{i=1}^N \sum_{j=1, j < i}^N J_{ij} x_i x_j \right), \quad (57)$$

where

$$Z = \sum_{X \in \{-1, +1\}^N} \exp \left( - \sum_{i=1}^N \sum_{j=1, j < i}^N J_{ij} x_i x_j \right) \quad (58)$$

is the so-called partition function.

There are several quantities of interest in the PGMs. First, it is the inference task - the computation of the quantity  $Z$  given by Eq. (58). The exact inference is the computation of  $Z$  with all possible assignments, which is a hard problem for an arbitrary graph. The running time of the exact algorithms of finding  $Z$  is exponential in the size of the largest cluster of corresponding graph nodes. There are rare cases of the Ising model graphs when it is possible to compute its partition function in polynomial time, but the problem of computing  $Z$  is generally hard. Hence, the approximate inference is widely used. Other quantities of interest can include finding the low-energy states (low energy sampling), worst margin violators, constituents of partition functions - assignment likelihood and marginal probabilities and certain moments concerning the partition function and the target value.

Some popular approximate inference methods include sampling (Monte Carlo), variational methods and message-passing algorithms [233]. Since many optical spin machines are not flexible in terms of programmability compared to conventional computers, one can hardly exploit sophisticated methods in hardware operations. That is why the sampling procedure is the most promising application from the hardware perspective, especially for

inference tasks. Expanding the spin machines' functionality is a promising direction, given the speed and energy efficiency of the optical efficiency domain.

The physical system often realises the symmetric coupling coefficients, making the model undirected. Using the system-specific devices that redirect light, it is possible to introduce the asymmetry in the variable connections, which opens the path to the directional PGM. In addition to the universality concept, one can see many practical tasks encoded into the Ising model (such as portfolio optimisation) as special cases of the PGMs. Moreover, the hardware's ability to realise the high-order interaction terms allows one to encode complicated conditional dependencies with little or no overhead on the number of variables.

However, the application scope of optical machines aimed at simulating PGMs is far beyond the scope of this problem. One can encode complicated large graphs with many factors, representing large-scale practical problems and efficiently use them as supporting decision-making networks. There are also applications in control theory and game theory. For example, PGM can compactly model joint probability distributions using sparse graphs to reflect conditional independence relationships in complex systems. It is possible to decompose similarly multi-attribute cost functions (or utility functions). For instance, let the general cost function be a sum of local cost functions. Each local term has parental nodes (random variables or factors), which it depends upon. Moreover, some of the utility nodes will also have action (control) nodes similar to parent nodes because they depend on the state of the environment and the performed actions. The resulting graph is called an influence diagram. Using such a diagram, one can perform sampling, similar to the inference task, and compute the optimal (sequence of) action(s) to maximise or minimise the cost function [233, 236]. The application of the same strategy was used in multi-person game theory [237]. In such a way, one can exploit optical spin machines to investigate dynamical systems and decision policy on factor graphs. There are many more applications of such correspondence between spin system functionality, control theory, and decision-making. The advantages of optical systems will benefit large complex graphs with complex connections between units [233]. Exploring the functionality of optical machines with respect to different paradigms is a promising research direction.

## V.8. Image processing

Several problems in computer vision can be formulated as binary quadratic programs, a particular case of QUBO. One can also see the similarity with PGMs. The conventional approach to such problems is to use the semidefinite relaxation technique, which appeared to be quite efficient [238]. The problems discussed include image co-segmentation, image segmentation with different constraints, graph matching, image deconvolution, graph bisection, and others. The computational complexity of these problems is high, which makes it necessary to propose an improved version of the semidefinite programming approach, which is more efficient and scalable. Some of these formulations are listed with little corresponding details, and we refer the reader to the original work [239].

$$\begin{aligned} \min_{\mathbf{x} \in \{-1, +1\}^N} \quad & \mathbf{x}^\top \mathbf{A} \mathbf{x} \\ \text{s.t.} \quad & (\mathbf{x}^\top \mathbf{t}_i)^2 \leq \kappa^2 n_i^2, i = 1, \dots, s, \end{aligned} \quad (59)$$

is the image co-segmentation task with the matrix  $\mathbf{A}$  [239],  $s$  is the number of images,  $n_i$  is the number of pixels for  $i$ -th image, and  $\mathbf{t} = \sum_{i=1}^s n_i \mathbf{t}_i \in \{0, 1\}^n$  is the indicator vector for the  $i$ -th image,  $\kappa \in (0, 1]$  is a parameter.

$$\begin{aligned} \min_{\mathbf{x} \in \{0, 1\}^{KL}} \quad & \mathbf{h}^\top \mathbf{x} + \mathbf{x}^\top \mathbf{H} \mathbf{x} \\ \text{s.t.} \quad & \sum_{j=1}^L \mathbf{x}_{(i-1)L+j} = 1, i = 1, \dots, K \\ & \sum_{i=1}^K \mathbf{x}_{(i-1)L+j} \leq 1, j = 1, \dots, L \end{aligned} \quad (60)$$

is the graph matching task and  $x_{(i-1)L+j} = 1$  if the  $i$ -th source point is matched to the  $j$ -th target point; otherwise it equals to 0.  $h_{(i-1)L+j}$  records the local feature similarity between source point  $i$  and target point  $j$ ;  $H_{(i-1)L+j, (k-1)L+l} = \exp(-(d_{ij} - d_{kl})^2 / \sigma^2)$  encodes the structural consistency of source point  $i, j$  and target point  $k, l$ . The corresponding details can be found in [240].

$$\min_{\mathbf{x} \in \{0, 1\}^n} \|\mathbf{q} - \mathbf{K} \mathbf{x}\|_2^2 + S(\mathbf{x}) \quad (61)$$

is the image deconvolution task, where  $\mathbf{K}$  is the convolution matrix corresponding to the blurring kernel  $\mathbf{k}$ ,  $S$  denotes the smoothness cost,  $\mathbf{x}$  and  $\mathbf{q}$  represent the input image and the blurred image respectively [238].

$$\begin{aligned}
& \min_{\mathbf{x} \in \{-1,1\}^n} -\mathbf{x}^\top \mathbf{W} \mathbf{x}, \\
& \text{s.t. } \mathbf{x}^\top \mathbf{1} = 0
\end{aligned} \tag{62}$$

is the graph bisection task with  $W_{ij} = \exp(-d_{ij}^2/\sigma^2)$ , if  $(i, j) \in \mathcal{E}$ ; and 0 otherwise, where  $d_{ij}$  denotes the Euclidean distance between  $i$  and  $j$ . These tasks can potentially be mapped into the special-purpose hardware dealing with quadratic assignments or low-level programmable tasks.

### V.9. Several examples of hardware embeddings

Here we consider the hardware representation of several tasks we considered previously. We characterise each assignment stating its possible embedding on the particular hardware type - spin machines and characterise several parameters of such embedding. We consider discrete and continuous variables (the latter can require additional overhead on the number of discrete operational units), direct mapping of the problem coefficients or partial concerning other factors, whether the hardware requires the consequent manner of operations or not, incorporating additional constraints into the coefficients of the problem and other details. Overall, these factors determine whether the possible embeddings are efficient or not (significant overhead, consequent operations, etc.). We present the examples in Table I.

## VI. MAIN DIRECTIONS OF TECHNOLOGICAL DEVELOPMENT IN OPTICAL COMPUTING

The demand for computational resources is gaining momentum due to their use in many practical applications. This trend is supported by a growing industrial interest from prominent IT companies (Microsoft, Google, IBM, Amazon, etc.) and fast-growing start-ups. To get a better global picture, one must understand the current paradigm of conventional heavy calculations and what advantages the optical machines can offer. First, we present several key metrics of the standard approaches and then show the benefits of optical devices. After that, we describe the strategies pursued in photonic neuromorphic computing.

TABLE I. Example of possible encoding for the several tasks

Assignment	Formulation	Details
MIN-2-SAT	$\min_{x_i \in \{0,1\}^n} \sum_{i,j < i} w_{ij} x_i x_j \quad (63)$	Discrete variables, direct mapping, straightforward operation with respect to dynamical updates, efficient.
Phase retrieval	$\begin{aligned} \min \sum_{ij} M_{ij} u_i u_j \\ \text{s.t. }  u_i  = 1, i = \overline{1, n} \end{aligned} \quad (64)$	Continuous variables, direct mapping on the QCO (Eq.(4)), straightforward operation, efficient concerning the QCO hardware.
Regression	$\min_{\beta_j} \sum_{i=1}^n \left( \sum_{j=0}^m \beta_j x_{ij} - y_i \right)^2 \quad (65)$	Continuous variables, partial mapping, straightforward operation, inefficient concerning the variables mapping.
SVM	$\begin{aligned} \min \ \mathbf{w}\  \Rightarrow \min(\sum_j w_j^2) \\ \text{s.t. } y_i (\mathbf{w}^T \mathbf{x}_i - b) \geq 1, \text{ for } i = 1, \dots, n \end{aligned} \quad (66)$	Continuous variables, partial mapping, straightforward operation, inefficient concerning the variables mapping.
k-means	$\min_{S_i} \sum_{i=1}^k \sum_{\mathbf{x} \in S_i} \ \mathbf{x} - \boldsymbol{\mu}_{S_i}\ ^2 \quad (67)$	Continuous variables, partial mapping, consequent operation, inefficient variables mapping and operation setup.
Graph bisection	$\begin{aligned} \min_{x_i \in \{-1,1\}} - \sum_{i,j} w_{ij} x_i x_j \\ \text{s.t. } \sum_i x_i = 0 \end{aligned} \quad (68)$	Discrete variables, partial mapping due to the constraints, straightforward operation, inefficient representation of the constraints.
Image co-segmentation	$\begin{aligned} \min_{x_i \in \{-1,+1\}} \sum_{i,j} a_{ij} x_i x_j \\ \text{s.t. } \left( \sum_j t_{i,j} x_j \right)^2 = 0 \leq \kappa^2 n_i^2, i = 1, \dots, s \end{aligned} \quad (69)$	Discrete variables, partial mapping due to the constraints, straightforward operation, overhead on auxiliary variables, inefficient concerning the constraints and overhead.

### VI.1. Performance of information processing systems

In general, Moore's law concerns several metrics. All of them are reaching saturation but at a different paces. To maintain the same effectiveness of the hardware, new technology

is required. However, the more significant demand for superior hardware is caused by the explosive growth of AI applications, which puts much more pressure on research and development performance. For example, the need for computational capabilities has increased by more than five orders of magnitude from 2012 to 2018 because of the AI developments shown in the OpenAI report [8].

Several key metrics characterise the performance of information processing systems. We will use MAC (multiply-accumulate operation containing one multiplication and one addition) and FLOP (floating-point operation). The relationship between them is that 1 MAC counts as 2 FLOP. One usually uses MACs and FLOPs to measure the speed performance of the device, which depends on the frequency or the characteristic intrinsic operation time on the hardware. Alternatively, one can use the operations per second (OPs), be it conventional mathematical operation or hardware state switching, but this notation is rarely used. Another important metric is energy consumption or efficiency, which can be measured in FLOPs/W (FLOPs per watt). One can consider alternative metrics, such as the total training energy in joules in the case of the training NN or J per spike in the operations performed on the spiking NN (SNN) architecture. Many combined metrics and their variations exist, such as speed per area (Op/s/mm), that are used to describe some other energy characteristics. Other important parameters of the hardware setup may include the analogue level of noise, scalability properties, specific architecture parameters, etc.

Data centres that use thousands of CPUs and hundreds of GPUs consume megawatts of power. Despite the versatility of conventional computers, their characteristics are not enough to achieve high performance in the key metrics. Thus, application-specific hardware that differs in architecture and logic reduces this gap between the desired efficiency and computer capabilities. One can find several discussions of these devices in [198, 241] with the corresponding comparison of the key metrics; see also Fig. 10. In addition, we mention some of these electronic devices as reference points for comparison with optical devices.

Classical computing architectures can differ in the details within one type of device. However, it is common to characterise them using two key metrics – the processing power or the computing speed using FLOPS and the energy efficiency. One can use the ratio of the FLOPS to the power consumption in watts (W) to get the energy efficiency metrics [198].

The standard estimate of the modern CPU efficiency is 2 TFLOPs, while the power efficiency is about 10 GFLOPs/W. Therefore, we can use the Intel Xeon processor as one of

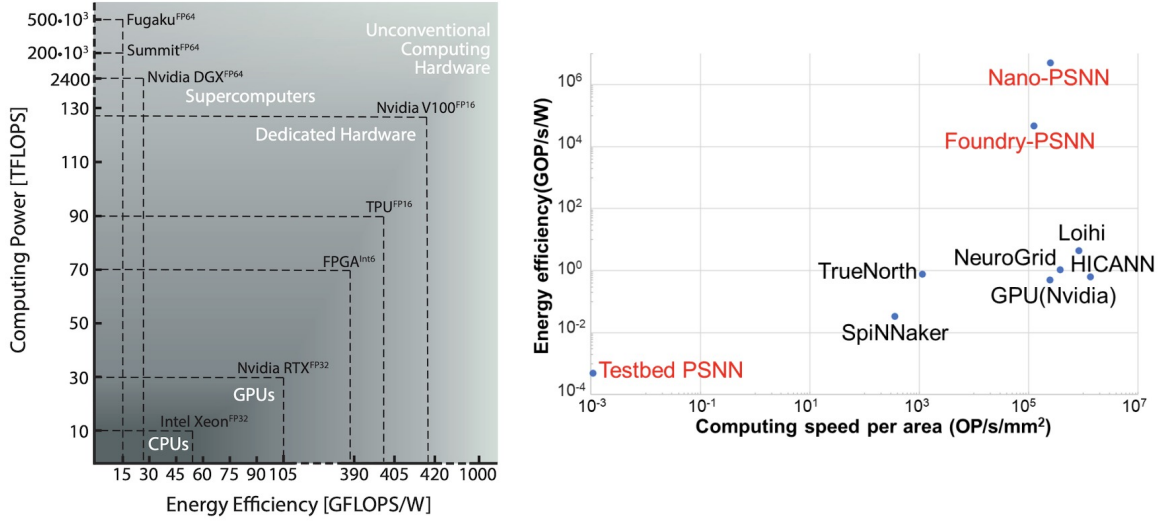


FIG. 10. Left panel: computing power and energy efficiency of different types of computing hardware. The schematic distribution of the processing power versus energy efficiency is shown for several CPUs, GPUs, FPGAs, supercomputers and potential unconventional computing devices based on optical systems, reproduced with permission from [198]. Right panel: energy efficiency values versus computing speed per area for spike-event hardware compared with results described in the literature. Reproduced with permission from [241].

the top devices in terms of efficiency for working with the double-precision format, which has 4.8 TFLOPs and 29 GFLOPs/W [242]. Graphics processing units (GPU) are the advanced specialised electronic architectures and workhorses of the current ML tasks in real applications because of the parallel computing options. Most of the GPUs operate at near 0.3 kW power consumption with the range of 0.5 to 7 TFLOPs and corresponding 1.6 to 23 GFLOPs/W energy efficiency for the work with the double-precision format.

Another type of classical hardware is powerful non-distributed computer systems that are not so energy efficient but have enormous computing power. The top 10 list starts with NVIDIA DGX SuperPOD with 2356 TFLOPs and nearly 26.2 GFLOPs/W. The most powerful supercomputer in processing power is Fujitsu’s Fugaku, with 442000 TFLOPs and 14.8 GFLOP/J. One can link several devices into the powerful distributed system to achieve much higher processing power with additional energy costs.

Another class of electronic devices can be named ”dedicated hardware”. Although the GPU is not usually attributed to this class, it performs a similar role. A good example is the field-programmable gate array (FPGA), an integrated circuit that can be configured by a customer using a hardware description language. On average, FPGA can achieve 10

TFLOPs with near 50 GFLOPs/W energy consumption rate and several times more ( $\times 5, \times 7$ ) by working with lower precision numbers [243]. Another example of dedicated hardware is Google’s Tensor processing unit (TPU). TPUs are custom-developed application-specific integrated circuits (ASICs) to accelerate ML workloads. The efficiency can be estimated as 90 TFLOPs, and 400 GFLOPs/W [244].

Further improvements in electronic special-purpose devices are expected to come from analogue architectures based on memristors [245], non-volatile memories, compact low-voltage field-effect transistors and engineering of heterostructures of two-dimensional materials taking into account the quantum effects. Another option is to explore the different architecture of the dedicated hardware. For example, IBM claims to achieve 176000 times better energy efficiency with their bio-inspired neuromorphic chip TrueNorth chip than the conventional general-purpose Intel i7 system for specific applications [246]. Nevertheless, TrueNorth has a relatively slow frequency rate of 1 kHz and an approximate energy efficiency of 2.3 pJ/bit. Moreover, it requires additional connections for the incoming neural spikes. One can further explore Intel’s Loihi [247] or NeuroGrid [248] devices, which are close to the modern GPU [249].

Despite impressive and innovative developments, more than the presented classical architectures are needed to satisfy the need. For example, some estimates on demand from future autonomous vehicles require the information processing at 100 TOPs rate with the energy consumption of less than 100 Watt with the additional low latency [250].

## **VI.2. Optical energy consumption**

Optical devices can process information instantaneously. Additional advantages include negligible energy consumption and heat generation. State-of-the-art for CPUs and GPUs metrics can be converted into 20 pJ/MAC [251]. The dedicated hardware and application-specific circuits can achieve 1 pJ/MAC with reduced precision of the calculations [252]. The same so-called “ideal” benchmark is supported by the work [49], where authors used a programmable nanophotonic processor with a cascaded array of 56 programmable MZIs in a silicon photonic integrated circuit to perform the vowel recognition task. Modern AI chips can reach the 100 mW/GOps operation power per second, but the future competitive requirements should be  $\sim 10 - 1$  mW/GOps [8].



We can consider several examples of photonic hardware and highlight their technical characteristics, such as speed and energy consumption. The photonic accelerator architecture based on coherent detection [51] enables a new class of ultra-low-energy processors operating at very low (sub-aJ) energies for MAC operation. These structures can be reprogrammed and trained on the fly and have good scalability of up to one million elements. Additionally, [51] discusses the “standard quantum limit” for optical NNs that can be bounded with 50 zJ/MAC values for irreversible digital computation.

Optical NNs can achieve accurate results with extremely low optical energies [253]. It was shown experimentally that optical NN with dot product calculated optically achieved high accuracy on the MNIST digits classification using few photons (of the order  $10^{-19}$  J of optical energy) per weight multiplication. The essential idea was to reduce the noise from accumulating scalar multiplications in dot-product sums.

Some optical machines can use pre-optimized mathematical structures for architectural benefits. A good example is energy-efficient, high-throughput, and compact tensorised optical NN exploiting the tensor-train decomposition [254]. Such a NN can improve the energy efficiency by a factor of  $1.4 \times 10^4$  compared with digital electronics ANN hardware and by a factor of  $2.9 \times 10^2$  compared with silicon photonic technologies. Moreover, it was possible to achieve better energy efficiency with fewer elements for footprint-energy efficiency calculation [254]. In general, neuromorphic photonic systems potentially offer petaMAC per second per  $\text{mm}^2$  processing speeds [61] and attojoule per MAC energy efficiencies [62].

Energy consumption is closely related to the physical properties of the neural architecture. For example, event-driven spiking neural networks (SNNs) outperform ANNs in energy efficiency. The dynamic of many models can be described using the universal Izhikevich model [249]. Event-driving neuromorphic computing overcomes traditional von-Neumann architectures’ limitations but has several specific problems with the throughput, scalability, training methods, etc.

The successful implementation of an optoelectronic spiking neuron inspired by the Izhikevich model was reported in [241]. A nanoscale optoelectronic neuron with 200 aJ/spike input can trigger the output from on-chip nanolasers with 10 fJ/spike. This neuron can support a fanout of  $\sim 80$  or overcome 19 dB excess optical loss while running at 10 GSpikes/second in the NN. Such a scheme corresponds to 100 throughput and 1000 times energy-efficiency improvement compared to state-of-art electrical neuromorphic hardware such as Loihi and

NeuroGrid [241]. The hybrid systems of quasiparticles can be another potential platform for spiking architectures. Exciton-polaritons can achieve 1 pJ/spike with 100 ps timescale [255, 256].

### VI.3. Evaluation of speed

A universal optical computer was not a viable option to compete with classical computers. Instead, a specified optical computer or optical block as a part of a hybrid classical/nonclassical architecture has become a focus of recent research. One of the first realisations of simple mathematical operations, such as a free-space fan-in/out vector-matrix multiplication, was introduced by Goodman in 1978 [257]. It is the essential linear algebra operation, where the input vector is loaded into an array of light sources, and the multiplication matrix is encoded into the SLM. The light propagation is analogous to broadcasting the initial vector into SLM, which performs element-wise multiplication, after which the lens gathers all the beams in the horizontal direction and summates the intensities. One can evaluate the performance of this device as  $N^2$  MAC for one multiplication of the vector with  $N$  elements and a square matrix  $N^2$ . However, the effective performance is limited by the system's frequency  $f$ , mainly of the SLM, resulting in  $fN^2$  MACs; see also [258]. Nevertheless, using 256-length input vector and 125 MHz frequency rate, the device's performance can reach impressive  $\sim 8$  TMACs.

Other schemes based on different forms of the free-space matrix-vector multiplication can reach similar values. In 2020, Lightmatter presented an optoelectrical hybrid chip 'Mars' with  $0.4 - 4$  TMACs depending on the frequency of weights [259]. A massively parallel convolution of 16x16' tensor core' scheme based on crossbar architecture has been built on a chip with 13 GHz modulation speed for the inputs, and approximate 2 TMACs [260]. Another scheme based on the electro-optical Mach-Zehnder modulators represents a universal optical vector convolutional accelerator and achieves more than ten TOPS speed, with a consequent successful use as an optical convolutional neural network in facial and handwritten digit images recognition [261]. Most of the photonic hardware with the feed-forward architecture can operate at high (GHz) speeds and usually have good scalability characteristics [51, 253, 254].

Another critical factor affecting the optical device's speed performance is the hardware's

architecture. From this perspective, RC might improve many aspects of optical computing devices. One could expect several orders of magnitude speed-up compared to the typical ANN structure. RC optoelectronic/optical implementations are usually divided into spatially distributed and time-delayed [80]. The RC scheme on a silicon photonic chip with optical waveguides, splitters and optical combiners can achieve the data processing rate of 0.12 and up to 12.5 Gbit/s [262]. Moreover, more exotic physical systems, such as exciton-polaritons, can reach similar performance so that the SNN architectures can achieve the characteristic operation time of the order of 100 ps with the energy efficiency of 1 pJ/spike [255, 256]

Optic-based spin machines also enjoy competitive speed characteristics. CIM evolved from having just 4 spins and 12 connections in 2014 (Stanford) to 16K spins and 256M connections in 2021. The 2000-node version achieves semidefinite relaxation minimum of a cost function in 0.1 ms and further improves the solution [263]. The new generation of CIMs based on Thin-Film LiNbO<sub>3</sub> (TFLM) photonic circuits will be released in 2022. It will feature an OPO network with  $\sim \mu W$  pump power,  $\sim$  fs pulse duration, 100 GHz – 1 THz clock frequency and the synchronized operation of multiple CIMs on a chip.

Exciton-polaritons possess even better ultrafast timescales. For example, the polariton graph simulator [136] is easily scalable to 10K elements and shows  $\sim$  100 ps operational times respectively, while the degenerate lasers [90] system have  $\sim \mu s$  characteristic timescale. However, all-to-all controllable couplings have yet to be experimentally implemented.

#### **VI.4. Other important properties**

Other essential factors are undoubtedly affecting optical devices' attractiveness and performance, such as intrinsic noise and analogue accuracy of the hardware. For example, the recognition results using MNIST handwritten digits can show different accuracy on different devices, which can be a good measure of how well a particular NN is adjusted to a specific task citelee2021izhikevich. The comprehensive analysis of the error sources and their classification for the electro-optical device can be found in [8].

The essential part of the hardware is its structure/architecture. It affects many other properties of the optical devices, be it the accuracy, scalability, the potential for future optimization, etc. The interplay between the hardware's electronic and photonic components

depends on the architecture. It directly affects optical/electronic conversion, storing and reading the data, and logic operations cost in the case of a hybrid architecture.

Scalability is one of the key metrics and is the consequence of the architecture choice. It measures the ability of a system to keep its algorithmic performance with a growing number of variables.

The optical setups enjoy additional degrees of freedom compared to the conventional electronic hardware. For example, two independent variables in the complex plane can parameterise short optical impulses. In addition, one can explore optics-specific degrees of freedom such as polarisation and orbit angular moments of light.

Lastly, current optical hardware is used to employ classical algorithms and NN architectures that are conventional for standard electronic architecture. These algorithms are designed using Boolean logic, which is suitable for a digital computing system. However, they are not always optimal for optics implementation. Therefore, developing specialised algorithms optimised for optical computer platforms is necessary, further reducing the operational complexity and execution time.

## **VI.5. Optical minimisers of spin Hamiltonians**

The optical systems described in this review as optical minimisers of spin Hamiltonians aim to find the global minimum of hard optimisation problems. They offer the potential for finding a better solution to a wide variety of nonlinear optimisation problems for a fixed time, finding a solution of a given precision faster, or solving more complex problems at fixed and limited cost. All these machines have advantages and limitations. They vary in scalability, ability to engineer the required couplings, the flexibility of turning the interactions, the precision of read-out, and factors facilitating the approach to global rather than the local minimum. However, they all have some parts of their operation that promise increased performance over the classical computations. To solve an optimisation problem on optical minimisers of spin Hamiltonians, one needs to think of an optimal mapping of the real-life problem onto a spin Hamiltonian, some of which are known [84], for others finding an optimal mapping will mean half of the success in solving.

While combinatorial optimization is often focused on finding just one of the absolute minima configurations, it is desirable in many applications to obtain many or all degenerate

absolute minima and, in some cases, to sample many low-energy excited states as well [264]. Such sampling capability benefits applications that obtain distributional information about optimal solutions, such as implementing Boltzmann machines as generative models for ML [265]. In industrial settings, accessing a pool of candidate solutions to an optimization problem can make processes more efficient and flexible; for example, in drug discovery [266], structure-based lead optimization could generate many candidate molecules for simultaneous testing.

Another approach is to decompose large optimisation problems into subproblems to be solved separately (e.g., to accommodate hardware limitations). Better solutions to the original problem can be constructed using multiple low-energy samples rather than just the optimum for each subproblem [267]. However, a spin minimiser designed for combinatorial optimisation is not necessarily well-suited to sample all ground and low-energy states. The nonlinear stochastic dynamics of such machines in the presence of quantum noise can be exploited to sample degenerate ground and low-energy spin configurations of the spin models. When such optical machines operate in a quantum-noise-dominated regime with short photon lifetimes (i.e., low cavity finesse), homodyne monitoring of the system can efficiently produce samples of low-energy spin configurations better than their classical analogues [268].

An additional advantage of discovered principles of operation of optical minimisers of spin Hamiltonians leads to the opportunity of formulating new optimisation algorithms to be realised on specialised but classical computing architectures: FPGAs, GPUs, etc. For example, the principle of operation of the CIM was implemented as the network of nonlinear oscillators described by simplified equations [269]. A similar approach has been recently realised using FPGAs using a network of Duffing oscillators [270].

To properly access the properties of such systems, one can use computer simulations in several scenarios. Such emulations allow one to avoid extensive labour experiments to predict properties of such systems properly, tune and optimise the parameters for optimal performance and even inspire new classes of algorithms for conventional computers. The emulation algorithms can be found in [122, 271]. Such techniques can apply to a broad type of NNs.

## VI.6. Efficiency of Artificial neural networks

Overall, ANNs help process large data sets and combine and analyze vast amounts of information quickly and without explicit instructions. Therefore, multiple NN architectures have been investigated and implemented in various applications. Furthermore, developing a variety of NNs is essential because different NNs can be represented through different architectures while maintaining a certain universality in approximating and representing many complex systems, which expands the already significant scope of NNs applicability.

Many linear transformations can be performed with passive optics without power consumption and minimal latency at rates over 50 Gb/s. The feasibility of optical logic gates has also been demonstrated [272–276]. However, the attempts to replicate the classical boolean electronic logic circuits in photonics did not prove to be successful. Analog photonic computing devices are especially suitable for NNs, which require fast and energy-efficient (although approximate) computations. Furthermore, in principle, many optical nonlinearities can be used to implement various nonlinear functions [277]. Recent developments suggest that optical implementations of NNs can overcome electronic solutions in terms of computational speed and energy efficiency. However, as discussed in our review, the challenge of developing truly deep NNs with photonics still needs to be solved. Photonic multilayer perceptrons and photonic SNNs have a lot of potential to realize all-optical ANNs. In the near term, photonic accelerators for convolution NNs (multiple layers, weight sharing, sparse topology) are the most promising photonic solutions to enhance inference speed and reduce power consumption.

However, there are still many other opportunities to explore and improve the implementation of photonic NN. For example, more research is needed to assess whether a specific type of deep NN can be implemented optically efficiently, i.e., in a way that provides advantages concerning fully electronic implementations. Furthermore, photonics has not yet implemented some deep NNs (long-short-term memory NNs, generative adversarial nets, geometric deep NNs, deep belief networks, etc.).

The ultimate goal is to demonstrate large networks with thousands of nodes and interconnections across many hidden layers, i.e., truly deep architectures. Therefore, it is essential to work on the photonic NN cascability (enabled by low propagation losses, crosstalk, and noise) and robustness to fabrication imperfections and parameter drifts over time [278].

For instance, resonant structures like microring resonators are susceptible to manufacturing deviations [279]. At the same time, because of their reconfigurability, linear optical processors based on MZI appear more robust to process inaccuracies. Some studies discuss how to achieve reliable photonic computations even with imperfect components [280].

The all-optical implementation of the nonlinear activation function requires further investigation. Nonlinearities can be emulated in software, but integrating nonlinear elements into hardware is still challenging. Several approaches to address this issue have been reported using MZIs [281], graphene and quantum well electro-optic absorption modulators, and photonic crystals [282]. Some technological breakthroughs would benefit photonic NN, particularly implementing an integrated, non-volatile and energy-efficient photonic memory element. In this scenario, using phase-change materials seems the most promising approach to achieve such photonic memories since they have also shown the potential for multi-level storage [283]. Moreover, the cells of such materials have been recently exploited in photonic NN, mainly for SNNs [56].

#### *VI.6.1. All-optical backpropagation*

When training NNs, one usually considers the backpropagation algorithm by default. The essential idea behind the backpropagation is to compute the gradient of the loss function with respect to each weight by the chain rule and doing it consequently, one layer at a time, iterating backwards from the last layer to avoid redundant calculations of intermediate terms in this sequence of steps [216, 218]. Such a procedure allows one to fit the weights of a NN for a given task. Still, the complexity of the backpropagation is enormous. It grows linearly with the number of training examples or batches, the number of iterations, which is not known in advance and the basic complexity of feedforward input propagations, which can be estimated as a consequent series of matrix-vector multiplications. These evaluations hold for many cases, assuming batch gradient descent algorithm and simple matrix multiplication for the input propagation. However, one can reduce the number of steps with some approximate schemes. At the moment, there are many different ways to train NNs, including variants of backpropagation or alternatives, such as learning without backpropagation [284].

Thus, the backpropagation algorithm remains one of the most expensive components to compute. The significant power and time consumption happens due to the sequential

computation of gradients in the backpropagation procedure of NN training. Backpropagation through nonlinear neurons is another challenge to the field of optical NNs and a significant conceptual barrier to all-optical training schemes. Although there exist several practical, simple solutions, such as using approximation provided in a pump-probe scheme that requires only passive optical elements [285] or by measuring the forward and backwards propagated optical fields based on light reciprocity and phase conjunction principles [286], the schemes still involve digital electronics or programming a high-speed SLM respectively. Therefore, having incomplete solutions, the work on the end-to-end optical training of NNs is in progress. Achieving the efficient all-optical backpropagation training method (besides the realization of depth and nonlinearities) will be a major achievement in the field. The question of such realisation is just a matter of time since there are no fundamental restrictions on such a development [287, 288].

### **VI.7. Statistical sampling**

Statistical sampling is another essential domain where using optical machines can be beneficial. PGMs can effectively represent the probability distributions of different factors in complex systems. Moreover, due to its universal structure, one can model complicated large graphs with many factors for various practical problems.

The correspondence between the Ising model and the probability measure of the pairwise PGM allows one to solve many tasks, such as inference based on the given observations or sampling. For example, the latter can obtain the most and the least probable states by exploiting the sign before the energy function. Furthermore, the additional specific mechanism presented in several types of hardware can enhance the sampling procedure to efficiently use them as a source of additional information for particular problems.

Unfortunately, the simulation of PGMs using optical machines needs to be better investigated. The obvious directions will be to increase the programmability of the optical spin models to access more options for manipulating the Ising/XY/Potts etc., states or decompose large and rich PGMs into their discrete approximations accessible by spin Hamiltonian simulators. Another option is to investigate additional hardware improvements in the context of PGMs. Finally, there are many more applications of such correspondence between spin system functionality, control theory, and decision-making.



### VI.7.1. *Neural architectures and transfer learning*

Many NN architectures can differ in forms (deep and shallow, feed-forward and recurrent), training methods, network topologies, and operational principles. Some photonic architectures were mentioned before; see Section II.3. Moreover, some of these structures are best suited for one purpose than another. For example, recurrent NNs are good at tackling temporal dependencies, while convolutional NN is a standard architecture in image processing tasks. However, one can not easily realise all of the architectures on particular hardware due to its physical limitations or the ineffectiveness of the design.

To deal with the transfer of functionality between different architectures, one can pay attention to the domain of transfer learning. Originally, transfer learning was a research direction in ML that aimed at gaining knowledge from solving one type of problem and using it in a different but related domain; see recent reviews [289, 290]. However, transfer learning is a way to transfer features of one architecture to another and make the problem more hardware-friendly.

Transfer of functionality will dramatically influence the ML domain and benefit the hardware computing field. It is of essential importance for optical devices, which have certain engineering limitations on the realisations of some architectures. Many more related research directions, like neural architecture search, can be adjusted to optimise the hardware systems.

## VII. OPTICAL QUANTUM COMPUTING

ANN in photonic integrated circuits and optical minimisers of spin Hamiltonians are the main paradigms for optical platforms that have already established an engineering base and clear development directions. Compared with emerging quantum technologies, a high-risk endeavour, classical optical devices offer advantages in speed, parallelism, energy consumption, or operational policy in short to medium term. Therefore, we can say that optical technologies are repeating their electronic special purpose hardware analogues development, with the technological progress making "another loop in its spiral development". Hence, they represent a solid investment in research and development activities with inevitable advantages.

The story of quantum computers is related to exciting developments in physics and the theory of computation. There has been a recent surge of investment by large public and startup companies. Such ramping up of industrial activity requires careful examination of the commercial potential of quantum computing technology. There are many hardware platforms on which quantum computing can be developed, and it is still being determined which technology, or a combination of technologies, will prove most successful.

This section assesses the current status and future potential of quantum computing based on photons. The current view of the academic community is to exert caution when discussing future practical applications of quantum computing technology because it is so different from the information technology we use now. Many believe that quantum technology will substantially impact society in the decades ahead [291]. Still, not many are confident about the commercial potential of quantum technology in the near term (five to ten years) [292]. Others are sceptical that quantum computers will ever become useful [293]. At the core of critics' argument against the feasibility of quantum computers lies the notion of complexity. So far, a very low-level complexity class of probability distributions has been identified and described by noisy intermediate-scale quantum computers. Such computers would allow neither good-quality quantum error correction nor a demonstration of "quantum supremacy" – the ability of quantum computers to make computations that are impossible or extremely hard for classical computers [293].

### **VII.1. Quantum optical devices**

The operation of quantum computers relies on three principles: quantum entanglement, quantum complexity and quantum error correction. Therefore, quantum computers exploit the characteristic correlations among the parts of a quantum system that make them robust and scalable to large devices solving hard problems.

By 2022, many advances in quantum computing were announced (but some were also refuted). The leading technology is based on superconducting qubits (Google, IBM, Rigetti) and trapped ions (IonQ, Honeywell). Google team has announced quantum supremacy using 53 qubits in 2019; IBM entangled 65 qubits while revealing a road map to more than 1000 by 2023. The advantages of superconducting qubit systems are that they are based on well-developed semiconductor technology; however, they have to be kept cold (10mK) and have

a short decoherence time ( $< 10\mu\text{s}$ ). In contrast, trapped ions are very stable with much longer decoherence times (minutes), longer range interactions (beyond nearest neighbours) and report the best quantum volume among any quantum computer systems. However, many lasers are needed to be controlled simultaneously, the operation could be faster, and it would be hard to put many ions on a chip. So far, IonQ has achieved 32 trapped ions in a chain, promised to achieve quantum supremacy by 2025 and solve interesting real-life problems by 2028. There are other proposals and small-scale realisations using silicon quantum dots [294], diamond vacancies [295], neutral atoms [296, 297], etc. One of the biggest disappointments was experienced by Microsoft in 2021 invested into topological qubits. In theory, a topological qubit created from a pair of Majorana zero modes could benefit from topological protection. The topological protection leads to stability and a lack of decoherence that could help topological quantum computers scale up in power more easily than other approaches. The theoretical existence of Majorana zero modes was realised experimentally in 2018 [298], but the paper was retracted following the discovery of erroneous data presented.

Quantum computers based on photons had been considered impractical in the early ages of quantum computer developments because of difficulties in generating and controlling the required quantum states. However, such computers are being developed by photonic companies such as Xanadu (Toronto) and PsiQuantum (Palo Alto, CA) in addition to intensive academic research. The advantages of photon-based quantum computers are room temperature operation, much longer decoherence times (from ms to hours), and the systems being cheaper and easier to build. However, they become large quickly (although PsiQuantum claims that one million qubits would still be possible).

For a photon-based quantum computer, boson sampling was proposed as a counterpart to a random quantum circuit of superconducting qubit systems. A sampling task is one where the computer generates samples from a specific probability distribution. Quantum algorithms allow sampling from probability distributions well beyond the capabilities of classical computers. The most famous example is Shor's factorisation algorithm which exploits the ability to sample a probability distribution efficiently based on the Fourier coefficients of a function on a quantum computer.

There is a quantum uncertainty associated with the amplitude and phase of any state of light. In squeezed states of light, this quantum uncertainty is unequally distributed between

the amplitude and phase and the more the state is squeezed, the more photons it contains. Multi-photon squeezed light is found in many quantum-optics experiments, and quantum computing models based on these states have been studied for over two decades [299].

In particular, it was proposed that even a relatively simple optical circuit that exploits the properties of squeezed light and consists of beam splitters and photon counters could carry out a sampling algorithm at speed beyond the reach of classical computers [300, 301]. It was also proposed that such an algorithm has many practical applications [302] such as finding matching configurations between molecules [303] or the different states of a molecule [304].

More rigorously, the boson sampler is a quantum optical device in which a linear optical network mixes many non-classical photon sources. As a result, the photons are indistinguishable and, when originating from different sources, lead to complex photon counting statistics of the output detectors. When the number of the input/output channels of the boson sampler is large, the emulation of such a device with a classical computer is believed to be  $\# \mathbb{P}$ -hard [300, 305]. In the original formulation, the boson sampler was introduced as a device consisting of single-photon sources, a linear interferometer and photon-counting detectors at the output channels. Several experiments implemented variations of this set-up: 5 input photons in 21-mode optical circuit [306], and 20 input photons in 60-mode interferometer [307].

Using single-photon sources creates various technological complications that reduce the scalability necessary to overcome the classical computer calculations (that roughly scale as  $2^k$  in the number of operations where  $k$  is the number of input photons). The lack of scalability in single-photon-based experiments on integrated platforms is due to non-deterministic state preparation and gate implementation. Instead, deterministically prepared squeezed states and linear optics with non-Gaussian operations provided by photon-counting detectors allow significant scaling up in the number of input/output channels. Therefore, the Gaussian boson sampling was proposed, where the single-photon sources are replaced by the single-mode squeezed light generated by parametric down-conversion sources [300]. A paper published in Science at the end of 2020 reported that they achieved "quantum computational advantage" while implementing Gaussian boson sampling using 50 input channels and a 100-mode interferometer [308]. The authors claim that their device provides 200 seconds samples requiring classical computers billions of years. Specifically, the paper reports a Gaussian boson

sampling experiment representing a quantum state in  $10^{30}$ -dimensional Hilbert space and a sampling rate that is  $10^{14}$  faster than that of using digital supercomputers. This paper was described as the first independent verification of Google’s quantum advantage claims and claimed to surpass Google’s supremacy by several orders of magnitude.

This huge computational advantage reported [308] is based on specific statistical tests measuring the proximity of the measured samples to the outcomes of noiseless simulations of the quantum experiment that were performed on a classical digital supercomputer. It was previously shown that a classically sampled distribution might pass the same statistical tests by only reproducing small-scale correlations of the actual theoretical distribution [309]. Moreover, a polynomial-time algorithm based on taking a truncated Fourier–Hermite expansion on the boson sampling distribution [309] may achieve similar or better sampling quality for the statistical methods of [308]. Another method for attaining similar sampling quality based on an algorithm of Clifford and Clifford [310] was also proposed [311]. Finally, very recently, a series of approximations were introduced to generate the probability distributions of any specific measurement outcome in a polynomial complexity [312]. The accuracy of the experiment was achieved at the fourth-order approximation using a laptop computer. The algorithm was tuned towards the actual experiment and applies only to the Gaussian boson sampling (not Fock-state boson sampling) [300], only for threshold detectors (not photon-counting detectors), and only for a small number of modes (not quadratic in the number of photons as in the original proposal [300]). Further experiments, however, reported nontrivial genuine high-order correlations in the GBS samples, which presented an evidence of robustness against possible classical simulation schemes [313].

So far, experimental implementations of GBS lack programmability (reconfigurability of the circuitry) or have prohibitive loss rates that limit the scalability. There is a need for rigorous theoretical evidence of the classical hardness of GBS, although some progress was recently made [314].

A more recent (2021) experiment by Xanadu and NIST attempted to remedy this [315]. The circuitry they implemented is programmable and potentially highly scalable. The system uses eight modes of strongly squeezed vacuum initialized as two-mode squeezed states in single temporal modes that pass through a fully programmable four-mode interferometer and photon number-resolving readout on all outputs. This technological advance was achieved by using strong squeezing and high sampling rates. The interferometer imple-

mented a user-programmable gate sequence based on a network of beam splitters and phase shifters. The resulting eight-mode Gaussian state is measured on the Fock basis using eight independent photon-number-resolving detectors. The total device was composed of a  $10\text{ mm} \times 4\text{ mm}$  photonic chip. The chip is coupled with a high-level application programming interface running on a classical computer.

There are many problems to overcome before the quantum sampling implemented on a quantum computer becomes useful for real-world applications. Photon losses need to be controlled and significantly decreased to enable photon travel through the circuitry to improve scalability. The improvement in the sampling fidelity and the quality of the squeezed states must be increased. The most exciting application would require individual control of the degree of squeezing and the amount of optical power in each squeezed state. The number of commercial applications that can be implemented using the current architecture is limited. Xanadu group implemented two potentially practical algorithms. By encoding the problems into the beam splitter network, they use the generated samples to determine energy spectra for transitions between molecular states and find the similarity between graph representations of different molecules. In particular, a graph can be encoded in a photonic circuit by mapping the graph’s adjacency matrix into the structure of a linear optical interferometer with squeezed light [316]. The photon-counting statistics can be used to specify so-called ”feature vectors”, which represent the graphs in Euclidean space [317] so that the distance between them can be used to quantify the similarity of the corresponding graphs. Such similarity measure between the graphs derived from a Gaussian boson sampling device is important, for instance, for classification in ML. Recently, other optical computing platforms based on squeezed states have been theoretically proposed on the route to a useful optical quantum computer [318, 319]; see Fig. 11.

## VII.2. Boson sampling and graph isomorphism

Using the light interference network for quantum analogue calculation has many practical advantages. We mentioned that operating with the boson sampling setup allows one to calculate the permanent of a specific matrix, which is extremely hard from the computational perspective. However, it is more complex to make this helpful computation and was an open question for some time with a few remaining debates. Recently the connection between a

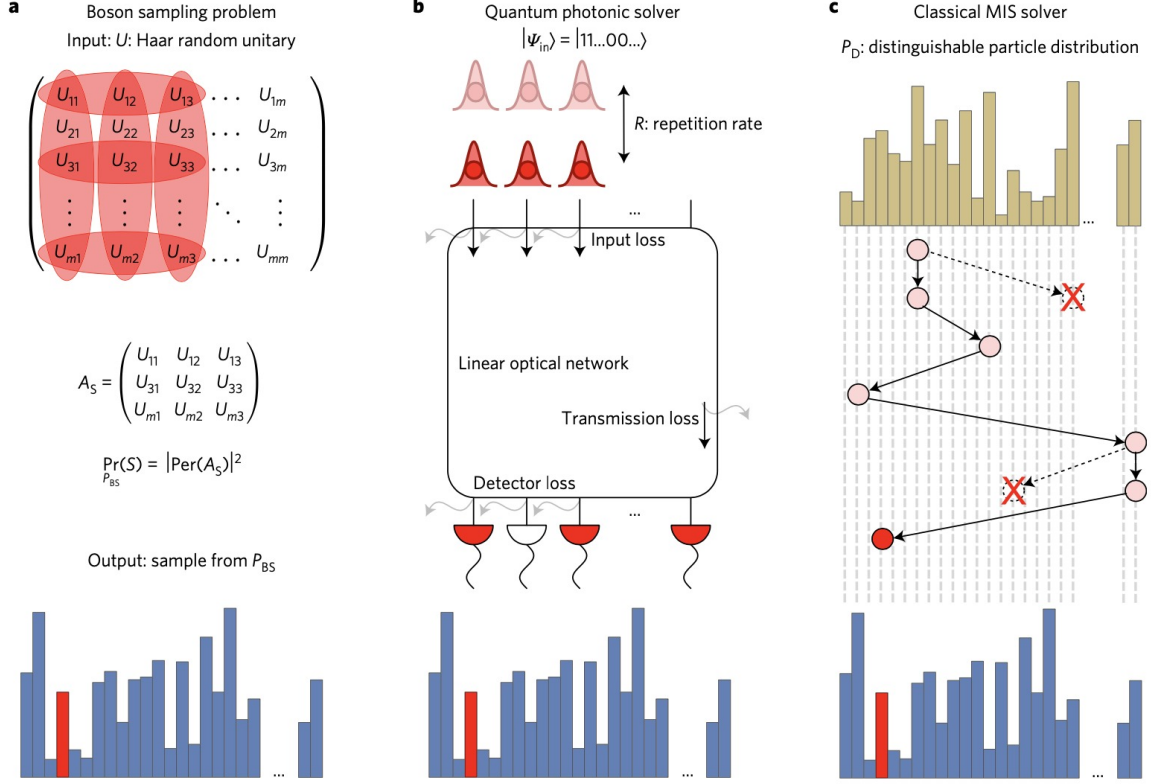


FIG. 11. a) Definition of the problem. Calculate the sample from the specific distribution defined by the modulus squared permanents of submatrices of a Haar random unitary matrix  $U$ . b) The scheme of the photonic experiments, i.e. single photons propagate through a linear optical network followed by its detection. c) A classical boson sampling algorithm based on Metropolis independence sampling using the distinguishable particle transition probabilities as the proposal distribution. Reproduced from [320] with permission.

Gaussian boson sampler and the graph isomorphism problem was established [321]. The graphs are encoded into quantum states of light, and then their properties are probed with photon-number-resolving detectors. Using a complete set of graph invariants, the authors prove that the probabilities in the setup can be combined, and the isomorphism between the two graphs can be established only in the case of equal detection probabilities on the output.

It is still an open question whether graph isomorphism has a specific complexity type. It is believed to belong to the class of  $\text{NP}$ -intermediate computational problems. The existence of a polynomial-time algorithm that can determine whether two graphs are isomorphic is under question; however, there are quasi-polynomial types of algorithms. One can find the recent advances in photonic boson sampling with the description of both the technological

improvements and future challenges [322]. The proposed connection between the graph isomorphism and boson sampling can be further extended to other practical tasks, such as constructing graph kernels for the ML applications operating with the graph-structured data [317].

### **VII.3. Quantum ML**

Programmable waveguide meshes can be configured to execute any linear transformation between sets of input and output waveguides. These operations are also at the core of photonic quantum computing. Here, the quantum information is represented by quantum states of light propagating through the photonic integrated circuits [323]. A typical scheme encodes a qubit as a single photon in a superposition of two rail waveguides [324]. Noisy intermediate-scale quantum (NISQ) devices have now shown potential in quantum ML that promises to process large data sets vastly faster than classical computers [325]. In these proposals, quantum ML parallels classical photonic deep NN accelerators: stages of linear waveguide meshes connected by activation layers. Still, these activation layers have strong reversible nonlinearities [326]. In such a ‘quantum optical neural network’ (QONN), programming a NISQ computer reduces to training the phases in the waveguide mesh through supervised learning on input and output quantum states. The QONN can be taught to perform a range of quantum information processing tasks, including quantum optical state compression and reinforcement learning. Recently, a QONN managed to program a one-way quantum repeater [326, 327]. However, these concepts and many other ideas in neural quantum architectures developed earlier are far from useful in practice with the current experiments state.

### **VII.4. Comparison with other quantum approaches to optimization**

As previously discussed, CIM has shown several orders of magnitude time-to-solution advantages compared to D-Wave2000Q quantum annealer on similar dense matrix instances. At the same time, the recent comparisons of (1) the quantum approximate optimization algorithm (QAOA) and two widely studied competing methods, quantum annealing and simulated annealing [328]; (2) the D-Wave2000Q quantum annealer with IBM Q Experi-



ence system that implements QAOA [329]; and (3) benchmarking of QAOA on Google "Sycamore" [330] allow us (to some extent) compare optical spin machines performance with QAOA.

In the QAOA, the variational wavefunction resembles a trotterised version of the quantum annealing procedure:

$$|\Psi(\beta, \gamma)\rangle = \prod_{i=1}^N e^{-i\beta_i H_0} e^{-i\gamma_i H_{\text{objective}}}, \quad (70)$$

where the starting state is  $|+\rangle$  is the product state of eigenstates of  $\sigma_x$  with eigenvalue 1,  $|+\rangle = \prod_i (|0\rangle_i + |1\rangle_i)/\sqrt{2}$  which is simultaneously the superposition of all computational basis states. In contrast to a trotterised version of quantum annealing, the parameters  $\beta_i$  and  $\gamma_i$  are adjusted in a classical learning loop to minimize the objective function. Such adjustments are considered as NP-hard problems themselves. As  $P \rightarrow \infty$ , QAOA approaches smooth QA. The results of [328] show that QAOA can deterministically find the solution of specially constructed optimization problems in cases where both quantum annealing and simulated annealing fail (wide and tall energy barriers of the function to be minimized). However, there exists an efficient classical algorithm for these instances.

In [329], small size (up to  $N = 18$ ) weighted Max-Cut problems and 2-SAT problems were tested using D-Wave2000Q quantum annealer with IBM Q Experience. The actual machine IBM Q on 16 qubits gave such poor solution quality that the real physical experiment on D-Wave200Q was compared to the simulation of QAOA. Even in this case, physical QA has shown much better success probabilities than QAOA (99.92 vs 8.84( $p = 1$ ) and 42.39( $p = 3$ ), respectively, on as small matrices as  $N = 8$ !) The conclusion was that for the set of problem instances considered, taking the success probability as a measure, "the QAOA cannot compete with quantum annealing". The corresponding plots can be found in Fig. 12.

In [330], the authors ran the Google Sycamore superconducting qubit quantum processor for combinatorial optimization problems with QAOA using the planar graph matching the hardware connectivity. They also applied the QAOA to the Sherrington-Kirkpatrick model and Max-Cut, both high-dimensional graph problems for which the QAOA requires significant compilation. The problems were solved up to  $N = 23$  numerically (without noise) and experimentally. For QAOA the theoretically optimal  $\beta, \gamma$  and  $p \in 1, 2, 3, 4, 5$  were used in experiments. The success probabilities on average of the problem on graph matching

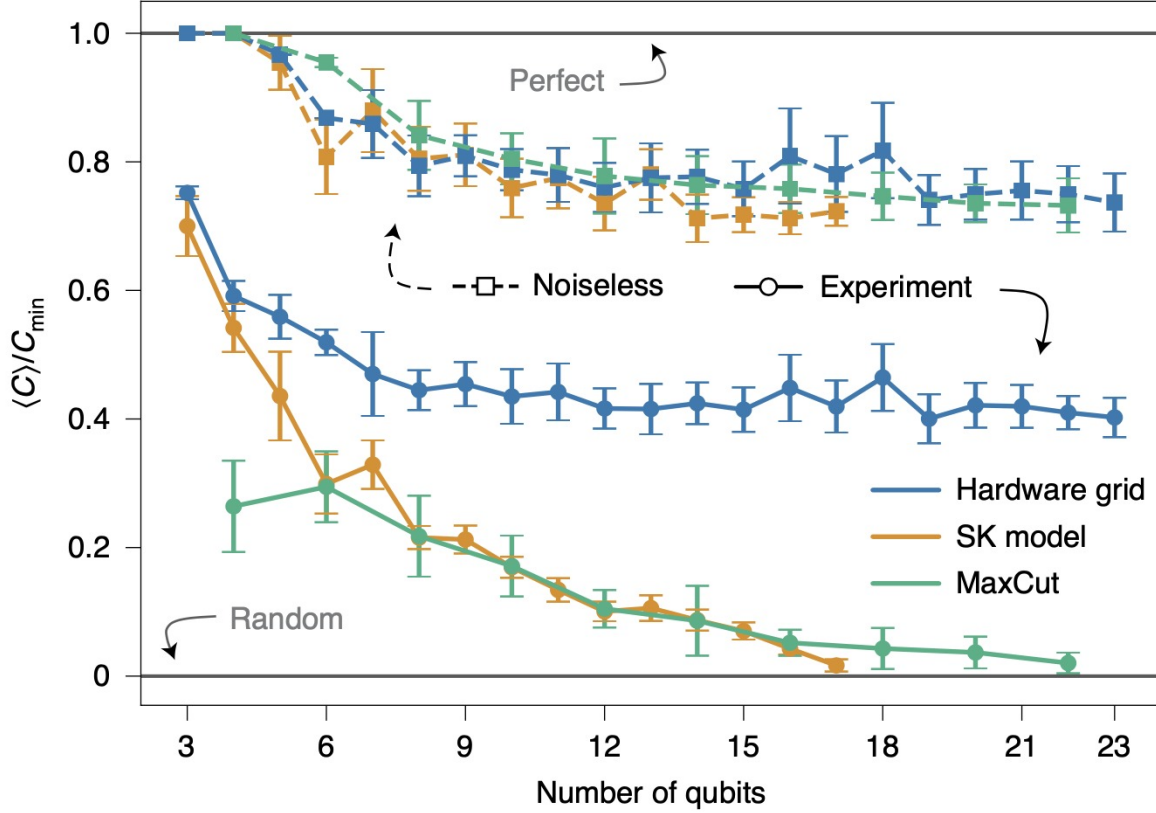


FIG. 12. The ratio of the found solution to the best solution when using QAOA for various problem sizes  $N$ . Each solution is averaged across ten random instances (standard deviation is given as error bars). The experimental solutions of the SK and Max-Cut models approach random as  $N$  increases. The figure is taken from [330].

hardware reached a plateau for  $N > 8$  at about 80 % (numerically) and about 45 % experimentally. For SK and Max-Cut problems, performance deteriorated quickly (for any  $p$ ) to the probability of finding a solution by random guessing (for  $N > 15$ ). The authors concluded that while no existing quantum processors can outperform classical optimization heuristics, applying popular methods such as the QAOA to prototypical problems can be a benchmark for comparing various hardware platforms. For quantum optimization to compete with classical methods for real-world problems, it is necessary to push beyond contrived problems at low circuit depth.

## VII.5. Quantum effects and optical machines

As we can see, various optical hardware uses different mechanisms for its operation. It can have the primary mechanism's pure classical, quantum, or hybrid nature. Even in the case of operating near the classical limit, the quantum effects can be essential and greatly influence the actual operation regime.

For example, it was shown that the nonlinear stochastic dynamics of the CIM in the presence of quantum noise could be efficiently exploited to sample degenerate ground and low-energy spin configurations of the Ising model on the example of Max-Cut problems [331]. Both quantum noise and optical nonlinearities play an essential role in system dynamics. Removing these essential elements will result in the degradation of sampling performance. The supplementary numerical results beyond the classical simulation complement the description of the quantum mechanism's role in the CIM operation. Another work [152] studies the performance scaling of three quantum algorithms for combinatorial optimization, such as CIM performance, discrete adiabatic quantum computation, and the Dürre-Høyer algorithm for quantum minimum finding that is based on Grover's search. Authors claim that the CIM performance is dramatically better for solving Max-Cut problems. Moreover, the CIM is competitive against various heuristic solvers implemented on CPUs, GPUs, and FPGAs.

Many optical devices fall under the category of open quantum systems. Such a formalism is necessary to account for many complicated effects. For this purpose, a Markovian open quantum systems framework has been developed [332, 333]. Such effective dynamics for the reduced density matrix of the system give rise to the Lindblad-form master equation, which allows one to trace such effects as equilibration with the pump and decay processes, thermalisation of the system and different aspects of interaction with the environment. Although the numerical methods for such processes are quite complicated, one usually develops approximated schemes that account for the omitted effects. There are many more systems where this approach could be beneficial for describing subtle but essential features—another example, except for the CIM, is the exciton-polariton system frequently mentioned before. Furthermore, one should pay attention to other microscopic processes in the EP system since such consideration gives more degrees of freedom to inspect compared to the simple mean-field theory [334–336].

## VIII. FINAL REMARKS

### VIII.1. Benchmarking optical machines

So far, the research and development of optical hardware are experiencing significant growth. The main problem is to compare the capabilities of optical machines as they are often tested on different problems of variable sizes and difficulty. Thus it is hard to figure out the scaling properties of the particular mechanism from either experiment or numerical emulation procedure. Another problem is lying in the biased results, which can be cherry-picked for better demonstrative purposes. In general, it is hard to find extensive, complete, up-to-date and unbiased results comparing different types of optical hardware.

Although the majority of the NN optical architectures can be compared using standard metrics concerning the accuracy of the particular datasets and the required workload, we outline what is known and how some of the optical machines can be compared. For example, in [337] comparisons between memristors, GPU, D-Wave and the CIMs were made using the same set of dense 60-node Max-Cut graphs. The time to solution (with 99 % probability to reach optimal solution) was  $600\mu$  s for the CIM and 1000 s for the D-Wave. In [117], it was reported that the Ising machine based on optoelectronic feedback systems solved Max-Cut optimization problems on regular and frustrated graphs with 100 spins showing similar or better performance compared to CIMs based on DOPOs. Since OEO-based CIMs can be implemented as integrated photonic circuits, the flexible spin coupling can be made optically with programmable silicon photonic circuits. This will take full advantage of the high bandwidth of the optical system and bring a significant speedup over existing CIM concepts.

Establishing universal benchmarks will attract more people since understanding the hardware's successes and failures on particular problems allows one to maximize utility. Moreover, such a research direction shares similar issues with the ongoing studies on the NN architectures and phase transitions in the statistical approaches to the computational problems [98], which is cross-beneficial for all of the domains.

### VIII.2. The most promising applications for optical computing

Our subjective perspective is that modern optical computing has the potential to give a significant computational advantage in three major applied areas: **Neural networks, Nonlinear optimization, and Statistical sampling.**

Optical hardware is a promising platform to get acceleration for these applications, with many computational advantages coming from the hybrid-quantum/classical mode of operation. The optics naturally supports these tasks but also benefit from many more factors, such as specific architectures and their interplay with the natural properties of light systems.

For example, a mode selection mechanism is one of the beneficial regimes of operation for a quantum system spanning a high-dimensional space of possible solutions and finding an optimal one while settling to the first possible coherent state with a large occupation. Another component is classical dynamical system behaviour that can mimic the NN dynamics, following the classical gradient dynamics on a changing energy landscape while tunnelling through barriers to the nearest energy minimum. The task is achieved if this minimum corresponds to the optimum solution to the problem. Finally, a similar mechanism is responsible for sampling the landscape's low-energy subspace.

### VIII.3. Future perspectives

The 'no free lunch' (NFL) theorem in optimisation states that any two optimisation algorithms have the same performance averaged across all possible problem instances. This theorem applies to the hardware instead of the algorithms with many more implications. One of the consequences of the NFL theorem is the correspondence between the solver/hardware structure and the hardness of the problem with the best-case and worst-case scenarios.

To use optical spin machines to speed up the solutions to specific industry real-life problems, one needs to think hard about the range of application that may go far from the QUBO. These application has to closely match the optical machine's operational principle to take advantage of all the potential advantages. Many questions need to be addressed before the optical spin machines become useful for the real-life applications. Which platforms should we use for comparison between different machines? What is the importance of optical

quantum vs classical, classical vs classical, hybrid vs classical, optical vs other physics-based hardware advantages? How does hardware performance compare to the best algorithms run on traditional systems? To answer these questions, we need to introduce a standard for fair comparisons between the machines and approaches. Which section of the workflow is more advantageous to optimize? Should sections that are closer to hardware or closer to a user be more important? How to properly optimise pre-processing and post-processing? How do we evaluate results and which metric should be used? The proximity between the found solutions of QUBO can be evaluated using, for instance, the Hamming distance, the distance in the energy space, the ratio of the energies, the accuracy of the neural architecture, or some other the generalisation of the error metrics can be used. How do we evaluate optimisation performance in several important dimensions, e.g. the computation time, the solution quality, the energy efficiency, the input scope, etc. all can be used for evaluation. How do we account for overheads concerning the given architecture and the task-specific constraints? How to optimize the implementation, translating, embedding, tuning, post-processing? How do we find inputs that are hard and relevant? How do we avoid using trivial ones? Drawing the possible phase diagrams should be built for the parametrised tasks. How do we maximise the generality of the conclusions, and to what extent if we can only test some combinations of inputs and hardware.

The advantage will come when we (i) develop purpose-built solutions tuned to specific applications, (ii) develop hybrid algorithms and approaches (e.g. including ML as a part of the hybrid solutions) and (iii) leverage programmable accelerators for core tasks. More research is needed to bring the potential of optical (or any other unconventional) computing systems to real-life applications. Answering the critical questions will bring us closer to a better understanding of the underlying principles of unconventional optical machines, improve their performance and hence achieve a significant practical impact.

## ACKNOWLEDGMENTS

N.G.B. thanks the Julian Schwinger Foundation grant JSF-19-02-0005 for the financial support.

---

- [1] G. E. Moore, “Cramming more components onto integrated circuits,” *Electronics*, vol. 38, April 1965.
- [2] G. E. Moore, M. Hill, N. Jouppi, and G. Sohi, “Readings in computer architecture,” *San Francisco, CA, USA: Morgan Kaufmann Publishers Inc*, pp. 56–59, 2000.
- [3] J. Von Neumann, “First draft of a report on the edvac,” *IEEE Annals of the History of Computing*, vol. 15, no. 4, pp. 27–75, 1993.
- [4] J. Edwards and S. O’Keefe, “Eager recirculating memory to alleviate the von neumann bottleneck,” in *2016 IEEE Symposium Series on Computational Intelligence (SSCI)*, pp. 1–5, IEEE, 2016.
- [5] M. Naylor and C. Runciman, “The reduceron: Widening the von neumann bottleneck for graph reduction using an fpga,” in *Symposium on Implementation and Application of Functional Languages*, pp. 129–146, Springer, 2007.
- [6] C. S. Lent, K. W. Henderson, S. A. Kandel, S. A. Corcelli, G. L. Snider, A. O. Orlov, P. M. Kogge, M. T. Niemier, R. C. Brown, J. A. Christie, *et al.*, “Molecular cellular networks: A non von neumann architecture for molecular electronics,” in *2016 IEEE International Conference on Rebooting Computing (ICRC)*, pp. 1–7, IEEE, 2016.
- [7] D. Shin and H.-J. Yoo, “The heterogeneous deep neural network processor with a non-von neumann architecture,” *Proceedings of the IEEE*, vol. 108, no. 8, pp. 1245–1260, 2019.
- [8] C. Li, X. Zhang, J. Li, T. Fang, and X. Dong, “The challenges of modern computing and new opportunities for optics,” *Photonix*, vol. 2, no. 1, pp. 1–31, 2021.
- [9] J. Wu, X. Lin, Y. Guo, J. Liu, L. Fang, S. Jiao, and Q. Dai, “Analog optical computing for artificial intelligence,” *Engineering*, 2021.
- [10] G. Genty, L. Salmela, J. M. Dudley, D. Brunner, A. Kokhanovskiy, S. Kobtsev, and S. K. Turitsyn, “Machine learning and applications in ultrafast photonics,” *Nature Photonics*, vol. 15, no. 2, pp. 91–101, 2021.

- [11] S. Xiang, Y. Han, Z. Song, X. Guo, Y. Zhang, Z. Ren, S. Wang, Y. Ma, W. Zou, B. Ma, *et al.*, “A review: Photonics devices, architectures, and algorithms for optical neural computing,” *Journal of Semiconductors*, vol. 42, no. 2, p. 023105, 2021.
- [12] Z. Chen and M. Segev, “Highlighting photonics: looking into the next decade,” *ELight*, vol. 1, no. 1, pp. 1–12, 2021.
- [13] B. J. Shastri, A. N. Tait, T. F. de Lima, W. H. Pernice, H. Bhaskaran, C. D. Wright, and P. R. Prucnal, “Photonics for artificial intelligence and neuromorphic computing,” *Nature Photonics*, vol. 15, no. 2, pp. 102–114, 2021.
- [14] G. Wetzstein, A. Ozcan, S. Gigan, S. Fan, D. Englund, M. Soljačić, C. Denz, D. A. Miller, and D. Psaltis, “Inference in artificial intelligence with deep optics and photonics,” *Nature*, vol. 588, no. 7836, pp. 39–47, 2020.
- [15] D. R. Solli and B. Jalali, “Analog optical computing,” *Nature Photonics*, vol. 9, no. 11, pp. 704–706, 2015.
- [16] P. Ambs, “Optical computing: A 60-year adventure,” *Advances in Optical Technologies*, 2010.
- [17] A. Maréchal and P. Croce, “Un filtre de fréquences spatiales pour lamélioration du contraste des images optiques,” *COMPTES RENDUS HEBDOMADAIRES DES SEANCES DE L ACADEMIE DES SCIENCES*, vol. 237, no. 12, pp. 607–609, 1953.
- [18] C. Weaver and J. W. Goodman, “A technique for optically convolving two functions,” *Applied optics*, vol. 5, no. 7, pp. 1248–1249, 1966.
- [19] E. Abbe, “Beiträge zur theorie des mikroskops und der mikroskopischen wahrnehmung,” *Archiv für mikroskopische Anatomie*, vol. 9, no. 1, pp. 413–468, 1873.
- [20] F. Zernike, “Diffraction theory of the knife-edge test and its improved form, the phase-contrast method,” *Monthly Notices of the Royal Astronomical Society*, vol. 94, pp. 377–384, 1934.
- [21] P. Elias, “Optics and communication theory,” *SPIE MILESTONE SERIES MS*, vol. 105, pp. 52–52, 1995.
- [22] P. Elias, D. S. Grey, and D. Z. Robinson, “Fourier treatment of optical processes,” *Josa*, vol. 42, no. 2, pp. 127–134, 1952.
- [23] D. Gabor, “A new microscopic principle,” *nature*, vol. 161, pp. 777–778, 1948.



- [24] T. Maiman, “Optical and microwave-optical experiments in ruby,” *Physical review letters*, vol. 4, no. 11, p. 564, 1960.
- [25] T. H. Maiman *et al.*, “Stimulated optical radiation in ruby,” 1960.
- [26] E. N. Leith and J. Upatnieks, “Wavefront reconstruction with continuous-tone objects,” *JOSA*, vol. 53, no. 12, pp. 1377–1381, 1963.
- [27] E. N. Leith and J. Upatnieks, “Wavefront reconstruction with diffused illumination and three-dimensional objects,” *Josa*, vol. 54, no. 11, pp. 1295–1301, 1964.
- [28] B. R. Brown and A. W. Lohmann, “Complex spatial filtering with binary masks,” *Applied optics*, vol. 5, no. 6, pp. 967–969, 1966.
- [29] A. W. Lohmann and D. Paris, “Binary fraunhofer holograms, generated by computer,” *Applied Optics*, vol. 6, no. 10, pp. 1739–1748, 1967.
- [30] F. Dumont, J. Hazan, and D. Rossier, “The phototitus optical converter,” *Philips Technical Review*, vol. 34, no. 10, pp. 274–287, 1974.
- [31] S. Iwasa, “Optical processing: a near real-time coherent system using two itek prom devices,” *Applied optics*, vol. 15, no. 6, pp. 1418–1424, 1976.
- [32] D. S. Oliver, “Real-time spatial modulators for optical/digital processing systems,” *Optical Engineering*, vol. 17, no. 3, p. 173288, 1978.
- [33] K. Jain and G. Pratt Jr, “Optical transistor,” *Applied Physics Letters*, vol. 28, no. 12, pp. 719–721, 1976.
- [34] R. Hauck and O. Bryngdahl, “Computer-generated holograms with pulse-density modulation,” *JOSA A*, vol. 1, no. 1, pp. 5–10, 1984.
- [35] T.-C. Poon, R. Juday, and T. Hara, “Spatial light modulators—research, development, and applications: introduction to the feature issue,” *Applied optics*, vol. 37, no. 32, pp. 7471–7471, 1998.
- [36] E. Abraham, C. T. Seaton, and S. D. Smith, “The optical computer,” *Scientific American*, vol. 248, no. 2, pp. 85–93, 1983.
- [37] D. J. Jackson, “Photonic processors: a systems approach,” *Applied optics*, vol. 33, no. 23, pp. 5451–5466, 1994.
- [38] R. S. Tucker, “The role of optics in computing,” *Nature Photonics*, vol. 4, no. 7, pp. 405–405, 2010.

- [39] W. Bogaerts, D. Pérez, J. Capmany, D. A. Miller, J. Poon, D. Englund, F. Morichetti, and A. Melloni, “Programmable photonic circuits,” *Nature*, vol. 586, no. 7828, pp. 207–216, 2020.
- [40] P. Singh, D. K. Tripathi, S. Jaiswal, and H. Dixit, “All-optical logic gates: Designs, classification, and comparison,” *Advances in Optical Technologies*, 2014.
- [41] V. Jandieri, R. Khomeriki, T. Onoprishvili, D. H. Werner, J. Berakdar, and D. Erni, “Functional all-optical logic gates for true time-domain signal processing in nonlinear photonic crystal waveguides,” *Optics Express*, vol. 28, no. 12, pp. 18317–18331, 2020.
- [42] P. Minzioni, C. Lacava, T. Tanabe, J. Dong, X. Hu, G. Csaba, W. Porod, G. Singh, A. E. Willner, A. Almaiman, *et al.*, “Roadmap on all-optical processing,” *Journal of Optics*, vol. 21, no. 6, p. 063001, 2019.
- [43] D. Woods and T. J. Naughton, “Optical computing,” *Applied Mathematics and Computation*, vol. 215, no. 4, pp. 1417–1430, 2009.
- [44] H. Wu and Q. Dai, “Artificial intelligence accelerated by light,” 2021.
- [45] E. G. Paek and D. Psaltis, “Optical associative memory using fourier transform holograms,” *Optical Engineering*, vol. 26, no. 5, p. 265428, 1987.
- [46] X. Lin, Y. Rivenson, N. T. Yardimci, M. Veli, Y. Luo, M. Jarrahi, and A. Ozcan, “All-optical machine learning using diffractive deep neural networks,” *Science*, vol. 361, no. 6406, pp. 1004–1008, 2018.
- [47] Y. Zuo, B. Li, Y. Zhao, Y. Jiang, Y.-C. Chen, P. Chen, G.-B. Jo, J. Liu, and S. Du, “All-optical neural network with nonlinear activation functions,” *Optica*, vol. 6, no. 9, pp. 1132–1137, 2019.
- [48] A. N. Tait, T. F. De Lima, E. Zhou, A. X. Wu, M. A. Nahmias, B. J. Shastri, and P. R. Prucnal, “Neuromorphic photonic networks using silicon photonic weight banks,” *Scientific reports*, vol. 7, no. 1, pp. 1–10, 2017.
- [49] Y. Shen, N. C. Harris, S. Skirlo, M. Prabhu, T. Baehr-Jones, M. Hochberg, X. Sun, S. Zhao, H. Larochelle, D. Englund, *et al.*, “Deep learning with coherent nanophotonic circuits,” *Nature Photonics*, vol. 11, no. 7, pp. 441–446, 2017.
- [50] H. Zhang, M. Gu, X. Jiang, J. Thompson, H. Cai, S. Paesani, R. Santagati, A. Laing, Y. Zhang, M. Yung, *et al.*, “An optical neural chip for implementing complex-valued neural network,” *Nature Communications*, vol. 12, no. 1, pp. 1–11, 2021.

- [51] R. Hamerly, L. Bernstein, A. Sludds, M. Soljačić, and D. Englund, “Large-scale optical neural networks based on photoelectric multiplication,” *Physical Review X*, vol. 9, no. 2, p. 021032, 2019.
- [52] K. Kravtsov, M. P. Fok, D. Rosenbluth, and P. R. Prucnal, “Ultrafast all-optical implementation of a leaky integrate-and-fire neuron,” *Optics express*, vol. 19, no. 3, pp. 2133–2147, 2011.
- [53] A. N. Tait, M. A. Nahmias, B. J. Shastri, and P. R. Prucnal, “Broadcast and weight: an integrated network for scalable photonic spike processing,” *Journal of Lightwave Technology*, vol. 32, no. 21, pp. 4029–4041, 2014.
- [54] J. M. Shainline, S. M. Buckley, R. P. Mirin, and S. W. Nam, “Superconducting optoelectronic circuits for neuromorphic computing,” *Physical Review Applied*, vol. 7, no. 3, p. 034013, 2017.
- [55] V. Bangari, B. A. Marquez, H. Miller, A. N. Tait, M. A. Nahmias, T. F. De Lima, H.-T. Peng, P. R. Prucnal, and B. J. Shastri, “Digital electronics and analog photonics for convolutional neural networks (deap-cnns),” *IEEE Journal of Selected Topics in Quantum Electronics*, vol. 26, no. 1, pp. 1–13, 2019.
- [56] J. Feldmann, N. Youngblood, C. D. Wright, H. Bhaskaran, and W. H. Pernice, “All-optical spiking neurosynaptic networks with self-learning capabilities,” *Nature*, vol. 569, no. 7755, pp. 208–214, 2019.
- [57] M. Reck, A. Zeilinger, H. J. Bernstein, and P. Bertani, “Experimental realization of any discrete unitary operator,” *Physical review letters*, vol. 73, no. 1, p. 58, 1994.
- [58] B. Gholipour, P. Bastock, C. Craig, K. Khan, D. Hewak, and C. Soci, “Amorphous metal-sulphide microfibers enable photonic synapses for brain-like computing,” *Advanced Optical Materials*, vol. 3, no. 5, pp. 635–641, 2015.
- [59] I. A. Williamson, T. W. Hughes, M. Minkov, B. Bartlett, S. Pai, and S. Fan, “Reprogrammable electro-optic nonlinear activation functions for optical neural networks,” *IEEE Journal of Selected Topics in Quantum Electronics*, vol. 26, no. 1, pp. 1–12, 2019.
- [60] A. N. McCaughan, V. B. Verma, S. M. Buckley, J. Allmaras, A. Kozorezov, A. Tait, S. Nam, and J. Shainline, “A superconducting thermal switch with ultrahigh impedance for interfacing superconductors to semiconductors,” *Nature electronics*, vol. 2, no. 10, pp. 451–456, 2019.
- [61] M. A. Nahmias, T. F. De Lima, A. N. Tait, H.-T. Peng, B. J. Shastri, and P. R. Prucnal, “Photonic multiply-accumulate operations for neural networks,” *IEEE Journal of Selected*

- Topics in Quantum Electronics*, vol. 26, no. 1, pp. 1–18, 2019.
- [62] K. Nozaki, S. Matsuo, T. Fujii, K. Takeda, A. Shinya, E. Kuramochi, and M. Notomi, “Femtofarad optoelectronic integration demonstrating energy-saving signal conversion and nonlinear functions,” *Nature Photonics*, vol. 13, no. 7, pp. 454–459, 2019.
  - [63] C. Ríos, M. Stegmaier, P. Hosseini, D. Wang, T. Scherer, C. D. Wright, H. Bhaskaran, and W. H. Pernice, “Integrated all-photonic non-volatile multi-level memory,” *Nature photonics*, vol. 9, no. 11, pp. 725–732, 2015.
  - [64] C. Ríos, N. Youngblood, Z. Cheng, M. Le Gallo, W. H. Pernice, C. D. Wright, A. Sebastian, and H. Bhaskaran, “In-memory computing on a photonic platform,” *Science advances*, vol. 5, no. 2, p. eaau5759, 2019.
  - [65] C. D. Schuman, T. E. Potok, R. M. Patton, J. D. Birdwell, M. E. Dean, G. S. Rose, and J. S. Plank, “A survey of neuromorphic computing and neural networks in hardware,” *arXiv preprint arXiv:1705.06963*, 2017.
  - [66] G. Tanaka, T. Yamane, J. B. Héroux, R. Nakane, N. Kanazawa, S. Takeda, H. Numata, D. Nakano, and A. Hirose, “Recent advances in physical reservoir computing: A review,” *Neural Networks*, vol. 115, pp. 100–123, 2019.
  - [67] W. Maass, T. Natschläger, and H. Markram, “Real-time computing without stable states: A new framework for neural computation based on perturbations,” *Neural computation*, vol. 14, no. 11, pp. 2531–2560, 2002.
  - [68] H. Jaeger, “The “echo state” approach to analysing and training recurrent neural networks—with an erratum note,” *Bonn, Germany: German National Research Center for Information Technology GMD Technical Report*, vol. 148, no. 34, p. 13, 2001.
  - [69] M. Nakajima, K. Tanaka, and T. Hashimoto, “Scalable reservoir computing on coherent linear photonic processor,” *Communications Physics*, vol. 4, no. 1, pp. 1–12, 2021.
  - [70] F. Duport, B. Schneider, A. Smerieri, M. Haelterman, and S. Massar, “All-optical reservoir computing,” *Optics express*, vol. 20, no. 20, pp. 22783–22795, 2012.
  - [71] C. Mesaritakis, A. Bogris, A. Kapsalis, and D. Syvridis, “High-speed all-optical pattern recognition of dispersive fourier images through a photonic reservoir computing subsystem,” *Optics letters*, vol. 40, no. 14, pp. 3416–3419, 2015.
  - [72] D. Brunner and I. Fischer, “Reconfigurable semiconductor laser networks based on diffractive coupling,” *Optics letters*, vol. 40, no. 16, pp. 3854–3857, 2015.

- [73] J. Bueno, S. Maktoobi, L. Froehly, I. Fischer, M. Jacquot, L. Larger, and D. Brunner, “Reinforcement learning in a large-scale photonic recurrent neural network,” *Optica*, vol. 5, no. 6, pp. 756–760, 2018.
- [74] Y. Paquot, F. Duport, A. Smerieri, J. Dambre, B. Schrauwen, M. Haelterman, and S. Massar, “Optoelectronic reservoir computing,” *Scientific reports*, vol. 2, no. 1, pp. 1–6, 2012.
- [75] L. Larger, M. C. Soriano, D. Brunner, L. Appeltant, J. M. Gutiérrez, L. Pesquera, C. R. Mirasso, and I. Fischer, “Photonic information processing beyond turing: an optoelectronic implementation of reservoir computing,” *Optics express*, vol. 20, no. 3, pp. 3241–3249, 2012.
- [76] R. Martinenghi, S. Rybalko, M. Jacquot, Y. K. Chembo, and L. Larger, “Photonic nonlinear transient computing with multiple-delay wavelength dynamics,” *Physical review letters*, vol. 108, no. 24, p. 244101, 2012.
- [77] M. C. Soriano, S. Ortín, D. Brunner, L. Larger, C. R. Mirasso, I. Fischer, and L. Pesquera, “Optoelectronic reservoir computing: tackling noise-induced performance degradation,” *Optics express*, vol. 21, no. 1, pp. 12–20, 2013.
- [78] S. Ortín, M. C. Soriano, L. Pesquera, D. Brunner, D. San-Martín, I. Fischer, C. Mirasso, and J. Gutiérrez, “A unified framework for reservoir computing and extreme learning machines based on a single time-delayed neuron,” *Scientific reports*, vol. 5, no. 1, pp. 1–11, 2015.
- [79] F. Duport, A. Smerieri, A. Akrou, M. Haelterman, and S. Massar, “Fully analogue photonic reservoir computer,” *Scientific reports*, vol. 6, no. 1, pp. 1–12, 2016.
- [80] G. Van der Sande, D. Brunner, and M. C. Soriano, “Advances in photonic reservoir computing,” *Nanophotonics*, vol. 6, no. 3, pp. 561–576, 2017.
- [81] G. E. Santoro, R. Martoňák, E. Tosatti, and R. Car, “Theory of quantum annealing of an ising spin glass,” *Science*, vol. 295, no. 5564, pp. 2427–2430, 2002.
- [82] E. Farhi, J. Goldstone, S. Gutmann, and M. Sipser, “Quantum computation by adiabatic evolution,” *arXiv preprint quant-ph/0001106*, 2000.
- [83] J. J. Hopfield, “Neural networks and physical systems with emergent collective computational abilities,” *Proceedings of the national academy of sciences*, vol. 79, no. 8, pp. 2554–2558, 1982.
- [84] A. Lucas, “Ising formulations of many np problems,” *Frontiers in Physics*, vol. 2, p. 5, 2014.
- [85] B. Molnár, F. Molnár, M. Varga, Z. Toroczkai, and M. Ercsey-Ravasz, “A continuous-time maxsat solver with high analog performance,” *Nature communications*, vol. 9, no. 1, p. 4864, 2018.

- [86] C. J. Burges, “Factoring as optimization,” *Microsoft Research MSR-TR-200*, 2002.
- [87] R. W. Harrison, “Phase problem in crystallography,” *JOSA a*, vol. 10, no. 5, pp. 1046–1055, 1993.
- [88] O. Bunk, A. Diaz, F. Pfeiffer, C. David, B. Schmitt, D. K. Satapathy, and J. F. Van Der Veen, “Diffractive imaging for periodic samples: retrieving one-dimensional concentration profiles across microfluidic channels,” *Acta Crystallographica Section A: Foundations of Crystallography*, vol. 63, no. 4, pp. 306–314, 2007.
- [89] J. Miao, T. Ishikawa, Q. Shen, and T. Earnest, “Extending x-ray crystallography to allow the imaging of noncrystalline materials, cells, and single protein complexes,” *Annu. Rev. Phys. Chem.*, vol. 59, pp. 387–410, 2008.
- [90] C. Tradonsky, I. Gershenzon, V. Pal, R. Chriki, A. Friesem, O. Raz, and N. Davidson, “Rapid laser solver for the phase retrieval problem,” *Science advances*, vol. 5, no. 10, p. eaax4530, 2019.
- [91] M. Ekeberg, C. Lövkvist, Y. Lan, M. Weigt, and E. Aurell, “Improved contact prediction in proteins: using pseudolikelihoods to infer potts models,” *Physical Review E*, vol. 87, no. 1, p. 012707, 2013.
- [92] N. Stroeve and N. G. Berloff, “Neural network architectures based on the classical xy model,” *Physical Review B*, vol. 104, no. 20, p. 205435, 2021.
- [93] F. Barahona, “On the computational complexity of ising spin glass models,” *Journal of Physics A: Mathematical and General*, vol. 15, no. 10, p. 3241, 1982.
- [94] G. De las Cuevas and T. S. Cubitt, “Simple universal models capture all classical spin physics,” *Science*, vol. 351, no. 6278, pp. 1180–1183, 2016.
- [95] K. P. Kalinin and N. G. Berloff, “Computational complexity continuum within ising formulation of np problems,” *Communications Physics*, vol. 5, no. 1, pp. 1–10, 2022.
- [96] L. Zdeborová, “Statistical physics of hard optimization problems,” *arXiv preprint arXiv:0806.4112*, 2008.
- [97] M. Mezard and A. Montanari, *Information, physics, and computation*. Oxford University Press, 2009.
- [98] L. Zdeborová and F. Krzakala, “Statistical physics of inference: Thresholds and algorithms,” *Advances in Physics*, vol. 65, no. 5, pp. 453–552, 2016.

- [99] F. Hamze, J. Raymond, C. A. Pattison, K. Biswas, and H. G. Katzgraber, “Wishart planted ensemble: A tunably rugged pairwise ising model with a first-order phase transition,” *Physical Review E*, vol. 101, no. 5, p. 052102, 2020.
- [100] M. X. Goemans and D. P. Williamson, “Approximation algorithms for max-3-cut and other problems via complex semidefinite programming,” *Journal of Computer and System Sciences*, vol. 68, no. 2, pp. 442–470, 2004.
- [101] S. Zhang and Y. Huang, “Complex quadratic optimization and semidefinite programming,” *SIAM Journal on Optimization*, vol. 16, no. 3, pp. 871–890, 2006.
- [102] N. Krislock, J. Malick, and F. Roupin, “Biqcrunch: A semidefinite branch-and-bound method for solving binary quadratic problems,” *ACM Transactions on Mathematical Software (TOMS)*, vol. 43, no. 4, p. 32, 2017.
- [103] F. Hamze, D. C. Jacob, A. J. Ochoa, D. Perera, W. Wang, and H. G. Katzgraber, “From near to eternity: spin-glass planting, tiling puzzles, and constraint-satisfaction problems,” *Physical Review E*, vol. 97, no. 4, p. 043303, 2018.
- [104] J. Hertz, A. Krogh, R. G. Palmer, and H. Horner, “Introduction to the theory of neural computation,” *Physics Today*, vol. 44, no. 12, p. 70, 1991.
- [105] H. Cao, R. Chriki, S. Bittner, A. A. Friesem, and N. Davidson, “Complex lasers with controllable coherence,” *Nature Reviews Physics*, p. 1, 2019.
- [106] D. Brunner, M. C. Soriano, C. R. Mirasso, and I. Fischer, “Parallel photonic information processing at gigabyte per second data rates using transient states,” *Nature communications*, vol. 4, p. 1364, 2013.
- [107] L. Bao, N.-H. Kim, L. J. Mawst, N. N. Elkin, V. N. Troshchieva, D. V. Vysotsky, and A. P. Napartovich, “Near-diffraction-limited coherent emission from large aperture antiguided vertical-cavity surface-emitting laser arrays,” *Applied physics letters*, vol. 84, no. 3, pp. 320–322, 2004.
- [108] F. Rogister, K. S. Thornburg Jr, L. Fabiny, M. Möller, and R. Roy, “Power-law spatial correlations in arrays of locally coupled lasers,” *Physical review letters*, vol. 92, no. 9, p. 093905, 2004.
- [109] V. Pal, C. Tradonsky, R. Chriki, A. A. Friesem, and N. Davidson, “Observing dissipative topological defects with coupled lasers,” *Physical review letters*, vol. 119, no. 1, p. 013902, 2017.

- [110] Y. Kuramoto, *Chemical oscillations, waves, and turbulence*. Courier Corporation, 2003.
- [111] Y. Kuramoto, “International symposium on mathematical problems in theoretical physics,” *Lecture notes in Physics*, vol. 30, p. 420, 1975.
- [112] H. K. Khalil, “Nonlinear systems,” *Upper Saddle River*, 2002.
- [113] P. L. McMahon, A. Marandi, Y. Haribara, R. Hamerly, C. Langrock, S. Tamate, T. Inagaki, H. Takesue, S. Utsunomiya, K. Aihara, *et al.*, “A fully programmable 100-spin coherent ising machine with all-to-all connections,” *Science*, vol. 354, no. 6312, pp. 614–617, 2016.
- [114] R. Hamerly, T. Inagaki, P. L. McMahon, D. Venturelli, A. Marandi, T. Onodera, E. Ng, C. Langrock, K. Inaba, T. Honjo, *et al.*, “Experimental investigation of performance differences between coherent ising machines and a quantum annealer,” *Science advances*, vol. 5, no. 5, p. eaau0823, 2019.
- [115] F. Böhm, T. Inagaki, K. Inaba, T. Honjo, K. Enbutsu, T. Umeki, R. Kasahara, and H. Takesue, “Understanding dynamics of coherent ising machines through simulation of large-scale 2d ising models,” *Nature communications*, vol. 9, no. 1, p. 5020, 2018.
- [116] Y. Haribara, H. Ishikawa, S. Utsunomiya, K. Aihara, and Y. Yamamoto, “Performance evaluation of coherent ising machines against classical neural networks,” *Quantum Science and Technology*, vol. 2, no. 4, p. 044002, 2017.
- [117] F. Böhm, G. Verschaffelt, and G. Van der Sande, “A poor man’s coherent ising machine based on opto-electronic feedback systems for solving optimization problems,” *Nature communications*, vol. 10, no. 1, pp. 1–9, 2019.
- [118] K. Takata, A. Marandi, and Y. Yamamoto, “Quantum correlation in degenerate optical parametric oscillators with mutual injections,” *Physical Review A*, vol. 92, no. 4, p. 043821, 2015.
- [119] T. Leleu, Y. Yamamoto, P. L. McMahon, and K. Aihara, “Destabilization of local minima in analog spin systems by correction of amplitude heterogeneity,” *Physical review letters*, vol. 122, no. 4, p. 040607, 2019.
- [120] A. D. King, W. Bernoudy, J. King, A. J. Berkley, and T. Lanting, “Emulating the coherent ising machine with a mean-field algorithm,” *arXiv preprint arXiv:1806.08422*, 2018.
- [121] M. Babaeian, D. T. Nguyen, V. Demir, M. Akbulut, P.-A. Blanche, Y. Kaneda, S. Guha, M. A. Neifeld, and N. Peyghambarian, “A single shot coherent ising machine based on a network of injection-locked multicore fiber lasers,” *Nature communications*, vol. 10, no. 1, 2019.



- pp. 1–11, 2019.
- [122] K. P. Kalinin and N. G. Berloff, “Global optimization of spin hamiltonians with gain-dissipative systems,” *Scientific reports*, vol. 8, no. 1, p. 17791, 2018.
  - [123] K. P. Kalinin and N. G. Berloff, “Networks of non-equilibrium condensates for global optimization,” *New Journal of Physics*, vol. 20, no. 11, p. 113023, 2018.
  - [124] D. Pierangeli, G. Marcucci, and C. Conti, “Large-scale photonic ising machine by spatial light modulation,” *Physical Review Letters*, vol. 122, no. 21, p. 213902, 2019.
  - [125] J. Kasprzak, M. Richard, S. Kundermann, A. Baas, P. Jeambrun, J. Keeling, F. Marchetti, M. Szymańska, R. André, J. Staehli, *et al.*, “Bose–einstein condensation of exciton polaritons,” *Nature*, vol. 443, no. 7110, p. 409, 2006.
  - [126] N. Berloff and J. Keeling, “Universality in modelling non-equilibrium pattern formation in polariton condensates,” in *Physics of Quantum Fluids*, pp. 19–38, Springer, 2013.
  - [127] J. Klaers, J. Schmitt, F. Vewinger, and M. Weitz, “Bose–einstein condensation of photons in an optical microcavity,” *Nature*, vol. 468, no. 7323, p. 545, 2010.
  - [128] J. Klaers, F. Vewinger, and M. Weitz, “Thermalization of a two-dimensional photonic gas in “a white wall” photon box,” *Nature Physics*, vol. 6, no. 7, p. 512, 2010.
  - [129] J. Klaers, J. Schmitt, T. Damm, F. Vewinger, and M. Weitz, “Bose–einstein condensation of paraxial light,” *Applied Physics B*, vol. 105, no. 1, p. 17, 2011.
  - [130] J. Schmitt, T. Damm, F. Vewinger, M. Weitz, and J. Klaers, “Thermalization of a two-dimensional photon gas in a polymeric host matrix,” *New Journal of Physics*, vol. 14, no. 7, p. 075019, 2012.
  - [131] H. Walther, B. T. Varcoe, B.-G. Englert, and T. Becker, “Cavity quantum electrodynamics,” *Reports on Progress in Physics*, vol. 69, no. 5, p. 1325, 2006.
  - [132] E. Wertz, L. Ferrier, D. Solnyshkov, R. Johne, D. Sanvitto, A. Lemaître, I. Sagnes, R. Grousson, A. V. Kavokin, P. Senellart, *et al.*, “Spontaneous formation and optical manipulation of extended polariton condensates,” *Nature physics*, vol. 6, no. 11, p. 860, 2010.
  - [133] F. Manni, K. G. Lagoudakis, T. C. H. Liew, R. André, and B. Deveaud-Plédran, “Spontaneous pattern formation in a polariton condensate,” *Physical review letters*, vol. 107, no. 10, p. 106401, 2011.
  - [134] G. Tosi, G. Christmann, N. Berloff, P. Tsotsis, T. Gao, Z. Hatzopoulos, P. Savvidis, and J. Baumberg, “Sculpting oscillators with light within a nonlinear quantum fluid,” *Nature*

- Physics*, vol. 8, no. 3, p. 190, 2012.
- [135] G. Tosi, G. Christmann, N. Berloff, P. Tsotsis, T. Gao, Z. Hatzopoulos, P. Savvidis, and J. Baumberg, “Geometrically locked vortex lattices in semiconductor quantum fluids,” *Nature communications*, vol. 3, p. 1243, 2012.
  - [136] N. G. Berloff, M. Silva, K. Kalinin, A. Askitopoulos, J. D. Töpfer, P. Cilibrizzi, W. Langbein, and P. G. Lagoudakis, “Realizing the classical xy hamiltonian in polariton simulators,” *Nature materials*, vol. 16, no. 11, p. 1120, 2017.
  - [137] C. Schneider, K. Winkler, M. Fraser, M. Kamp, Y. Yamamoto, E. Ostrovskaya, and S. Höfling, “Exciton-polariton trapping and potential landscape engineering,” *Reports on Progress in Physics*, vol. 80, no. 1, p. 016503, 2016.
  - [138] A. Amo and J. Bloch, “Exciton-polaritons in lattices: A non-linear photonic simulator,” *Comptes Rendus Physique*, vol. 17, no. 8, pp. 934–945, 2016.
  - [139] D. Dung, C. Kurtscheid, T. Damm, J. Schmitt, F. Vewinger, M. Weitz, and J. Klaers, “Variable potentials for thermalized light and coupled condensates,” *Nature Photonics*, vol. 11, no. 9, p. 565, 2017.
  - [140] K. P. Kalinin and N. G. Berloff, “Polaritonic network as a paradigm for dynamics of coupled oscillators,” *Physical Review B*, vol. 100, no. 24, p. 245306, 2019.
  - [141] K. P. Kalinin and N. G. Berloff, “Simulating ising and n-state planar potts models and external fields with nonequilibrium condensates,” *Physical review letters*, vol. 121, no. 23, p. 235302, 2018.
  - [142] N. Stroeve and N. G. Berloff, “Discrete polynomial optimization with coherent networks of condensates and complex coupling switching,” *Physical Review Letters*, vol. 126, no. 5, p. 050504, 2021.
  - [143] R. Lang and K. Kobayashi, “External optical feedback effects on semiconductor injection laser properties,” *IEEE journal of Quantum Electronics*, vol. 16, no. 3, pp. 347–355, 1980.
  - [144] J. A. Acebrón, L. L. Bonilla, C. J. P. Vicente, F. Ritort, and R. Spigler, “The kuramoto model: A simple paradigm for synchronization phenomena,” *Reviews of modern physics*, vol. 77, no. 1, p. 137, 2005.
  - [145] M. Syed and N. G. Berloff, “Physics-enhanced bifurcation optimisers: All you need is a canonical complex network,” *arXiv preprint arXiv:2207.11256*, 2022.

- [146] S. K. Vaddlamani, T. P. Xiao, and E. Yablonovitch, “Physics successfully implements lagrange multiplier optimization,” *Proceedings of the National Academy of Sciences*, vol. 117, no. 43, pp. 26639–26650, 2020.
- [147] B. T. Polyak, “Some methods of speeding up the convergence of iteration methods,” *Ussr computational mathematics and mathematical physics*, vol. 4, no. 5, pp. 1–17, 1964.
- [148] Y. Nesterov, “A method for unconstrained convex minimization problem with the rate of convergence  $O(1/k^2)$ ,” in *Doklady an ussr*, vol. 269, pp. 543–547, 1983.
- [149] Y. Kuramoto, “International symposium on mathematical problems in theoretical physics,” *Lecture notes in Physics*, vol. 30, p. 420, 1975.
- [150] Y. Kuramoto and T. Tsuzuki, “On the formation of dissipative structures in reaction-diffusion systems: Reductive perturbation approach,” *Progress of Theoretical Physics*, vol. 54, no. 3, pp. 687–699, 1975.
- [151] J. A. Acebrón, L. L. Bonilla, C. J. P. Vicente, F. Ritort, and R. Spigler, “The kuramoto model: A simple paradigm for synchronization phenomena,” *Reviews of modern physics*, vol. 77, no. 1, p. 137, 2005.
- [152] K. Sankar, A. Scherer, S. Kako, S. Reifenstein, N. Ghadermarzy, W. B. Krayenhoff, Y. Inui, E. Ng, T. Onodera, P. Ronagh, *et al.*, “Benchmark study of quantum algorithms for combinatorial optimization: unitary versus dissipative,” *arXiv preprint arXiv:2105.03528*, 2021.
- [153] Y. Inui and Y. Yamamoto, “Entanglement and photon anti-bunching in coupled non-degenerate parametric oscillators,” *Entropy*, vol. 23, no. 5, p. 624, 2021.
- [154] H. Goto, “Bifurcation-based adiabatic quantum computation with a nonlinear oscillator network,” *Scientific reports*, vol. 6, no. 1, pp. 1–8, 2016.
- [155] H. Goto, K. Tatsumura, and A. R. Dixon, “Combinatorial optimization by simulating adiabatic bifurcations in nonlinear hamiltonian systems,” *Science advances*, vol. 5, no. 4, p. eaav2372, 2019.
- [156] H. Goto, K. Endo, M. Suzuki, Y. Sakai, T. Kanao, Y. Hamakawa, R. Hidaka, M. Yamasaki, and K. Tatsumura, “High-performance combinatorial optimization based on classical mechanics,” *Science Advances*, vol. 7, no. 6, p. eabe7953, 2021.
- [157] H. Ramsauer, B. Schäfl, J. Lehner, P. Seidl, M. Widrich, T. Adler, L. Gruber, M. Holzleitner, M. Pavlović, G. K. Sandve, *et al.*, “Hopfield networks is all you need,” *arXiv preprint arXiv:2008.02217*, 2020.

- [158] D. Krotov and J. Hopfield, “Large associative memory problem in neurobiology and machine learning,” *arXiv preprint arXiv:2008.06996*, 2020.
- [159] J. E. Marsden and M. McCracken, *The Hopf bifurcation and its applications*, vol. 19. Springer Science & Business Media, 2012.
- [160] A. A. Andronov, *Theory of bifurcations of dynamic systems on a plane*. Israel Program for Scientific Translations;[available from the US Department . . . , 1971.
- [161] V. Pal, S. Mahler, C. Tradonsky, A. A. Friesem, and N. Davidson, “Rapid fair sampling of the x y spin hamiltonian with a laser simulator,” *Physical Review Research*, vol. 2, no. 3, p. 033008, 2020.
- [162] F. C. Hoppensteadt and E. M. Izhikevich, *Weakly connected neural networks*, vol. 126. Springer Science & Business Media, 1997.
- [163] F. C. Hoppensteadt and E. M. Izhikevich, “Synaptic organizations and dynamical properties of weakly connected neural oscillators,” *Biological cybernetics*, vol. 75, no. 2, pp. 117–127, 1996.
- [164] F. C. Hoppensteadt and E. M. Izhikevich, “Synaptic organizations and dynamical properties of weakly connected neural oscillators ii. learning phase information,” *Biological Cybernetics*, vol. 75, no. 2, pp. 129–135, 1996.
- [165] F. C. Hoppensteadt and E. M. Izhikevich, “Synchronization of mems resonators and mechanical neurocomputing,” *IEEE Transactions on Circuits and Systems I: Fundamental Theory and Applications*, vol. 48, no. 2, pp. 133–138, 2001.
- [166] T. Leleu, F. Khoiratee, T. Levi, R. Hamerly, T. Kohno, and K. Aihara, “Scaling advantage of chaotic amplitude control for high-performance combinatorial optimization,” *Communications Physics*, vol. 4, no. 1, pp. 1–10, 2021.
- [167] N. G. Berloff and B. V. Svistunov, “Scenario of strongly nonequilibrated bose-einstein condensation,” *Physical Review A*, vol. 66, no. 1, p. 013603, 2002.
- [168] D. O. Hebb and W. Penfield, “Human behavior after extensive bilateral removal from the frontal lobes,” *Archives of Neurology & Psychiatry*, vol. 44, no. 2, pp. 421–438, 1940.
- [169] D. O. Hebb, “Distinctive features of learning in the higher animal,” *Brain mechanisms and learning*, vol. 37, p. 46, 1961.
- [170] D. J. Amit, H. Gutfreund, and H. Sompolinsky, “Storing infinite numbers of patterns in a spin-glass model of neural networks,” *Physical Review Letters*, vol. 55, no. 14, p. 1530, 1985.

- [171] R. McEliece, E. Posner, E. Rodemich, and S. Venkatesh, “The capacity of the hopfield associative memory,” *IEEE transactions on Information Theory*, vol. 33, no. 4, pp. 461–482, 1987.
- [172] I. Kanter and H. Sompolinsky, “Associative recall of memory without errors,” *Physical Review A*, vol. 35, no. 1, p. 380, 1987.
- [173] E. Ising, “Contribution to the theory of ferromagnetism,” *Z. Phys*, vol. 31, no. 1, pp. 253–258, 1925.
- [174] R. M. Karp, “Reducibility among combinatorial problems,” in *Complexity of computer computations*, pp. 85–103, Springer, 1972.
- [175] J. J. Hopfield and D. W. Tank, ““neural” computation of decisions in optimization problems,” *Biological cybernetics*, vol. 52, no. 3, pp. 141–152, 1985.
- [176] D. Krotov and J. Hopfield, “Dense associative memory is robust to adversarial inputs,” *Neural computation*, vol. 30, no. 12, pp. 3151–3167, 2018.
- [177] M. Fernández-Delgado, E. Cernadas, S. Barro, and D. Amorim, “Do we need hundreds of classifiers to solve real world classification problems?,” *The journal of machine learning research*, vol. 15, no. 1, pp. 3133–3181, 2014.
- [178] G. Klambauer, T. Unterthiner, A. Mayr, and S. Hochreiter, “Self-normalizing neural networks,” in *Proceedings of the 31st international conference on neural information processing systems*, pp. 972–981, 2017.
- [179] M. Leonetti, E. Hörmann, L. Leuzzi, G. Parisi, and G. Ruocco, “Optical computation of a spin glass dynamics with tunable complexity,” *Proceedings of the National Academy of Sciences*, vol. 118, no. 21, 2021.
- [180] B. P. Marsh, Y. Guo, R. M. Kroeze, S. Gopalakrishnan, S. Ganguli, J. Keeling, and B. L. Lev, “Enhancing associative memory recall and storage capacity using confocal cavity qed,” *Physical Review X*, vol. 11, no. 2, p. 021048, 2021.
- [181] B. P. Marsh, Y. Guo, R. M. Kroeze, S. Gopalakrishnan, S. Ganguli, J. Keeling, and B. L. Lev, “Enhancing associative memory recall and storage capacity using confocal cavity qed,” *Physical Review X*, vol. 11, no. 2, p. 021048, 2021.
- [182] D. Krotov and J. J. Hopfield, “Dense associative memory for pattern recognition,” *Advances in neural information processing systems*, vol. 29, pp. 1172–1180, 2016.

- [183] G. Joya, M. Atencia, and F. Sandoval, “Hopfield neural networks for optimization: study of the different dynamics,” *Neurocomputing*, vol. 43, no. 1-4, pp. 219–237, 2002.
- [184] S. A. Cook, “The complexity of theorem-proving procedures,” in *Proceedings of the third annual ACM symposium on Theory of computing*, pp. 151–158, 1971.
- [185] M. R. Garey, D. S. Johnson, and L. Stockmeyer, “Some simplified np-complete problems,” in *Proceedings of the sixth annual ACM symposium on Theory of computing*, pp. 47–63, 1974.
- [186] H. Markowitz, “Portfolio selection in the journal of finance vol. 7,” 1952.
- [187] A. Fernández and S. Gómez, “Portfolio selection using neural networks,” *Computers & Operations Research*, vol. 34, no. 4, pp. 1177–1191, 2007.
- [188] A. N. Sadigh, H. Mokhtari, M. Iranpoor, and S. Ghomi, “Cardinality constrained portfolio optimization using a hybrid approach based on particle swarm optimization and hopfield neural network,” *Advanced Science Letters*, vol. 17, no. 1, pp. 11–20, 2012.
- [189] I. Waldspurger, A. d’Aspremont, and S. Mallat, “Phase recovery, maxcut and complex semidefinite programming,” *Mathematical Programming*, vol. 149, no. 1-2, pp. 47–81, 2015.
- [190] E. Fix, *Discriminatory analysis: nonparametric discrimination, consistency properties*, vol. 1. USAF school of Aviation Medicine, 1985.
- [191] N. S. Altman, “An introduction to kernel and nearest-neighbor nonparametric regression,” *The American Statistician*, vol. 46, no. 3, pp. 175–185, 1992.
- [192] V. Vapnik and A. Y. Lerner, “Recognition of patterns with help of generalized portraits,” *Avtomat. i Telemekh*, vol. 24, no. 6, pp. 774–780, 1963.
- [193] C. Cortes and V. Vapnik, “Support-vector networks,” *Machine learning*, vol. 20, no. 3, pp. 273–297, 1995.
- [194] S. Brin and L. Page, “The anatomy of a large-scale hypertextual web search engine,” 1998.
- [195] L. Page, S. Brin, R. Motwani, and T. Winograd, “The pagerank citation ranking: Bringing order to the web,” tech. rep., Stanford InfoLab, 1999.
- [196] L. Ermann, K. M. Frahm, and D. L. Shepelyansky, “Google matrix analysis of directed networks,” *Reviews of modern physics*, vol. 87, no. 4, p. 1261, 2015.
- [197] D. F. Gleich, “Pagerank beyond the web,” *SIAM Review*, vol. 57, no. 3, pp. 321–363, 2015.
- [198] K. P. Kalinin and N. G. Berloff, “Large-scale sustainable search on unconventional computing hardware,” *arXiv preprint arXiv:2104.02553*, 2021.

- [199] M. Kim, R. Sumbaly, and S. Shah, “Root cause detection in a service-oriented architecture,” *ACM SIGMETRICS Performance Evaluation Review*, vol. 41, no. 1, pp. 93–104, 2013.
- [200] B. Jiang, S. Zhao, and J. Yin, “Self-organized natural roads for predicting traffic flow: a sensitivity study,” *Journal of statistical mechanics: Theory and experiment*, vol. 2008, no. 07, p. P07008, 2008.
- [201] S. V. Aiyer, M. Niranjan, and F. Fallside, “A theoretical investigation into the performance of the hopfield model,” *IEEE transactions on neural networks*, vol. 1, no. 2, pp. 204–215, 1990.
- [202] L. Van Der Maaten, E. Postma, and J. Van den Herik, “Dimensionality reduction: a comparative,” *J Mach Learn Res*, vol. 10, no. 66-71, p. 13, 2009.
- [203] C. O. S. Sorzano, J. Vargas, and A. P. Montano, “A survey of dimensionality reduction techniques,” *arXiv preprint arXiv:1403.2877*, 2014.
- [204] B. Sarwar, G. Karypis, J. Konstan, and J. Riedl, “Application of dimensionality reduction in recommender system-a case study,” tech. rep., Minnesota Univ Minneapolis Dept of Computer Science, 2000.
- [205] R. Jensen and Q. Shen, “Semantics-preserving dimensionality reduction: rough and fuzzy-rough-based approaches,” *IEEE Transactions on knowledge and data engineering*, vol. 16, no. 12, pp. 1457–1471, 2004.
- [206] K. Pearson, “Liii. on lines and planes of closest fit to systems of points in space,” *The London, Edinburgh, and Dublin Philosophical Magazine and Journal of Science*, vol. 2, no. 11, pp. 559–572, 1901.
- [207] T. Hofmann, “Learning the similarity of documents: An information-geometric approach to document retrieval and categorization,” in *Advances in neural information processing systems*, pp. 914–920, 2000.
- [208] T. K. Landauer, “Lsa as a theory of meaning,” *Handbook of latent semantic analysis*, vol. 3, p. 32, 2007.
- [209] S. Lloyd, “Least squares quantization in pcm,” *IEEE transactions on information theory*, vol. 28, no. 2, pp. 129–137, 1982.
- [210] H. Steinhaus, “Sur la division des corps matériels en parties,” *Bull. Acad. Polon. Sci*, vol. 1, no. 804, p. 801, 1956.

- [211] J. MacQueen *et al.*, “Some methods for classification and analysis of multivariate observations,” in *Proceedings of the fifth Berkeley symposium on mathematical statistics and probability*, vol. 1, pp. 281–297, Oakland, CA, USA, 1967.
- [212] K. Gurney, *An introduction to neural networks*. CRC press, 1997.
- [213] J. A. Anderson, *An introduction to neural networks*. MIT press, 1995.
- [214] B. Kröse, B. Krose, P. van der Smagt, and P. Smagt, “An introduction to neural networks,” 1993.
- [215] B. Yegnanarayana, *Artificial neural networks*. PHI Learning Pvt. Ltd., 2009.
- [216] I. Goodfellow, Y. Bengio, and A. Courville, *Deep learning*. MIT press, 2016.
- [217] G. Cybenko, “Approximation by superpositions of a sigmoidal function,” *Mathematics of control, signals and systems*, vol. 2, no. 4, pp. 303–314, 1989.
- [218] R. Hecht-Nielsen, “Theory of the backpropagation neural network,” in *Neural networks for perception*, pp. 65–93, Elsevier, 1992.
- [219] Y. Chauvin and D. E. Rumelhart, *Backpropagation: theory, architectures, and applications*. Psychology press, 1995.
- [220] J. Ba and R. Caruana, “Do deep nets really need to be deep?,” *Advances in neural information processing systems*, vol. 27, 2014.
- [221] T. Poggio, H. Mhaskar, L. Rosasco, B. Miranda, and Q. Liao, “Why and when can deep-but not shallow-networks avoid the curse of dimensionality: a review,” *International Journal of Automation and Computing*, vol. 14, no. 5, pp. 503–519, 2017.
- [222] H. N. Mhaskar and T. Poggio, “Deep vs. shallow networks: An approximation theory perspective,” *Analysis and Applications*, vol. 14, no. 06, pp. 829–848, 2016.
- [223] V. Khrulkov, A. Novikov, and I. Oseledets, “Expressive power of recurrent neural networks,” *arXiv preprint arXiv:1711.00811*, 2017.
- [224] K. Kashinath, M. Mustafa, A. Albert, J. Wu, C. Jiang, S. Esmaeilzadeh, K. Azizzadenesheli, R. Wang, A. Chattopadhyay, A. Singh, *et al.*, “Physics-informed machine learning: case studies for weather and climate modelling,” *Philosophical Transactions of the Royal Society A*, vol. 379, no. 2194, p. 20200093, 2021.
- [225] J.-L. Wu, H. Xiao, and E. Paterson, “Physics-informed machine learning approach for augmenting turbulence models: A comprehensive framework,” *Physical Review Fluids*, vol. 3, no. 7, p. 074602, 2018.



- [226] A. T. Mohan, D. Tretiak, M. Chertkov, and D. Livescu, “Spatio-temporal deep learning models of 3d turbulence with physics informed diagnostics,” *Journal of Turbulence*, vol. 21, no. 9-10, pp. 484–524, 2020.
- [227] W. Chen, Q. Wang, J. S. Hesthaven, and C. Zhang, “Physics-informed machine learning for reduced-order modeling of nonlinear problems,” *Journal of Computational Physics*, vol. 446, p. 110666, 2021.
- [228] G. E. Karniadakis, I. G. Kevrekidis, L. Lu, P. Perdikaris, S. Wang, and L. Yang, “Physics-informed machine learning,” *Nature Reviews Physics*, vol. 3, no. 6, pp. 422–440, 2021.
- [229] S. L. Brunton, M. Budišić, E. Kaiser, and J. N. Kutz, “Modern koopman theory for dynamical systems,” *SIAM Review*, vol. 64, no. 2, pp. 229–340, 2022.
- [230] E. Celledoni, M. J. Ehrhardt, C. Etmann, R. I. McLachlan, B. Owren, C.-B. SCHONLIEB, and F. Sherry, “Structure-preserving deep learning,” *European Journal of Applied Mathematics*, vol. 32, no. 5, pp. 888–936, 2021.
- [231] E. Weinan, “A proposal on machine learning via dynamical systems,” *Communications in Mathematics and Statistics*, vol. 1, no. 5, pp. 1–11, 2017.
- [232] A. Bravetti, M. L. Daza-Torres, H. Flores-Arguedas, and M. Betancourt, “Optimization algorithms inspired by the geometry of dissipative systems,” *arXiv preprint arXiv:1912.02928*, 2019.
- [233] K. Murphy, “An introduction to graphical models,” *Rap. tech*, vol. 96, pp. 1–19, 2001.
- [234] S. L. Lauritzen, *Graphical models*, vol. 17. Clarendon Press, 1996.
- [235] M. I. Jordan, “Graphical models,” *Statistical science*, vol. 19, no. 1, pp. 140–155, 2004.
- [236] R. G. Cowell, P. Dawid, S. L. Lauritzen, and D. J. Spiegelhalter, *Probabilistic networks and expert systems: Exact computational methods for Bayesian networks*. Springer Science & Business Media, 2006.
- [237] M. Kearns, M. Littman, and S. Singh, “Graphical models for game theory uai-01: Proc. 17th conf. annual conf. on uncertainty in artificial intelligence,” 2001.
- [238] P. Wang, C. Shen, A. van den Hengel, and P. H. Torr, “Large-scale binary quadratic optimization using semidefinite relaxation and applications,” *IEEE transactions on pattern analysis and machine intelligence*, vol. 39, no. 3, pp. 470–485, 2016.
- [239] A. Joulin, F. Bach, and J. Ponce, “Discriminative clustering for image co-segmentation,” in *2010 IEEE Computer Society Conference on Computer Vision and Pattern Recognition*,

- pp. 1943–1950, IEEE, 2010.
- [240] C. Schellewald and C. Schnörr, “Probabilistic subgraph matching based on convex relaxation,” in *International Workshop on Energy Minimization Methods in Computer Vision and Pattern Recognition*, pp. 171–186, Springer, 2005.
  - [241] Y.-j. Lee, M. B. On, X. Xiao, R. Proietti, and S. Yoo, “Izhikevich-inspired optoelectronic neurons with excitatory and inhibitory inputs for energy-efficient photonic spiking neural networks,” *arXiv preprint arXiv:2105.02809*, 2021.
  - [242] Y. Sun, N. B. Agostini, S. Dong, and D. Kaeli, “Summarizing cpu and gpu design trends with product data,” *arXiv preprint arXiv:1911.11313*, 2019.
  - [243] E. Nurvitadhi, G. Venkatesh, J. Sim, D. Marr, R. Huang, J. Ong Gee Hock, Y. T. Liew, K. Srivatsan, D. Moss, S. Subhaschandra, *et al.*, “Can fpgas beat gpus in accelerating next-generation deep neural networks?,” in *Proceedings of the 2017 ACM/SIGDA International Symposium on Field-Programmable Gate Arrays*, pp. 5–14, 2017.
  - [244] N. P. Jouppi, C. Young, N. Patil, D. Patterson, G. Agrawal, R. Bajwa, S. Bates, S. Bhatia, N. Boden, A. Borchers, *et al.*, “In-datacenter performance analysis of a tensor processing unit,” in *Proceedings of the 44th annual international symposium on computer architecture*, pp. 1–12, 2017.
  - [245] H. Jeong and L. Shi, “Memristor devices for neural networks,” *Journal of Physics D: Applied Physics*, vol. 52, no. 2, p. 023003, 2018.
  - [246] P. A. Merolla, J. V. Arthur, R. Alvarez-Icaza, A. S. Cassidy, J. Sawada, F. Akopyan, B. L. Jackson, N. Imam, C. Guo, Y. Nakamura, *et al.*, “A million spiking-neuron integrated circuit with a scalable communication network and interface,” *Science*, vol. 345, no. 6197, pp. 668–673, 2014.
  - [247] M. Davies, N. Srinivasa, T.-H. Lin, G. Chinya, Y. Cao, S. H. Choday, G. Dimou, P. Joshi, N. Imam, S. Jain, *et al.*, “Loihi: A neuromorphic manycore processor with on-chip learning,” *Ieee Micro*, vol. 38, no. 1, pp. 82–99, 2018.
  - [248] B. V. Benjamin, P. Gao, E. McQuinn, S. Choudhary, A. R. Chandrasekaran, J.-M. Bussat, R. Alvarez-Icaza, J. V. Arthur, P. A. Merolla, and K. Boahen, “Neurogrid: A mixed-analog-digital multichip system for large-scale neural simulations,” *Proceedings of the IEEE*, vol. 102, no. 5, pp. 699–716, 2014.
  - [249] E. M. Izhikevich, *Dynamical systems in neuroscience*. MIT press, 2007.

- [250] C. V. Poulton, M. J. Byrd, P. Russo, E. Timurdogan, M. Khandaker, D. Vermeulen, and M. R. Watts, “Long-range lidar and free-space data communication with high-performance optical phased arrays,” *IEEE Journal of Selected Topics in Quantum Electronics*, vol. 25, no. 5, pp. 1–8, 2019.
- [251] S. W. Keckler, W. J. Dally, B. Khailany, M. Garland, and D. Glasco, “Gpus and the future of parallel computing,” *IEEE micro*, vol. 31, no. 5, pp. 7–17, 2011.
- [252] V. Sze, Y.-H. Chen, T.-J. Yang, and J. S. Emer, “Efficient processing of deep neural networks: A tutorial and survey,” *Proceedings of the IEEE*, vol. 105, no. 12, pp. 2295–2329, 2017.
- [253] T. Wang, S.-Y. Ma, L. G. Wright, T. Onodera, B. C. Richard, and P. L. McMahon, “An optical neural network using less than 1 photon per multiplication,” *Nature Communications*, vol. 13, no. 1, pp. 1–8, 2022.
- [254] X. Xiao, M. B. On, T. Van Vaerenbergh, D. Liang, R. G. Beausoleil, and S. B. Yoo, “Large-scale and energy-efficient tensorized optical neural networks on iii–v-on-silicon moscap platform,” *APL Photonics*, vol. 6, no. 12, p. 126107, 2021.
- [255] K. Tyszka, M. Furman, R. Mirek, M. Król, A. Opala, B. Seredyński, J. Suffczyński, W. Pacuski, M. Matuszewski, J. Szczytko, *et al.*, “Leaky integrate-and-fire mechanism in exciton-polariton condensates for photonic spiking neurons,” *arXiv preprint arXiv:2111.13123*, 2021.
- [256] A. Opala, S. Ghosh, T. C. Liew, and M. Matuszewski, “Neuromorphic computing in ginzburg-landau polariton-lattice systems,” *Physical Review Applied*, vol. 11, no. 6, p. 064029, 2019.
- [257] J. W. Goodman, A. Dias, and L. Woody, “Fully parallel, high-speed incoherent optical method for performing discrete fourier transforms,” *Optics Letters*, vol. 2, no. 1, pp. 1–3, 1978.
- [258] D. E. Tamir, N. T. Shaked, P. J. Wilson, and S. Dolev, “High-speed and low-power electro-optical dsp coprocessor,” *JOSA A*, vol. 26, no. 8, pp. A11–A20, 2009.
- [259] C. Ramey, “Silicon photonics for artificial intelligence acceleration: Hotchips 32,” in *2020 IEEE hot chips 32 symposium (HCS)*, pp. 1–26, IEEE, 2020.
- [260] J. Feldmann, N. Youngblood, M. Karpov, H. Gehring, X. Li, M. Stappers, M. Le Gallo, X. Fu, A. Lukashchuk, A. S. Raja, *et al.*, “Parallel convolutional processing using an integrated photonic tensor core,” *Nature*, vol. 589, no. 7840, pp. 52–58, 2021.
- [261] X. Xu, M. Tan, B. Corcoran, J. Wu, A. Boes, T. G. Nguyen, S. T. Chu, B. E. Little, D. G. Hicks, R. Morandotti, *et al.*, “11 tops photonic convolutional accelerator for optical neural

- networks,” *Nature*, vol. 589, no. 7840, pp. 44–51, 2021.
- [262] K. Vandoorne, P. Mechet, T. Van Vaerenbergh, M. Fiers, G. Morthier, D. Verstraeten, B. Schrauwen, J. Dambre, and P. Bienstman, “Experimental demonstration of reservoir computing on a silicon photonics chip,” *Nature communications*, vol. 5, no. 1, pp. 1–6, 2014.
- [263] T. Inagaki, Y. Haribara, K. Igarashi, T. Sonobe, S. Tamate, T. Honjo, A. Marandi, P. L. McMahon, T. Umeki, K. Enbutsu, *et al.*, “A coherent ising machine for 2000-node optimization problems,” *Science*, vol. 354, no. 6312, pp. 603–606, 2016.
- [264] Z. Zhu, A. J. Ochoa, and H. G. Katzgraber, “Fair sampling of ground-state configurations of binary optimization problems,” *Physical Review E*, vol. 99, no. 6, p. 063314, 2019.
- [265] G. E. Hinton, “Training products of experts by minimizing contrastive divergence,” *Neural computation*, vol. 14, no. 8, pp. 1771–1800, 2002.
- [266] H. Sakaguchi, K. Ogata, T. Isomura, S. Utsunomiya, Y. Yamamoto, and K. Aihara, “Boltzmann sampling by degenerate optical parametric oscillator network for structure-based virtual screening,” *Entropy*, vol. 18, no. 10, p. 365, 2016.
- [267] Z. Bian, F. Chudak, R. B. Israel, B. Lackey, W. G. Macready, and A. Roy, “Mapping constrained optimization problems to quantum annealing with application to fault diagnosis,” *Frontiers in ICT*, vol. 3, p. 14, 2016.
- [268] E. Ng, T. Onodera, S. Kako, P. L. McMahon, H. Mabuchi, and Y. Yamamoto, “Efficient sampling of ground and low-energy ising spin configurations with a coherent ising machine,” *Physical Review Research*, vol. 4, no. 1, p. 013009, 2022.
- [269] T. Leleu, Y. Yamamoto, S. Utsunomiya, and K. Aihara, “Combinatorial optimization using dynamical phase transitions in driven-dissipative systems,” *Physical Review E*, vol. 95, no. 2, p. 022118, 2017.
- [270] H. Goto, K. Tatsumura, and A. R. Dixon, “Combinatorial optimization by simulating adiabatic bifurcations in nonlinear hamiltonian systems,” *Science advances*, vol. 5, no. 4, p. eaav2372, 2019.
- [271] E. S. Tiunov, A. E. Ulanov, and A. Lvovsky, “Annealing by simulating the coherent ising machine,” *Optics express*, vol. 27, no. 7, pp. 10288–10295, 2019.
- [272] F. Bontempi, S. Pinna, N. Andriolli, A. Bogoni, X. J. Leijtens, J. Bolk, and G. Contestabile, “Multifunctional current-controlled inp photonic integrated delay interferometer,” *IEEE Journal of Quantum Electronics*, vol. 48, no. 11, pp. 1453–1461, 2012.

- [273] D. Ballarini, M. De Giorgi, E. Cancellieri, R. Houdré, E. Giacobino, R. Cingolani, A. Bramati, G. Gigli, and D. Sanvitto, “All-optical polariton transistor,” *Nature communications*, vol. 4, no. 1, pp. 1–8, 2013.
- [274] W. Chen, K. M. Beck, R. Bücker, M. Gullans, M. D. Lukin, H. Tanji-Suzuki, and V. Vuletić, “All-optical switch and transistor gated by one stored photon,” *Science*, vol. 341, no. 6147, pp. 768–770, 2013.
- [275] A. V. Zasedatelev, A. V. Baranikov, D. Urbonas, F. Scafrimuto, U. Scherf, T. Stöferle, R. F. Mahrt, and P. G. Lagoudakis, “A room-temperature organic polariton transistor,” *Nature Photonics*, vol. 13, no. 6, pp. 378–383, 2019.
- [276] A. V. Baranikov, A. V. Zasedatelev, D. Urbonas, F. Scafrimuto, U. Scherf, T. Stöferle, R. F. Mahrt, and P. G. Lagoudakis, “All-optical cascable universal logic gate with sub-picosecond operation,” *arXiv preprint arXiv:2005.04802*, 2020.
- [277] K. Nozaki, T. Tanabe, A. Shinya, S. Matsuo, T. Sato, H. Taniyama, and M. Notomi, “Sub-femtojoule all-optical switching using a photonic-crystal nanocavity,” *Nature Photonics*, vol. 4, no. 7, pp. 477–483, 2010.
- [278] T. F. De Lima, H.-T. Peng, A. N. Tait, M. A. Nahmias, H. B. Miller, B. J. Shastri, and P. R. Prucnal, “Machine learning with neuromorphic photonics,” *Journal of Lightwave Technology*, vol. 37, no. 5, pp. 1515–1534, 2019.
- [279] A. Tait, A. Wu, T. F. De Lima, M. Nahmias, B. Shastri, and P. Prucnal, “Microring weight bank designs with improved channel density and tolerance,” in *2017 IEEE Photonics Conference (IPC)*, pp. 101–102, IEEE, 2017.
- [280] D. A. Miller, “Perfect optics with imperfect components,” *Optica*, vol. 2, no. 8, pp. 747–750, 2015.
- [281] G. Mourgias-Alexandris, A. Tsakyridis, N. Passalis, A. Tefas, K. Vysokinos, and N. Pleros, “An all-optical neuron with sigmoid activation function,” *Optics express*, vol. 27, no. 7, pp. 9620–9630, 2019.
- [282] H. Sharifi, S. M. Hamidi, and K. Navi, “A new design procedure for all-optical photonic crystal logic gates and functions based on threshold logic,” *Optics Communications*, vol. 370, pp. 231–238, 2016.
- [283] M. Wuttig, H. Bhaskaran, and T. Taubner, “Phase-change materials for non-volatile photonic applications,” *Nature Photonics*, vol. 11, no. 8, pp. 465–476, 2017.

- [284] B. M. Wilamowski and H. Yu, “Neural network learning without backpropagation,” *IEEE Transactions on Neural Networks*, vol. 21, no. 11, pp. 1793–1803, 2010.
- [285] X. Guo, T. D. Barrett, Z. M. Wang, and A. Lvovsky, “Backpropagation through nonlinear units for the all-optical training of neural networks,” *Photonics Research*, vol. 9, no. 3, pp. B71–B80, 2021.
- [286] T. Zhou, L. Fang, T. Yan, J. Wu, Y. Li, J. Fan, H. Wu, X. Lin, and Q. Dai, “In situ optical backpropagation training of diffractive optical neural networks,” *Photonics Research*, vol. 8, no. 6, pp. 940–953, 2020.
- [287] V. Lopez Pastor and F. Marquardt, “Design of self-learning machines using hamiltonian echo backpropagation,” *Bulletin of the American Physical Society*, 2022.
- [288] F. Marquardt and V. Lopez-Pastor, “How a time-reversal-invariant physical system can be turned into a self-learning machine,” *Bulletin of the American Physical Society*, 2022.
- [289] K. Weiss, T. M. Khoshgoftaar, and D. Wang, “A survey of transfer learning,” *Journal of Big data*, vol. 3, no. 1, pp. 1–40, 2016.
- [290] F. Zhuang, Z. Qi, K. Duan, D. Xi, Y. Zhu, H. Zhu, H. Xiong, and Q. He, “A comprehensive survey on transfer learning,” *Proceedings of the IEEE*, vol. 109, no. 1, pp. 43–76, 2020.
- [291] A. Fedorov, N. Gisin, S. Beloussov, and A. Lvovsky, “Quantum computing at the quantum advantage threshold: a down-to-business review,” *arXiv preprint arXiv:2203.17181*, 2022.
- [292] J. Preskill, “Quantum computing in the nisq era and beyond,” *Quantum*, vol. 2, p. 79, 2018.
- [293] G. Kalai, “The argument against quantum computers, the quantum laws of nature, and google’s supremacy claims,” *arXiv preprint arXiv:2008.05188*, 2020.
- [294] M. Fuechsle, S. Mahapatra, F. Zwanenburg, M. Friesen, M. Eriksson, and M. Y. Simmons, “Spectroscopy of few-electron single-crystal silicon quantum dots,” *Nature Nanotechnology*, vol. 5, no. 7, pp. 502–505, 2010.
- [295] C. Bradley, J. Randall, M. Abobeih, R. Berrevoets, M. Degen, M. Bakker, M. Markham, D. Twitchen, and T. Taminiau, “A ten-qubit solid-state spin register with quantum memory up to one minute,” *Physical Review X*, vol. 9, no. 3, p. 031045, 2019.
- [296] H. Bernien, S. Schwartz, A. Keesling, H. Levine, A. Omran, H. Pichler, S. Choi, A. S. Zibrov, M. Endres, M. Greiner, *et al.*, “Probing many-body dynamics on a 51-atom quantum simulator,” *Nature*, vol. 551, no. 7682, pp. 579–584, 2017.

- [297] L. Henriët, L. Beguin, A. Signoles, T. Lahaye, A. Browaeys, G.-O. Reymond, and C. Jurczak, “Quantum computing with neutral atoms,” *Quantum*, vol. 4, p. 327, 2020.
- [298] H. Zhang, C.-X. Liu, S. Gazibegovic, D. Xu, J. A. Logan, G. Wang, N. Van Loo, J. D. Bommer, M. W. De Moor, D. Car, *et al.*, “Quantized majorana conductance,” *Nature*, vol. 556, no. 7699, pp. 74–79, 2018.
- [299] N. C. Menicucci, P. Van Loock, M. Gu, C. Weedbrook, T. C. Ralph, and M. A. Nielsen, “Universal quantum computation with continuous-variable cluster states,” *Physical review letters*, vol. 97, no. 11, p. 110501, 2006.
- [300] S. Aaronson and A. Arkhipov, “The computational complexity of linear optics,” in *Proceedings of the forty-third annual ACM symposium on Theory of computing*, pp. 333–342, 2011.
- [301] C. S. Hamilton, R. Kruse, L. Sansoni, S. Barkhofen, C. Silberhorn, and I. Jex, “Gaussian boson sampling,” *Physical review letters*, vol. 119, no. 17, p. 170501, 2017.
- [302] T. R. Bromley, J. M. Arrazola, S. Jahangiri, J. Izaac, N. Quesada, A. D. Gran, M. Schuld, J. Swinarton, Z. Zabaneh, and N. Killoran, “Applications of near-term photonic quantum computers: software and algorithms,” *Quantum Science and Technology*, vol. 5, no. 3, p. 034010, 2020.
- [303] L. Banchi, M. Fingerhuth, T. Babej, C. Ing, and J. M. Arrazola, “Molecular docking with gaussian boson sampling,” *Science advances*, vol. 6, no. 23, p. eaax1950, 2020.
- [304] J. Huh, G. G. Guerreschi, B. Peropadre, J. R. McClean, and A. Aspuru-Guzik, “Boson sampling for molecular vibronic spectra,” *Nature Photonics*, vol. 9, no. 9, pp. 615–620, 2015.
- [305] B. Wu, B. Cheng, F. Jia, J. Zhang, M.-H. Yung, and X. Sun, “Speedup in classical simulation of gaussian boson sampling,” *Science Bulletin*, vol. 65, no. 10, pp. 832–841, 2020.
- [306] J. Carolan, J. D. Meinecke, P. J. Shadbolt, N. J. Russell, N. Ismail, K. Wörhoff, T. Rudolph, M. G. Thompson, J. L. O’Brien, J. C. Matthews, *et al.*, “On the experimental verification of quantum complexity in linear optics,” *Nature Photonics*, vol. 8, no. 8, pp. 621–626, 2014.
- [307] H. Wang, J. Qin, X. Ding, M.-C. Chen, S. Chen, X. You, Y.-M. He, X. Jiang, L. You, Z. Wang, *et al.*, “Boson sampling with 20 input photons and a 60-mode interferometer in a 1 0 14-dimensional hilbert space,” *Physical review letters*, vol. 123, no. 25, p. 250503, 2019.
- [308] H.-S. Zhong, H. Wang, Y.-H. Deng, M.-C. Chen, L.-C. Peng, Y.-H. Luo, J. Qin, D. Wu, X. Ding, Y. Hu, *et al.*, “Quantum computational advantage using photons,” *Science*, vol. 370,

- no. 6523, pp. 1460–1463, 2020.
- [309] G. Kalai and G. Kindler, “Gaussian noise sensitivity and bosonsampling,” *arXiv preprint arXiv:1409.3093*, 2014.
  - [310] P. Clifford and R. Clifford, “The classical complexity of boson sampling,” in *Proceedings of the Twenty-Ninth Annual ACM-SIAM Symposium on Discrete Algorithms*, pp. 146–155, SIAM, 2018.
  - [311] J. J. Renema, “Marginal probabilities in boson samplers with arbitrary input states,” *arXiv preprint arXiv:2012.14917*, 2020.
  - [312] A. Popova and A. Rubtsov, “Cracking the quantum advantage threshold for gaussian boson sampling,” in *Quantum 2.0*, pp. QW2A–15, Optica Publishing Group, 2022.
  - [313] H.-S. Zhong, Y.-H. Deng, J. Qin, H. Wang, M.-C. Chen, L.-C. Peng, Y.-H. Luo, D. Wu, S.-Q. Gong, H. Su, *et al.*, “Phase-programmable gaussian boson sampling using stimulated squeezed light,” *Physical review letters*, vol. 127, no. 18, p. 180502, 2021.
  - [314] A. Deshpande, A. Mehta, T. Vincent, N. Quesada, M. Hinsche, M. Ioannou, L. Madsen, J. Lavoie, H. Qi, J. Eisert, *et al.*, “Quantum computational advantage via high-dimensional gaussian boson sampling,” *Science advances*, vol. 8, no. 1, p. eabi7894, 2022.
  - [315] J. Arrazola, V. Bergholm, K. Brádler, T. Bromley, M. Collins, I. Dhand, A. Fumagalli, T. Gerrits, A. Goussev, L. Helt, *et al.*, “Quantum circuits with many photons on a programmable nanophotonic chip,” *Nature*, vol. 591, no. 7848, pp. 54–60, 2021.
  - [316] K. Brádler, P.-L. Dallaire-Demers, P. Reberntrost, D. Su, and C. Weedbrook, “Gaussian boson sampling for perfect matchings of arbitrary graphs,” *Physical Review A*, vol. 98, no. 3, p. 032310, 2018.
  - [317] M. Schuld, K. Brádler, R. Israel, D. Su, and B. Gupt, “Measuring the similarity of graphs with a gaussian boson sampler,” *Physical Review A*, vol. 101, no. 3, p. 032314, 2020.
  - [318] J. E. Bourassa, R. N. Alexander, M. Vasmer, A. Patil, I. Tzitrin, T. Matsuura, D. Su, B. Q. Baragiola, S. Guha, G. Dauphinais, *et al.*, “Blueprint for a scalable photonic fault-tolerant quantum computer,” *Quantum*, vol. 5, p. 392, 2021.
  - [319] M. V. Larsen, C. Chamberland, K. Noh, J. S. Neergaard-Nielsen, and U. L. Andersen, “Fault-tolerant continuous-variable measurement-based quantum computation architecture,” *Prx Quantum*, vol. 2, no. 3, p. 030325, 2021.



- [320] A. Neville, C. Sparrow, R. Clifford, E. Johnston, P. M. Birchall, A. Montanaro, and A. Laing, “Classical boson sampling algorithms with superior performance to near-term experiments,” *Nature Physics*, vol. 13, no. 12, pp. 1153–1157, 2017.
- [321] K. Brádler, S. Friedland, J. Izaac, N. Killoran, and D. Su, “Graph isomorphism and gaussian boson sampling,” *Special Matrices*, vol. 9, no. 1, pp. 166–196, 2021.
- [322] D. J. Brod, E. F. Galvão, A. Crespi, R. Osellame, N. Spagnolo, and F. Sciarrino, “Photonic implementation of boson sampling: a review,” *Advanced Photonics*, vol. 1, no. 3, p. 034001, 2019.
- [323] J. Wang, F. Sciarrino, A. Laing, and M. G. Thompson, “Integrated photonic quantum technologies,” *Nature Photonics*, vol. 14, no. 5, pp. 273–284, 2020.
- [324] J. Carolan, C. Harrold, C. Sparrow, E. Martín-López, N. J. Russell, J. W. Silverstone, P. J. Shadbolt, N. Matsuda, M. Oguma, M. Itoh, *et al.*, “Universal linear optics,” *Science*, vol. 349, no. 6249, pp. 711–716, 2015.
- [325] J. Biamonte, P. Wittek, N. Pancotti, P. Rebentrost, N. Wiebe, and S. Lloyd, “Quantum machine learning,” *Nature*, vol. 549, no. 7671, pp. 195–202, 2017.
- [326] G. R. Steinbrecher, J. P. Olson, D. Englund, and J. Carolan, “Quantum optical neural networks,” *npj Quantum Information*, vol. 5, no. 1, pp. 1–9, 2019.
- [327] F. M. Miatto, M. Epping, and N. Lütkenhaus, “Hamiltonians for one-way quantum repeaters,” *Quantum*, vol. 2, p. 75, 2018.
- [328] M. Streif and M. Leib, “Comparison of qaoa with quantum and simulated annealing,” *arXiv preprint arXiv:1901.01903*, 2019.
- [329] M. Willsch, D. Willsch, F. Jin, H. De Raedt, and K. Michielsen, “Benchmarking the quantum approximate optimization algorithm,” *Quantum Information Processing*, vol. 19, pp. 1–24, 2020.
- [330] M. P. Harrigan, K. J. Sung, M. Neeley, K. J. Satzinger, F. Arute, K. Arya, J. Atalaya, J. C. Bardin, R. Barends, S. Boixo, *et al.*, “Quantum approximate optimization of non-planar graph problems on a planar superconducting processor,” *Nature Physics*, vol. 17, no. 3, pp. 332–336, 2021.
- [331] E. Ng, T. Onodera, S. Kako, P. L. McMahon, H. Mabuchi, and Y. Yamamoto, “Efficient sampling of ground and low-energy ising spin configurations with a coherent ising machine,” *Physical Review Research*, vol. 4, no. 1, p. 013009, 2022.

- [332] G. Lindblad, “On the generators of quantum dynamical semigroups,” *Communications in Mathematical Physics*, vol. 48, no. 2, pp. 119–130, 1976.
- [333] V. Gorini, A. Kossakowski, and E. C. G. Sudarshan, “Completely positive dynamical semigroups of  $n$ -level systems,” *Journal of Mathematical Physics*, vol. 17, no. 5, pp. 821–825, 1976.
- [334] J. Levinsen, G. Li, and M. M. Parish, “Microscopic description of exciton-polaritons in microcavities,” *Physical Review Research*, vol. 1, no. 3, p. 033120, 2019.
- [335] M. A. Bastarrachea-Magnani, A. Camacho-Guardian, and G. M. Bruun, “Attractive and repulsive exciton-polariton interactions mediated by an electron gas,” *Physical Review Letters*, vol. 126, no. 12, p. 127405, 2021.
- [336] D. K. Efimkin, E. K. Laird, J. Levinsen, M. M. Parish, and A. H. MacDonald, “Electron-exciton interactions in the exciton-polaron problem,” *Physical Review B*, vol. 103, no. 7, p. 075417, 2021.
- [337] F. Cai, S. Kumar, T. Van Vaerenbergh, X. Sheng, R. Liu, C. Li, Z. Liu, M. Foltin, S. Yu, Q. Xia, *et al.*, “Power-efficient combinatorial optimization using intrinsic noise in memristor hopfield neural networks,” *Nature Electronics*, vol. 3, no. 7, pp. 409–418, 2020.